IMPERIAL COLLEGE LONDON

Department of Earth Science and Engineering
Centre for Petroleum Studies

A sensitivity study of the sub-volume and resolution on the prediction of petrophysical properties

By

Mohammed F. Alzayer

A report submitted in partial fulfilment of the requirements for the MSc and/or the DIC

September 2014

DECLARATION OF OWN WORK

I declare that this thesis

A sensitivity study of the sub-volume on the prediction of petrophysical properties

is entirely my own work and that where any material could be construed as the work of others, it is fully cited and referenced, and/or with appropriate acknowledgement given.

Signature:...

Name of student: Mohammed F. Alzayer

Name of Supervisors: Professor Martin J. Blunt and Nayef Al-Ansi

Acknowledgement

First, I thank Allah, the most merciful, for guiding me and providing me the high strength and endurance to achieve this important milestone of my life.

Special thanks to Nayef Al-Ansi for his support in the project. From day one, I am very grateful to his professionalism, competence, and guidance in my research. I am very grateful to Professor Martin Blunt for his inspirational and thought-stimulating incredible teaching style as well as his guidance and encouragement.

I am always grateful to my father Fuad and my mother Mona for inspiring me to pursue my dreams and never let a life setback hold me back from making them real. They always stimulated me to think more, work harder, develop myself and be always a distinguished person. Thank you for being proud of me.

My lovely wife, Bayan Alshammasi, who kept cheering me since I applied to the school, I deeply appreciate your encouragement and value your continuous patience while we are away from each other to complete your B.Sc. degree in Cardiac Technology. Nonetheless, your unlimited love lifted me every time I fell and made me believe more and more in myself and my abilities in the challenging one-year journey at Imperial College. Without you, my life would be boring, distasteful, and sad. Thanks for making me happy and thanks to Allah for giving me his blessing that is your love.

Contents

List of Figures

List of Tables

Imperial College
London

A Sensitivity Study of the Sub-volume on the Prediction of Petrophysical Properties

Mohammed F. Alzayer

Imperial College supervisors: Professor Martin J. Blunt and Nayef Al-Ansi

Abstract

Oil and gas are becoming more and more difficult to extract as most major hydrocarbon fields are maturing and with steady production decline. Understanding reservoir behavior at the pore scale is vital in order to unlock the potential and get more of the hydrocarbon resources. Pore-scale simulation takes into account all the factors that affect the movement of fluids within the pore space. This study focuses on porosity and absolute permeability.

The objective of this study is to find out the various effects of different sub volumes (100-1024 voxel^3) and resolutions (2.7-27 µm) on the petrophysical properties. Topologically representative networks were utilized to understand the effects of different sub-volumes and resolutions on basic petrophysical properties of four different rock types: Berea (medium permeability sandstone), Doddington (high permeability sandstone), Estaillades (medium permeability limestone), and Ketton (high permeability limestone).

At 2.7 µm, Berea shows convergence toward both porosity and permeability experimental values at sample volumes between 400 and 1024 voxel^3 (1.11 and 2.85 mm^3). In Doddington, porosity is close to the experimental values between 400-1024 voxel^3, whereas, permeability estimates were better at 100-200 voxel^3 and at 1024 voxel^3. It is impossible to get a representative elementary volume, REV, for porosity from µ-CT images due to the presence of micro-pores. Permeability of Estaillades and Ketton was close to the experimental value at 800 and at 600-1024 voxel^3 respectively.

In the resolution study, the input is a larger image of 1024 voxel^3 (2.85 mm^3) that is interpolated to coarser resolutions; simulation shows that the inclusion of more sample volume increased the ability to predict basic properties accurately. Sandstone porosity estimates were not affected by coarsening and their absolute permeability was predicted accurately at up to 18 µm in Berea and between 8-27 µm in Doddington. The portion of micro-pores to macro-pores can be an indication of the accuracy of pore-scale simulation results in limestone. Results can be improved by increasing sample size beyond 1024 voxel^3 then coarsening it to be a computationally feasible simulation.

Introduction

Pore scale simulation takes into account all the factors that affect the movement of fluids within the pore space. A study by (Blunt et. al., 2012) provides an overview of the techniques and methods of applying pore-scale imaging and modeling in difference advanced areas of study. Porosity and absolute permeability are the basic predicted properties. In addition, special core analysis data such as relative permeability and capillary pressure can be generated as well. One of the methods of pore-scale studies is simulating the flow in an extracted topological network from µ-CT binary images.

In conventional reservoir simulation models, having more cells allows capturing heterogeneity to get results that are more representative. However, at some point, simulation becomes impractical and resource intensive as the size of the model is increased. Similarly, µ-CT images of pore-scale structure have various resolutions and simulating large volumes of fine resolution pore-scale samples is a challenge. In this project, the bases of the study are 1024 voxel^3 images of Berea (medium permeability sandstone), Doddington (high permeability sandstone), Estaillades (medium permeability limestone), and Ketton (high permeability limestone). The four rock samples were µ-CT scanned with a resolution of ≈2.7 µm.

The objective of this study is to find out the various effects of different sub volumes (100-1024 voxel^3) and resolutions (2.7-27 µm) on the petrophysical properties. Topologically representative networks were utilized to understand the effects of different sub-volumes and resolutions on basic petrophysical properties of the four different rock types.

At 2.7 µm, Berea shows convergence toward both porosity and permeability experimental values at sample volumes between 400 and 1024 voxel^3 (1.11 and 2.85 mm^3). In Doddington, porosity is close to the experimental values between 400-1024 voxel^3, whereas, permeability estimates were better at 100-200 voxel^3 and at 1024 voxel^3. It is impossible to get a representative elementary volume, REV, for porosity from µ-CT images due to the presence of micro-pores in limestone samples. Permeability of Estaillades and Ketton was close to the experimental value at 800 and at 600-1024 voxel^3 respectively.

In the resolution study, the input is a larger image of 1024 voxel^3 (2.85 mm^3) that is interpolated to coarser resolutions; simulation shows that the inclusion of more sample volume increased the ability to predict basic properties accurately. Sandstone porosity estimates were not affected by coarsening and their absolute permeability was predicted accurately at up to 18 µm in Berea and between 8-27 µm in Doddington. The portion of micro-pores to macro-pores can be an indication of the accuracy of pore-scale simulation results in limestone. Results can be improved by increasing sample size beyond 1024 voxel^3 then coarsening it to be computationally feasible simulation.

Background

Representative elementary volume, REV, first introduced by (Bear, 1972), is a parameter of great importance not only in the petroleum industry but also in all other sciences that study heterogeneous materials. An important goal of determining REV is to find effective properties of heterogeneous medium. It must be large enough to be statically being representative of total volume but not extremely large as it will be purposeless. As a result, REV must include all micro heterogeneities of the material. In the scope of pore-scale modeling, REV needs to include all features that appear repeatedly within a sample by capturing a wide distribution of pores and throats that represent the main sample (Kanit, 2003).

REV is not an exact volume. It starts with a minimum volume at which the micro-scale properties become homogenous and representative of a large sample. It also ends with a maximum volume where any extra inclusion additional sample volume will introduce heterogeneities to the sample rendering it unrepresentative. (Bear, 1972), first introduced the REV concept based on porosity. An REV for porosity is commonly referred to as the REV of a particular rock type however; it will not be the same REV that represents other parameters especially for advance properties such as capillary pressure and relative permeability (Al-Raoush and Papadopoulos, 2010). REV is widely studied in soil science (Li, 2010), (O'Donnel, 2010). Also, it is used to assess mechanical properties of rocks (Wang, 2002). Due to the difficulty of REV determination, many researchers followed advanced statistical methodologies to study the REV for different purposes (Li, 2010), (Salmi, 2012). Authors who follow a statistical approach acknowledge the fact that even if they determine and REV, it will not be 100% applicable to the sample of interest. Statistical methods assume that the certain modeled properties follow a specific distribution, which enables the researcher to generate wide variety of samples to study. This study is different in the way it takes an actual μ-CT images that does not contain any user generated features.

A recent study by (Mostaghimi, et. al., 2012) compared absolute permeability prediction methods to experimental data. In addition, the authors examined the REV of different rock types and its significance. The REV of absolute permeability, compared to porosity, is larger in order to account for tortuosity and connectivity of the pore space. Moreover, the authors concluded that the REV of carbonate samples appears to be larger than the image itself.

Some available studies, (Peng, 2012), obtained a specific REV for Berea sandstone which is studied thoroughly in this paper. The author determined that 2.8 mm in height and diameter is sufficient at different resolutions for porosity and pore connectivity. Moreover, the study emphasizes the differences between high and low resolution with respect to pore structure details. High resolution images reveal more details of pore structure. Low resolution on the other hand, gets a wide view of the sample and captures large pores and large throats. (Vik, 2013) proved experimentally that for highly heterogeneous limestone, properties decrease in variability with increasing size. It indicates a transition from a variable property regime into an REV.

Moreover, (Al-Ansi et. al., 2013) had a similar objective in examining resolution effects on Clashach and Doddington sandstone rocks. The study covered resolutions between $\approx$6 to 20 μm. It concluded that a resolution of 6 μm is not sufficient to capture network properties correctly as the average throat radius is close to the image resolution. Regardless of that deficiency, 5-10 μm resolution is enough to accurately predict flow properties in homogenous high permeability rocks. In contrast, this study examines petrophysical properties of the same Doddington and other rocks that were scanned at a finer resolution, $\approx$2.7 μm. A detailed literature review is available in Appendix I.

Input data

Subject rocks were scanned with μ-CT scanners. The main advantage of μ-CT is the ability to perform 3D imaging of rock samples non-destructively through multiple slices of 2D images. (Cnudde and Boone, 2013) provide an extensive overview of μ-CT technology, recent advances and its vast applications. μ-CT imaging produces images with shades of grey. Network extraction input should include only pores and grains, i.e. segment images, as the network cannot be generated directly from raw grey μ-CT images.

In this study, I used images that had been already segmented and quality checked using Otsu's algorithm (Otsu, 1979) that maximizes the separability of gray levels. The optimal threshold is selected based on global property of the images' histograms which is a practical way to segment dry μ-CT images. Using the published images (Al-Ansi, 2012) ensured consistency and kept the project on track because the purpose of this project is to directly study the effect of sub-volume and resolution on single phase properties. In this report, the term "base image" always refers to the 1024 voxels^3 segmented image with resolution of $\approx$2.7 μm.

Sample	Rock type	Resolution (μm)	Size (voxel^3)
Berea	Sandstone	2.7745	1024
Doddington	Sandstone	2.7745	1024
Estaillades	Limestone	2.6825	1024
Ketton	Limestone	2.654	1024

Table 1 μ-CT image details of the analysed rock samples. Images of the rock samples are published in ".raw" format from which a pore network can be directly generated (Al-Ansi, 2012).

Rock samples

Four different rock types have been studied. Two sandstone and two limestone rocks with varying permeability range. This section discusses each rock individually. Additional images can be found in Appendix II and Appendix III. In this section, each rock is described briefly using different sources. Then, a sample of the segmented images is shown with a graph representing the variation of porosity in each individual 2D image slice along the sample. No line smoothing was performed to observe the variation in porosity between adjacent image slices.

Sample	Rock type	Place of origin	ϕ_{Helium}	Permeability [m^2]	n
Berea	Sandstone	Berea, Ohio, US	0.22	$(4.4 \pm 0.2) \times 10^{-13}$	2
Doddington	Sandstone	Doddington, UK	0.22	$(1.1 \pm 0.1) \times 10^{-12}$	1
Estaillades	Limestone	Oppède, France	0.28	$(1.6393 \pm 0.0005) \times 10^{-13}$	2
Ketton	Limestone	Ketton, UK	0.23	$(2.884 \pm 0.006) \times 10^{-12}$	1

Table 2 Rock types and basic petrophysical properties of subject rocks. 'n' refers to the number of independent measurements of permeability, (Tanino and Blunt, 2012).

Berea

Berea sandstone is a standard testing material in the petroleum industry as it is widely studied in the literature. The sandstone is brittle and is made of 93.13% silica (Berea Sandstone, 2014). Berea is a medium- to fine-grained sandstone from the vicinity of Berea, Ohio, US. (Pepper, 1954). Porosity in the Berea is inter-granular as shown in a Focused Ion Beam "FIB" cut through the grain, which reveals no micro porosity.

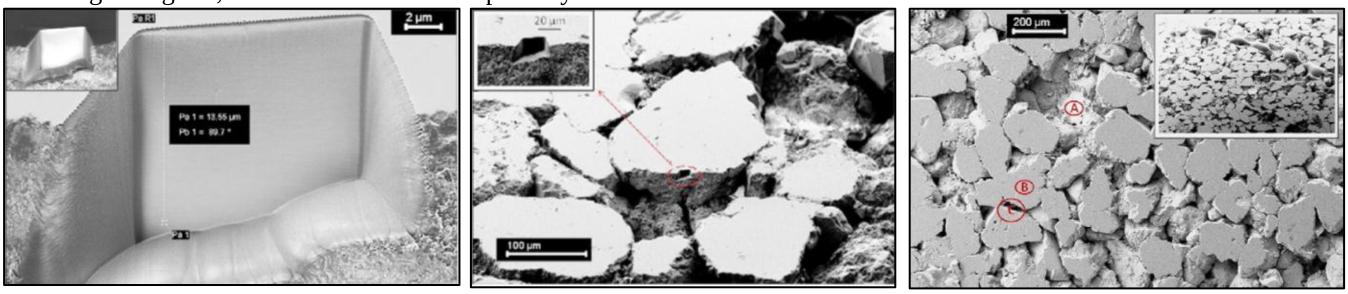

Figure 1. [Left] No micro-pores are present in a grain cut by FIB milling. [Centre] The sandstone matrix is surrounded by crater-like small pores. [Right] Micro-pores are also not present in a thin section milling (Bara, 2010). We expect to capture Berea's flow properties accurately with no micro-pores because pore structure is fully captured by 2.7μm resolution scanning.

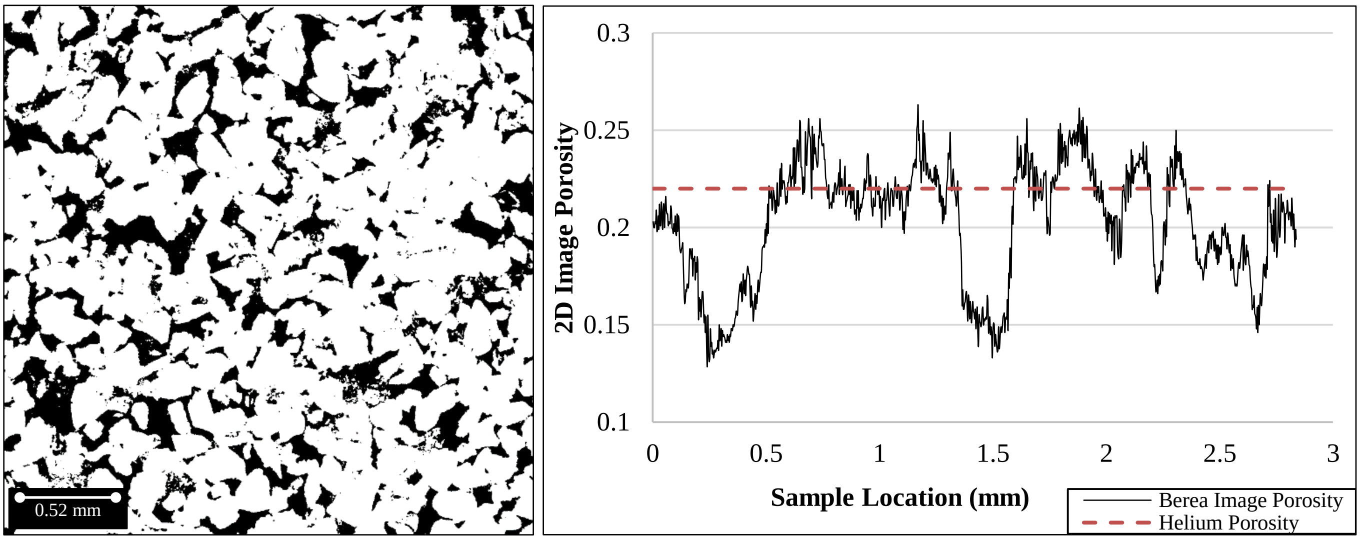

Figure 2. [Left] Segmented μ-CT image scan of Berea sandstone. The pores and grains shapes look very similar in the image. [Right] A z-axis profile plot of porosity of individual segmented image along the Berea sample.

Berea sandstone heterogeneity is identified from the several wide variations of porosity values, a 10 p.u. range, along the sample. Compared to other samples, Berea's z-axis plot is the most disturbed line. This is attributed to the small grain size that widens the slice-to-slice porosity variation window.

Doddington

Doddington is carboniferous sandstone. The studied sample has same porosity as the Berea; however, its permeability is 2.5 times higher. For the purpose of this study, it is classified as high permeability sandstone.

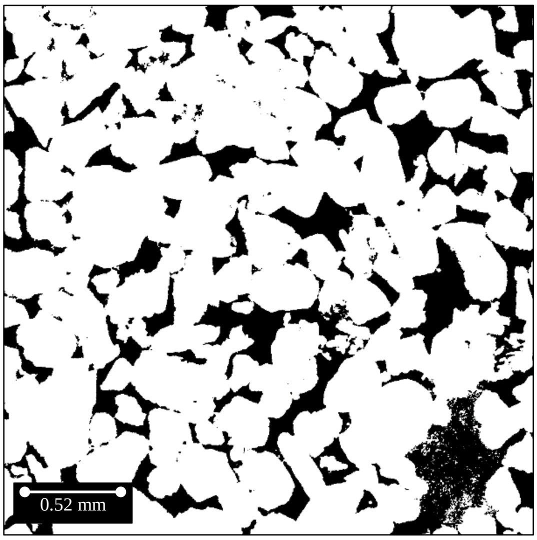

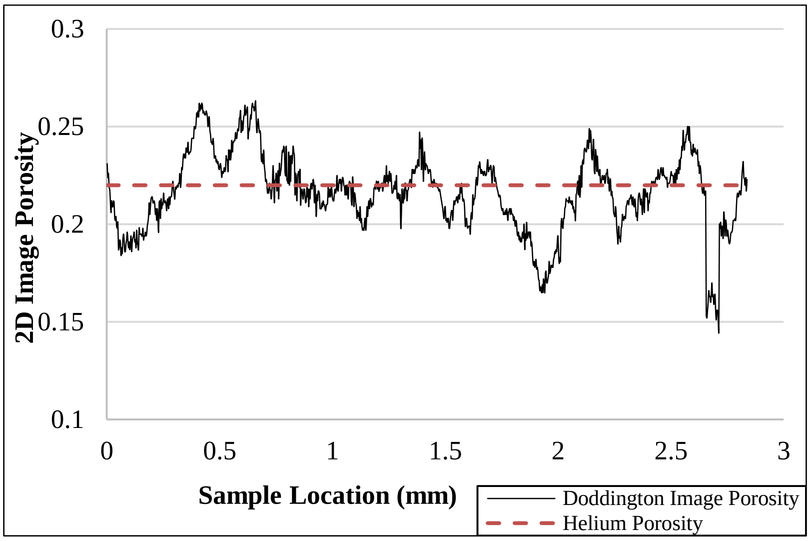

Figure 3. [Left] Segmented µ-CT image scan of Doddington sandstone. The pores and grains are larger than Berea, thus fewer pores and grains are present in the image. Pore bodies are clear can be easily traces by eye between images. [Right] A z-axis profile plot of porosity of individual segmented image along the Doddington sample.

Most of the images are within a range of 5 p.u. making Doddington much more homogeneous than Berea. In addition, the line is smoother indicating smaller slice-to-slice change in characteristics. Visual inspection of Figure 3 Figure 4 of Berea and Doddington sandstones show that the REV is approximately 1mm in sample length. It is approximately the same length that was found from the 3D images with 400 voxel^3.

Estaillades

Estaillades limestone has porosity up to 30%. It contains approximately 95% calcite and is considered to be a mid-range permeability rock between 1.97x10^{-13} to 3.95x10^{-13} m^2. The µ-CT and Scanning Electron Microscope "SME" show the high degree of heterogeneity in the pore space (Renard, 2006). Micro-porosity is present vastly in the Estaillades, producing a bimodal distribution of pore size, and cannot be detected with µ-CT scanning (Bejeljic, 2013). In addition, the presence of micro-scale grains ranging between 1 to 10 µm creates structural heterogeneity represented as local variations in porosity NMR and MICP experiments confirm the double porosity characteristic of Estaillades (Gland, 2009).

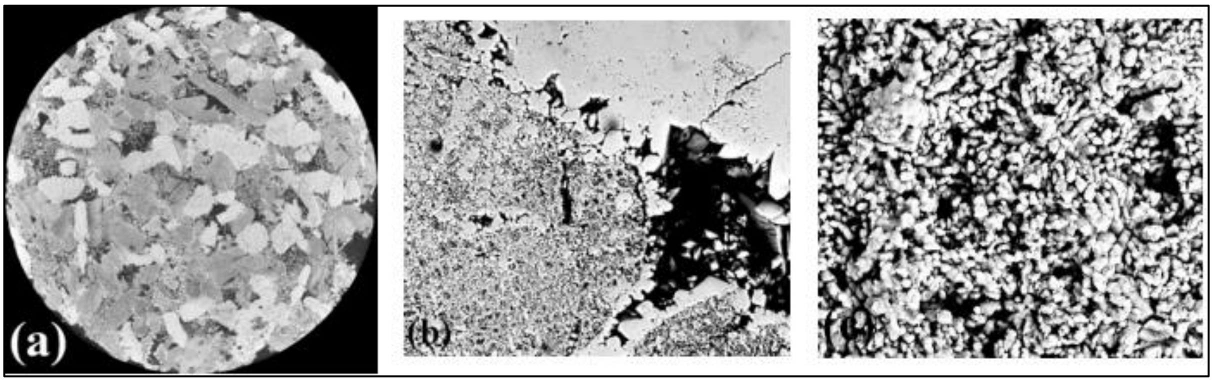

Figure 4. (a) A µ-CT scan of Estaillades showing only micro-grains. However, (b) displays the micro-porous structure on the left, the dense structure on the top and on the right a large pore is clearly shown (Gland, 2009).

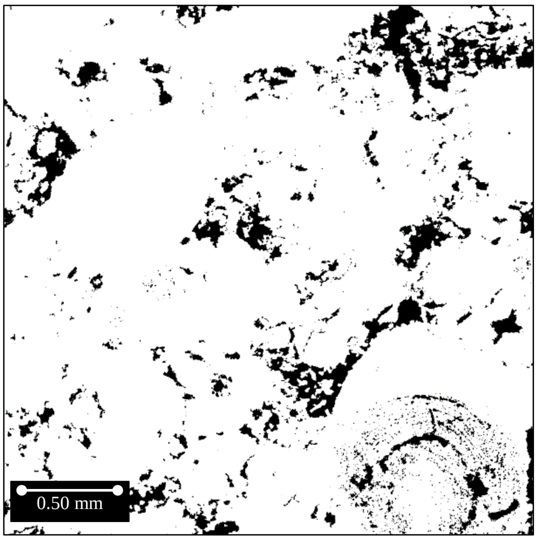

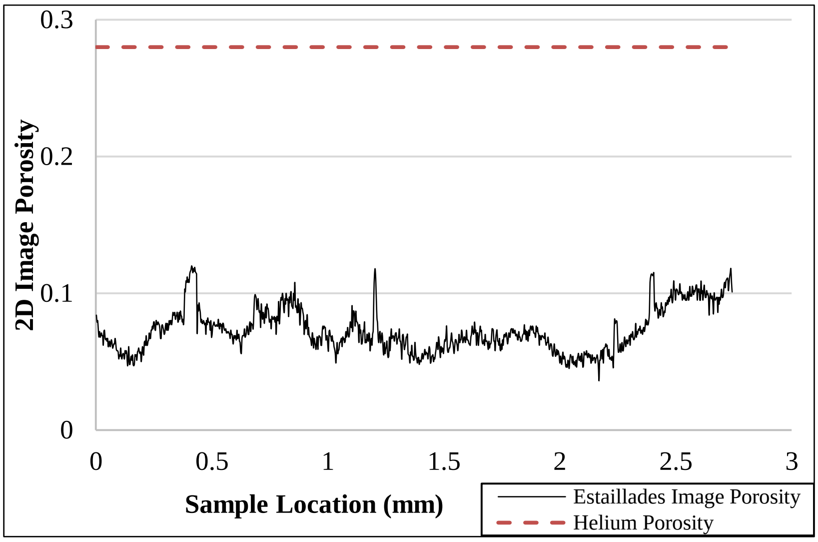

Figure 5. [Left] segmented µ-CT image scan of Estaillades limestone. Many different shapes of pores are clear in the picture. Limestone deposition has great impact on the structure of the rock. [Right] A z-axis profile plot of porosity of individual segmented image along the Estaillades sample.

Two-thirds of the porosity is micro-porous and cannot be identified in the image. That is why the line looks smooth, straight and 20 p.u. less than helium porosity value. Helium gas is used to measure porosity by applying Boyle's law. It's the smallest molecule in size, after hydrogen, allowing it to penetrate micro-pores rapidly. That is the main reason why µ-CT imaging underestimates helium porosity in limestone samples. Also, helium has high diffusivity allows determining porosity in low permeability rocks (Yu, 2013). Porosity from µ-CT images will match the helium porosity in the presence on micro-pores only when the scanning resolution is at the same scale as the micro-pores.

Ketton

The Ketton is almost pure limestone present in the Upper Lincolnshire limestone in Ketton, Rutland, UK. The grain stone are all oolitic in shape and up to 600µm in size. Like Estaillades, it has micro-porosity that cannot be captured by µ-CT imaging (Andrew, 2014). The permeability of the Ketton sample is about 18 times higher than Estaillades.

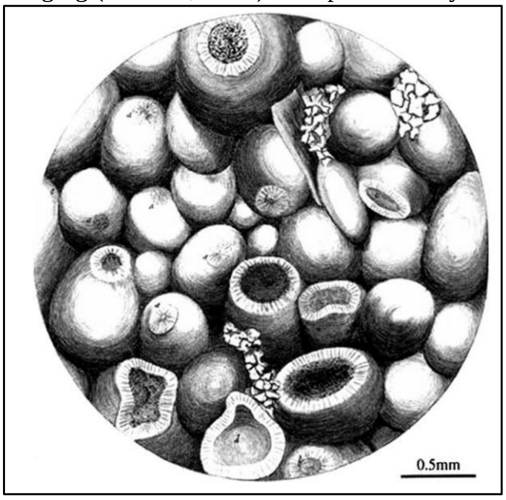

Figure 6. Hand-sketched Ketton surface showing the distribution of oolitic shape bodies (Azevedo, 2010).

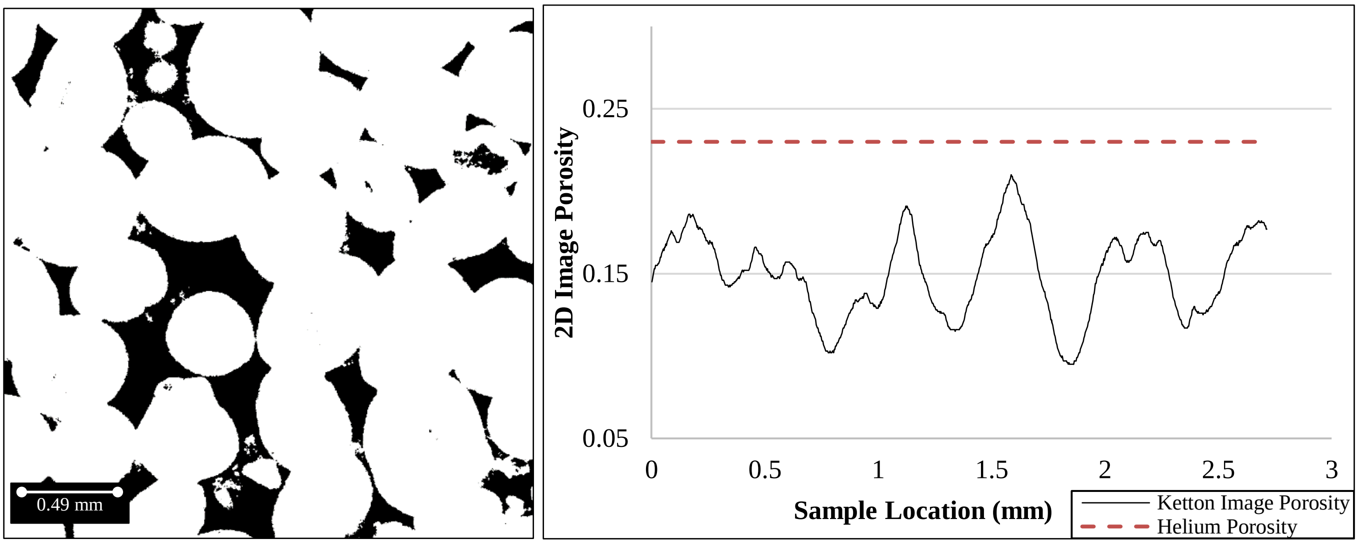

Figure 7. [Left] segmented µ-CT image scan of Ketton limestone. The image shows smooth oolitic grain. The shape of the grains is same all over the rock and they vary smoothly in size and shape across the sample. [Right] A z-axis profile plot of porosity of individual segmented image along the Ketton sample.

About one third of the porosity is micro-porous and cannot be identified in the image. The line is closer to experimental value than the Estaillades sample. Ketton has the smoothest porosity profile in a slice-to-slice basis. Ellipsoidal grains are large and change uniformly in size across the images.

Research Method

Studying the effects of different sub-volumes and resolutions of an image involves two separate parts. The first uses the base image of 1024 voxel^3 and crops it in smaller sizes without altering the resolution. The latter takes the same 1024 voxel^3 and reduces its size by interpolating the pores and grains with the intent of producing an image that is as similar as a µ-CT scan of the same rock with coarser resolution and smaller voxel^3 size.

Sub-volume study

The base images of 1024 voxel^3 were cropped into 4 different sizes that are 800, 400, 200, and 100 voxel^3. Cropping was always done by making the x-y center of the 1024^3 cube the same as the x-y center of the smaller cubes. The z-axis cropping always started from the first image. This procedure produces more consistent results that actually show the sensitivity of the sub-volume instead of randomly cropping a smaller cube anywhere in the base image. Table 3 illustrates the cropping concept on a Doddington sample. Note that a complete set of 2D and 3D images is available in Appendix II and Appendix III. No changes to resolution were made at any point in the sub-volume study.

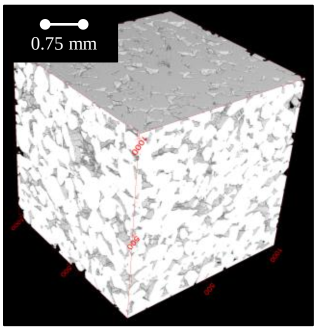	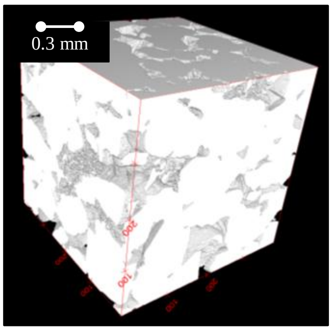	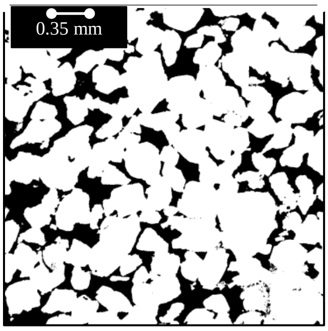	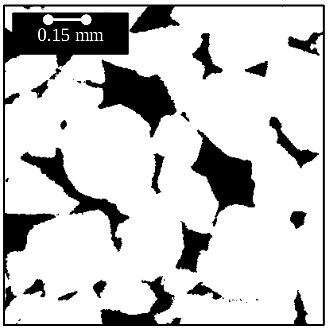
1024^3 Doddington base 3D image	400^3 Doddington sub-volume example 3D image	Full 1024 pixels Doddington 2D image	Full 400 pixels Doddington 2D sub-volume image
All images at resolution of 2.7745 µm			

Table 3. Illustration of the sub-volume concept of the study.

Resolution study

In the resolution study, the base is the same 1024 voxel^3 image. The image is reduced in size without cropping by interpolating its pores and grains. There are several interpolation algorithms that are coded in image processing software packages ranging from very simple nearest neighbor and linear algorithms into complex high-order ones like cubic convolution and quintic B-spline. All readily available interpolation algorithms were tested. The preferred algorithm is the quintic B-Spline.

The “spline” is a numeric function that is piecewise-defined by polynomial functions and provides smooth interpolation results that are similar to high degree polynomial interpolation but are better in stability (Judd, 1998). This interpolation method is well known in the fields of mathematics, physics, and engineering to solve nonlinear higher order evolution equations and was first identified to provide smooth piecewise polynomial approximation by (Schoenberg, 1946).

Complexity of interpolation does not guarantee the best results. The quality of interpolation in is checked by comparing the pores and throats in the original image and the interpolated image across the entire cube. Quintic B-spline always produced interpolated images that are consistent with the original. Other interpolation methods produce artifacts and non-representative interpolated images that are not comparable to the base image.

The images are reduced by choosing a reduction factor between 0 and 1. The factors were chosen in a way that produces meaningful spacing between their respected resolutions. Specifically, more images were produced to examine effects of less than 10µm resolution as shown in Table 4 because samples are more commonly scanned at that range.

Image reduction factor	1	0.800	0.601	0.500	0.400	0.350	0.300	0.200	0.150	0.120	0.101
Cubic Voxels	1024	819	615	512	410	358	307	205	154	123	103
Berea (µm)	2.7745	3.47	4.62	5.55	6.93	7.94	9.25	13.9	18.4	23.1	27.6
Doddington (µm)	2.7745	3.47	4.62	5.55	6.93	7.94	9.25	13.9	18.4	23.1	27.6
Estaillades (µm)	2.6824	3.35	4.47	5.36	6.70	7.67	8.95	13.4	17.8	22.3	26.7
Ketton (µm)	2.654	3.32	4.42	5.31	6.63	7.59	8.85	13.3	17.6	22.1	26.4

Table 4. Coarsened resolutions and image voxel^3 sizes for each rock sample.

As the original images are binary having only black and white pixels, interpolating them will produce shades of grey. Directly trying to extract pore network from the gray shades does not work because it will confuse the code about what a pore and what a grain is. As a result, a manually set threshold based on the histogram of each individual image allows for better representation of the pore structure.

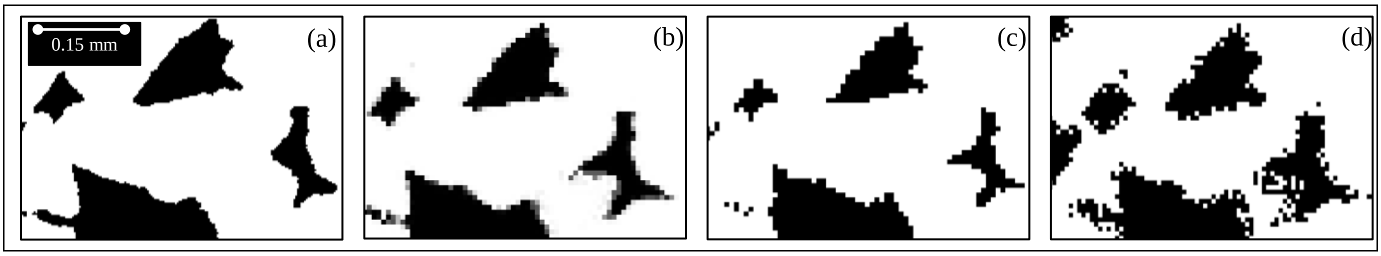

Figure 8. Illustrative images of interpolating Doddington sandstone sample and the effects of different grey scale thresholds. (A): Original Doddington image scanned at 2.7745 µm resolution. (B): Quintic b-spline interpolated image with grey shades with an interpolated resolution of 7.93µm. (C): Manually set grey scale appropriate threshold based on grey shades histogram. This was performed manually on all coarsened images. (D): Excessive inclusion of grey shades as pore space shown for illustrative purposes only and was avoided at all parts of the resolution study.

Figure 9 and Figure 10 show how the pore and throat structure change at different coarsened resolutions. In Berea sandstone, coarser resolutions have significant effects on the pore structure because the pores and throats are small in size. Some pores are completely missed out at the resolution of 23.1 µm. On the other hand, Ketton has larger pores. There is no visible change in the structure when the resolution is coarsened from 2.654 µm to 4.42 µm. Even at 22.1 µm, the effect is insignificant.

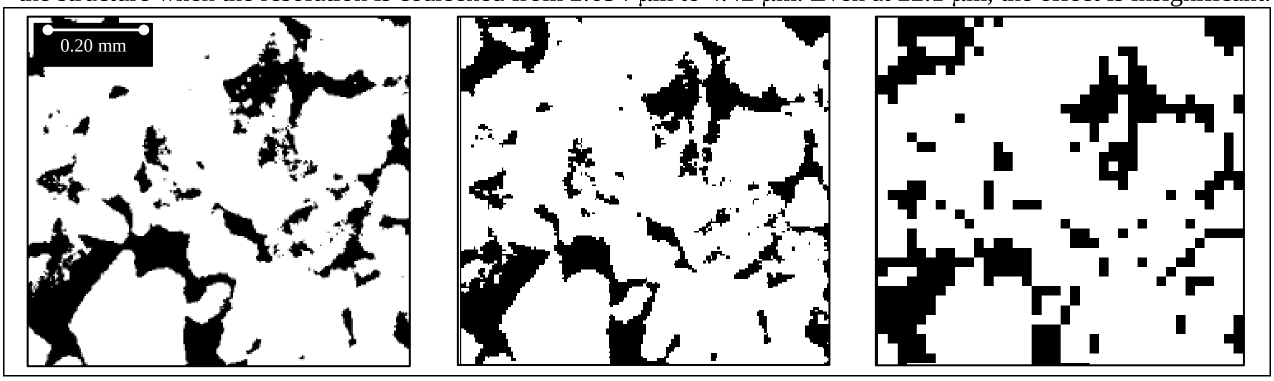

Figure 9. Resolution coarsening effects on Berea sandstone. [Left] original Berea image of resolution 2.7745 µm. [Centre] Berea image with an interpolated resolution of 5.55µm. [Right] Berea image with an interpolated resolution of 23.1µm

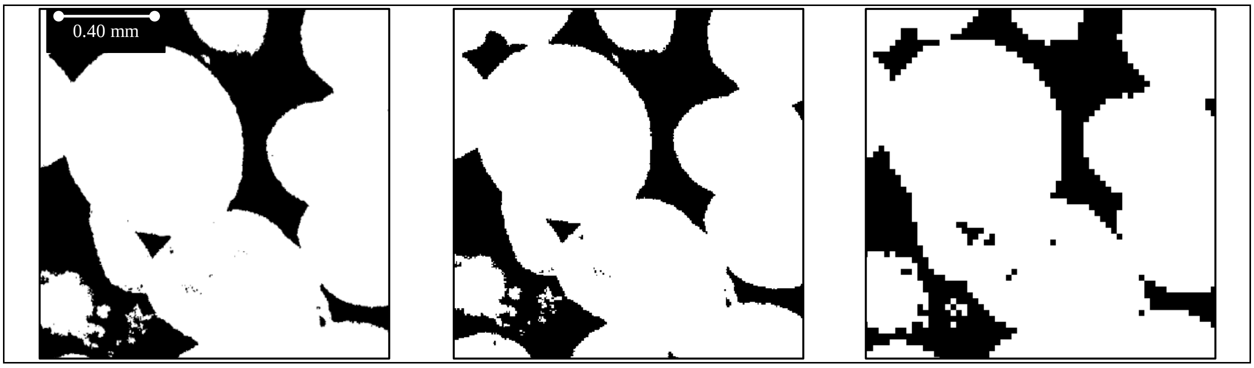

Figure 10. Resolution coarsening effects on Ketton limestone. [Left] original Ketton image of resolution 2.654 μm. [Centre] interpolated Ketton image with an interpolated resolution of 4.42 μm. [Right] interpolated Ketton image with an interpolated resolution of 22.1 μm.

In the Ketton sample, the pores and throats are much larger. There is only a small chance that the structures are undetected or misrepresented when the resolution is coarsened from 2.654 to 4.42 μm. For Ketton, even very coarse resolutions do not look very different from the original fine picture as indicated in Figure 10. A complete set of pictures for all samples and resolutions is available in Appendix III to show the effect of coarser resolution at all levels.

Topologically representative network extraction results

The first step after image processing is the extraction of topologically representative networks. The networks represent the void space by a lattice of pores that are connected by throats. These networks provide a representation of the 3D structure to be input into the two phase simulation codes. A modified maximal ball algorithm that is described in (Dong and Blunt, 2009) is robust with all of its critical output parameters such as coordination number and pore and throat size distributions are benchmarked and proven consistent with experimental data. It uses an algorithm that treats the large spheres as a pore while the small spheres that connect large spheres are pore throats.

Effects of sub-volume changes on networks

Sandstone topological networks are distinguished clearly from the limestone networks. The histograms of the pore and throat radii are almost identical in the case of Berea and Doddington sandstones. They vary at the radii above 30 μm where Doddington has more pores and pore-throats in that range due to its higher permeability. The volume of samples in the study is less than 3 mm^3. It is a small scale to observe sandstone sorting and pore size anomalies. At such a small scale, the sandstones appear to be homogeneous and the reduction of sub-volume does not significantly skew the radii histograms. Most lines appear identical to each other except the line of the smallest studied sub-volume of 100 $voxel^3$.

The same logic applies when comparing Ketton to Estaillades. The pores and throats of Ketton are very large compared to Estaillades. Also, they are all oolitic in variety of sizes. What is shown in the histograms and later in simulation of Ketton and Estaillades is based totally on the detectable macro-pores and throats at a scanning resolution of 2.7 μm. At the smallest size of 100 $voxel^3$, Ketton and Estaillades have poor representation in their networks. Many images in Estaillades will be purely grain without any pores whereas in Ketton the smallest images are mostly pore-space.

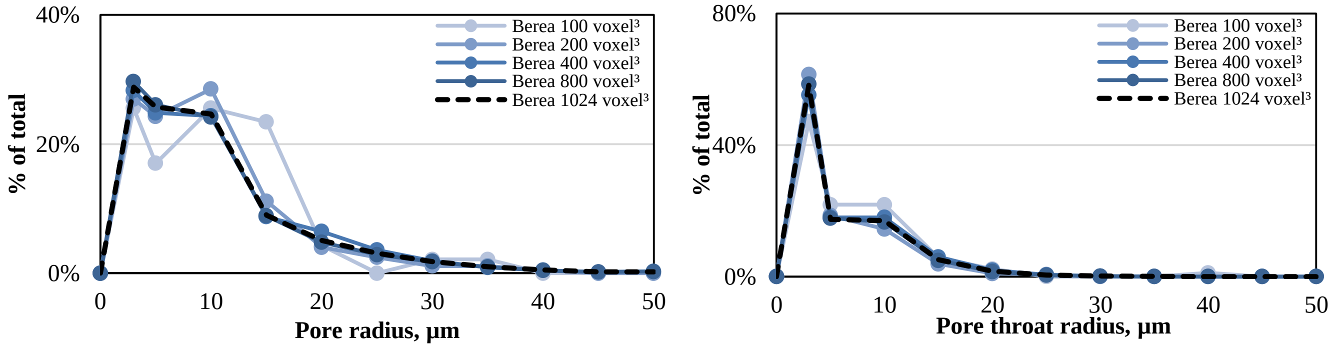

Figure 11. Pore and pore-throat radii size change with decreasing sub-volume in Berea sandstone that is scanned at ≈2.7 μm. The bin used in this and most following histograms is (3, 5, 10, 15, 20, 25, 30, 35, 40, and 45) μm. The dashed line here and all following histograms represents the 1024 $voxel^3$ base case.

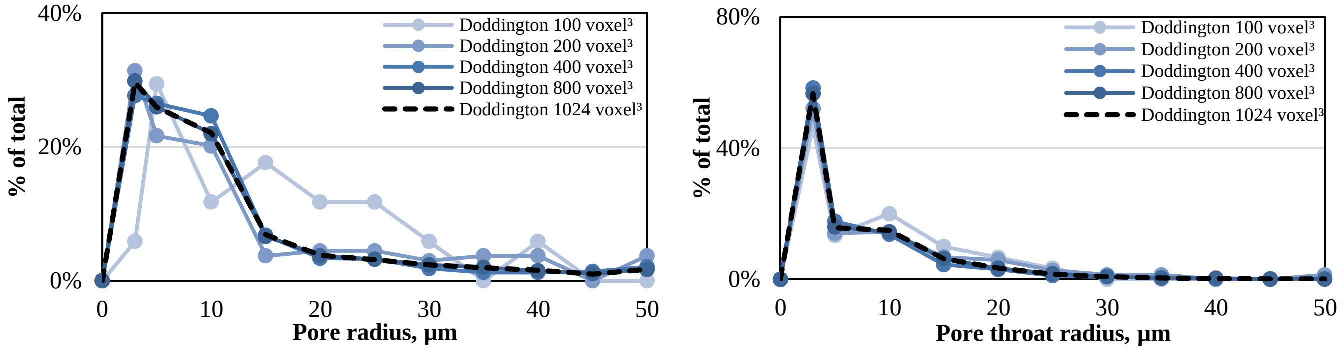

Figure 12. Pore and pore-throat radii size change with decreasing sub-volume in Doddington sandstone that is scanned at ≈2.7 µm.

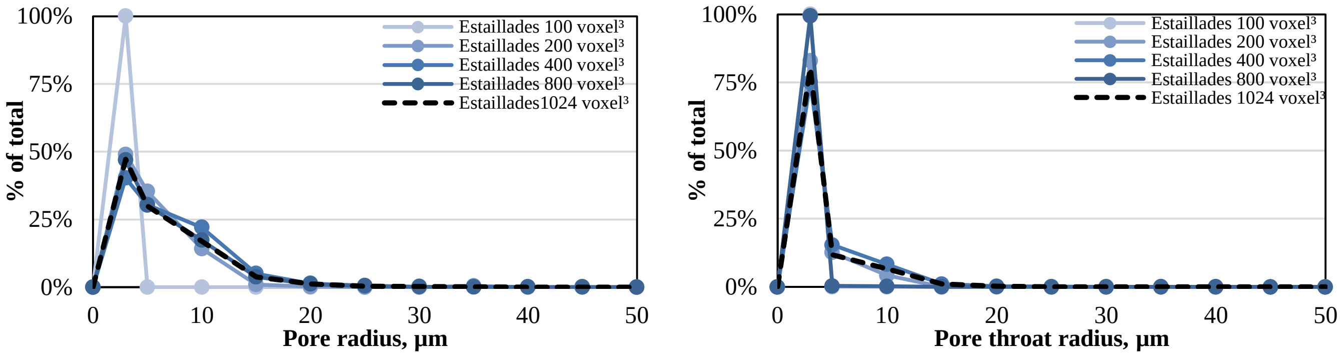

Figure 13. Pore and pore-throat radii size change with decreasing sub-volume in Estaillades limestone that is scanned at ≈2.7 µm.

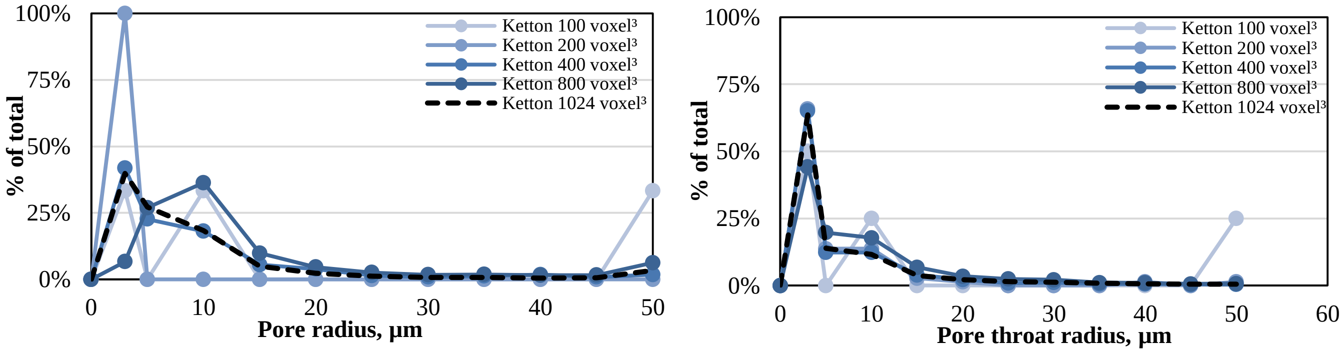

Figure 14. Pore and pore-throat radii size change with decreasing sub-volume in Ketton limestone that is scanned at ≈2.7 µm

Effect of coarsened resolution on network properties

The basis of this section is the coarsening of the original 1024 voxels^3 image into smaller sizes. This section here compares the networks of 4 out of the 10 different resolutions that were tested in the project namely 3.4, 7, 14, and 27 µm. Regardless of different rock types and characteristics, the effect of coarsening the resolution on the size of pores and throats is identical. At the first coarse resolution of 3.4 µm the majority of pores and throats are less than 5 µm in radius. The histograms lines skew to the larger sizes as the resolution coarsens creating pores and throats that are very large in size and at the same time missing pores and throats that are below the resolution limits. In all samples, the 27µm is shown as the extreme example where the histogram lines are nearly flat indicating a mix of all sizes as opposed to the finer resolution of 3.4 µm which shows more realistic distribution. These effects have direct impact on the petrophysical results, but one must bear in mind that the coarsened images source is a 1024^3 voxel image which is an excellent representation of the samples. Simulation results in the next section will show that pore connectivity is well captured in the interpolated images with a fine 1024^3 voxel base.

Due to their large grains and pores, Doddington and Ketton pore radius histogram bins were extended to 100 µm. In Ketton, about 8% of pore radii fall between 70-90 µm. These networks histograms represent only the captured porosity at 2.7µm and they will be different if the micro-porosity is accounted for. When large pore space voxel sizes are adjacent to each other without a detection of a grain between them, the scanner sees them as either all pore space or all grain depending on the several factors such as segmentation process, and grey scale thresholds. Berea and Estaillades show a modest shift toward larger pore and pore-throat sizes as the resolution coarsens because they have generally smaller pores.

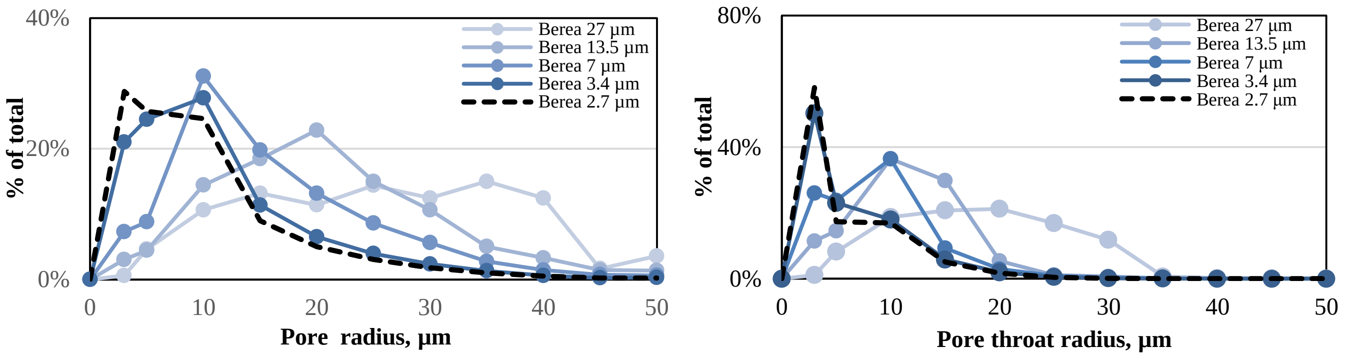

Figure 15. Pore and pore-throat radii size change with coarsening resolution in Berea sandstone.

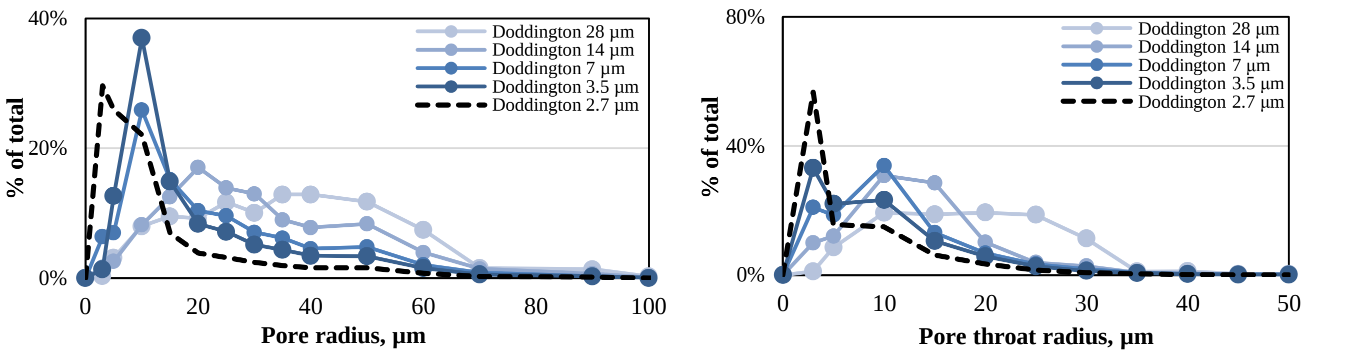

Figure 16. Pore and pore-throat radii size change with coarsening resolution in Doddington sandstone

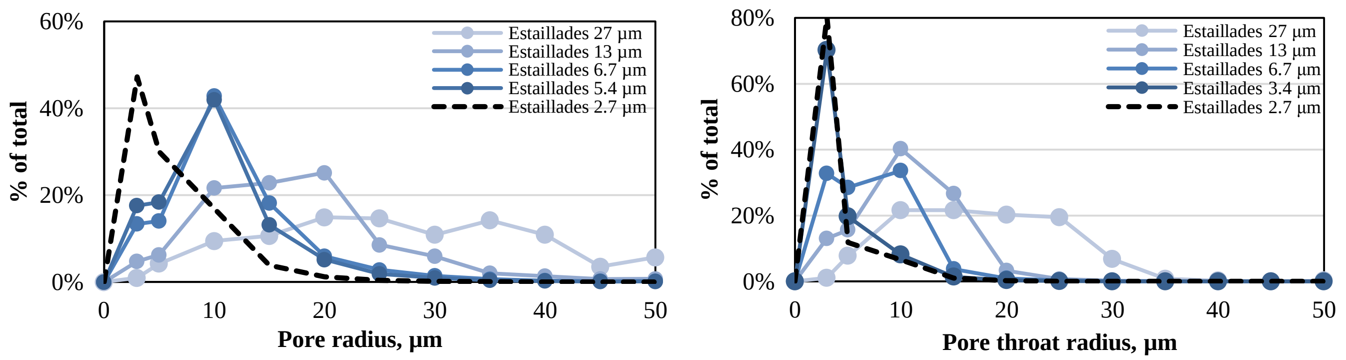

Figure 17. Pore and pore-throat radii size change with coarsening resolution in Estaillades sandstone

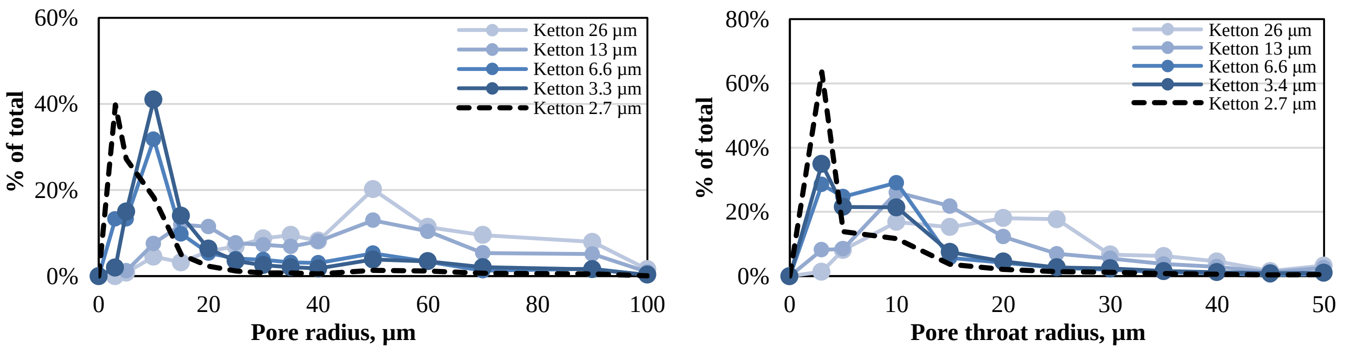

Figure 18. Pore and pore-throat radii size change with coarsening resolution in Ketton sandstone

Simulation results

A published two phase code, (Valvatne and Blunt, 2004) is used to predict the permeability, formation factor, capillary pressure and relative permeability. The input code which contains variety of parameters and constrains is included in Appendix IV. The scope of this project is to study the effects of sub-volume and resolution changes on porosity and permeability only. Porosity and absolute permeability are the most successfully predicted values in pore-scale modeling. Porosity can be directly measured from the segmented images, which matches the extracted network. On the other hand, permeability is measured by Darcy's law,

$$K_{absolute} = \frac{\mu_p q_{tsb} L}{A\,(\Phi_{inlet} - \Phi_{outlet})} \quad \ldots\ldots\ldots\ldots\ldots\ldots\ldots\ldots\ldots\ldots\ldots\ldots\ldots\ldots (1)$$

Equation 1. Absolute permeability equation where $K_{absolute}$ is absolute permeability, μ_p is single phase viscosity, q_{tsb} is total single-phase flow rate, L is the length across measured sample, A is the cross-sectional area of the model, P is the pressure, ρ_p is phase density, g is the gravitational constant and h is the height above datum. The term $(\Phi_{inlet} - \Phi_{outlet})$ refers to the potential drop across length L and area A. The potential Φ is equal to $P - \rho_p gh$. (Valvatne and Blunt, 2004).

The network extraction allows us to characterize the tested samples and understand the pore structure. Several parameters such as the number of pores, number of throats, average connection number, connections to inlet and outlet, physical isolated elements and net porosity. In addition, absolute permeability is calculated from the two-phase simulation code along with formation factor, relative permeability and capillary pressure in drainage and imbibition cycles. All these parameters are plotted in appendices V, VI, and VII for reference. The details of the capillary pressure and relative permeability predictions are explained thoroughly in (Valvatne and Blunt, 2004).

Figure 19, Figure 20, Figure 21, and Figure 22 compare the pore-scale porosity from the network and absolute permeability values to experimental results. Note that the two-phase simulation code did not run in some large sub-volumes making some figures look incomplete. This will be addressed in the following section. Simulation results are shown as rhombus points. There is only one experimental value of porosity. Both porosity and absolute permeability are plotted as straight lines.

Sub-volume study results

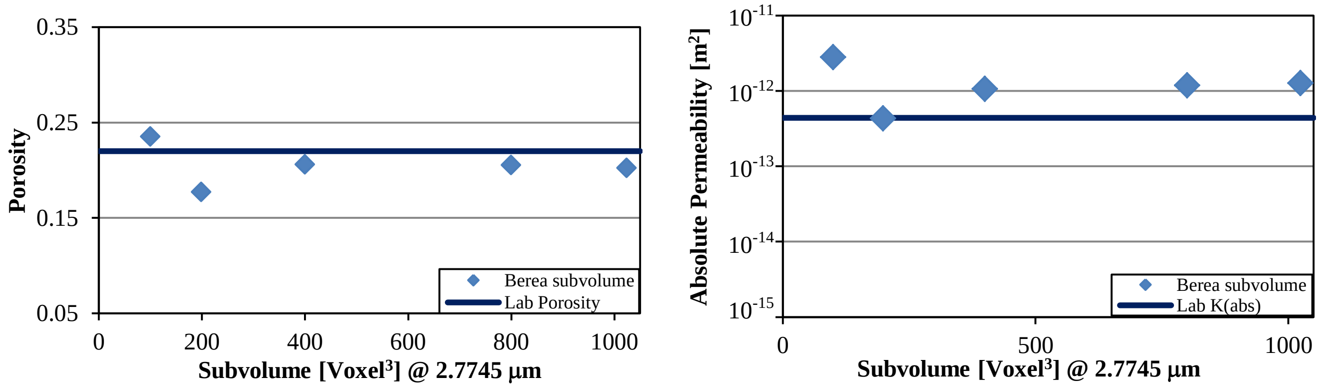

Figure 19. Porosity and absolute permeability comparison of sub-volume images of Berea sandstone.

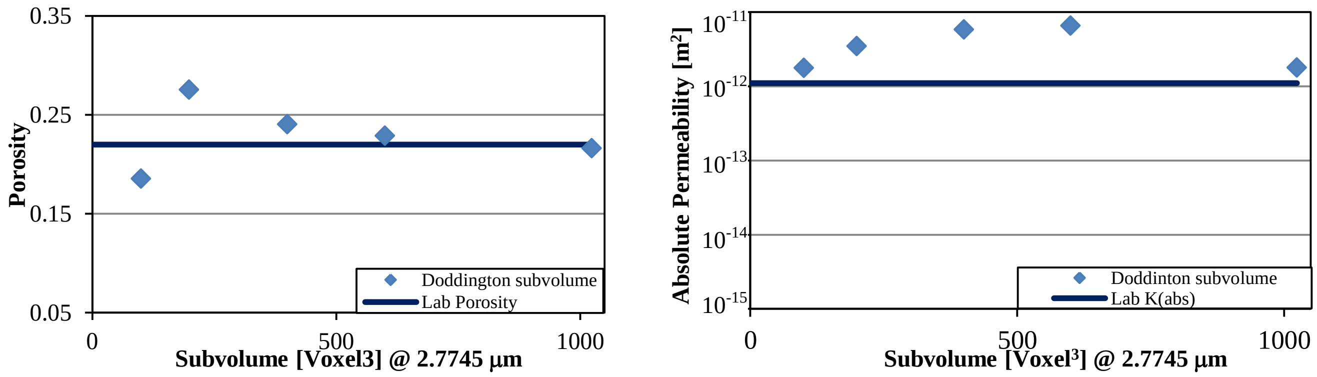

Figure 20. Porosity and absolute permeability comparison of sub-volume images of Doddington sandstone

Accurate porosity predictions in sandstones can be easily achieved at images with greater than 400 voxels^3 or 1.11 mm^3 considering scanning resolution of 2.7745µm. At images with less than 400 voxel^3, simulation values stray away from the experimental value. The majority of image features disappear when cropping the image to less than 400 voxels^3. In the sandstone case, as image size exceeds 400 voxel^3 image porosity value porosity becomes asymptotic to the experimental value. The REV includes also up to 1024 voxel^3, largest tested volume.

Permeability estimation on the other hand is different. Pore networks match permeability better in medium range permeability sandstone like the Berea. Estimation of permeability is accurate in both cases of high and medium permeability sandstone but it is more precise in medium range permeability such as Berea than in high permeability range such as Doddington. At fine resolution, large-pore rocks such as Doddington cause computational problems that will be described in the next section.

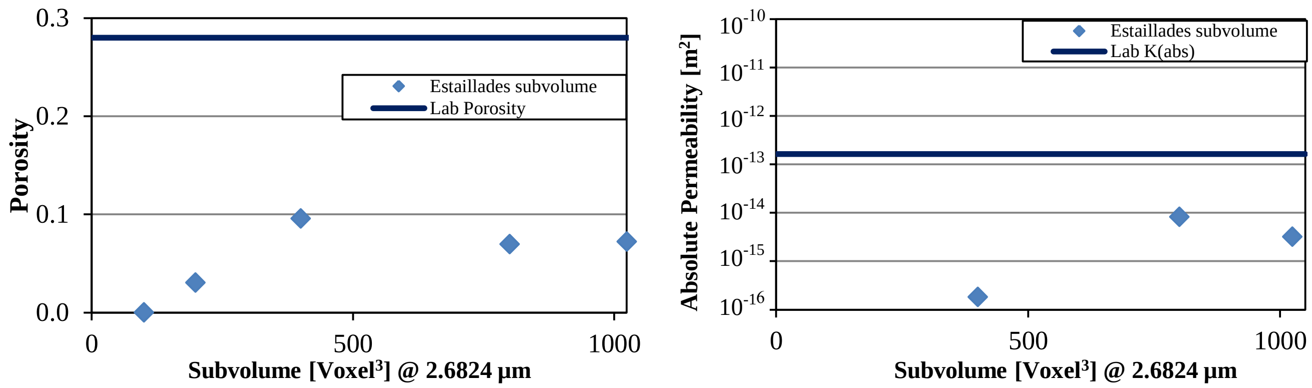

Figure 21. Porosity and absolute permeability comparison of sub-volume images of Estaillades limestone

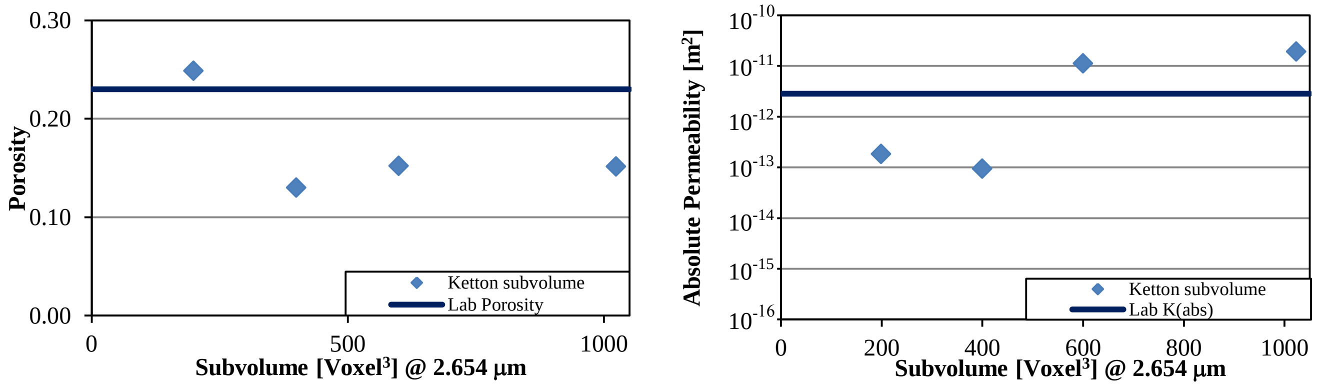

Figure 22. Porosity and absolute permeability comparison of sub-volume images of Ketton limestone

The right sub-volume in carbonate rocks is difficult to determine. In rock like Estaillades pore size distribution and pore shapes are diverse and vary greatly across the sample. Moreover, the missing micro-porosity in both Estaillades and Ketton magnifies the challenge because we simply assume it does not exist when running the simulation code. Porosity estimation of Ketton is much better than Estaillades because the significance of micro-pores is lower; this leads to better estimation of porosity as well as permeability.

In limestone, the criterion that governs the accuracy of predictions is the portion of micro to macro-pores. In Ketton, pore connectivity is dominated by macro-pores which lead to modest permeability predictions in the large samples. In contrast, micro-porosity is dominant in Estaillades which result in underestimated permeability.

Resolution study results

The main difference between sub-volume and resolution study is the fact that in sub-volume the rock sample is cropped which means that features of rock were removed. In resolution study, the considerably large 2.85 mm^3 sample [1024^3 voxels at ≈2.7 µm] is coarsened by upscaling it without removing parts of. Only by lumping detectable pores and throats at each resolution point. This is the main reason why data points in the resolution study Figure 23, Figure 24, Figure 25, and Figure 26 do not vary as much as the sub-volume data points within a sample. The study agrees with some claims by (Keehm, 2004). The author explained that the overestimation of permeability at coarser resolutions is because of the improper representation of complex pore geometry as structural complexity is lost. His generalized explanation is not true for all rock types or consistent across all resolutions. Coarse resolutions have different effects that are rock-type and resolution dependent.

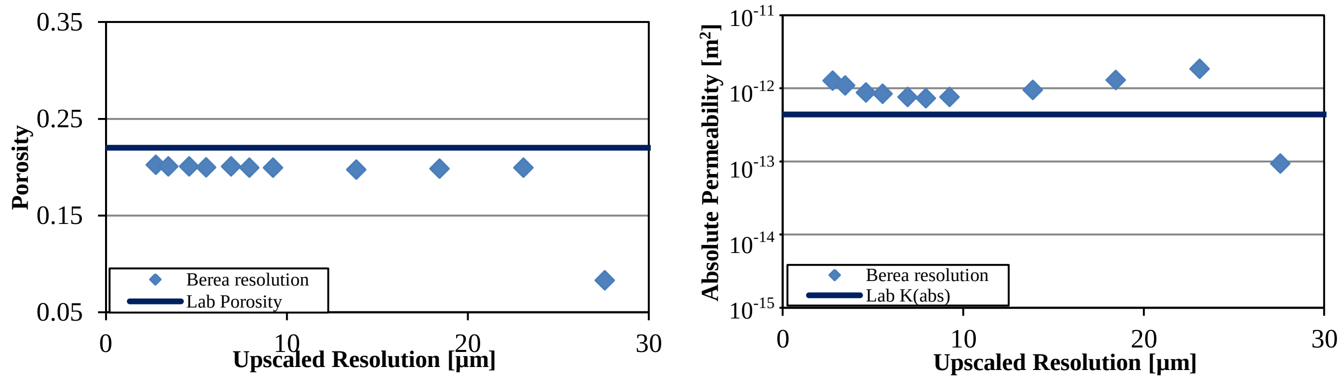

Figure 23. Porosity and absolute permeability comparison of resolution images of Berea sandstone.

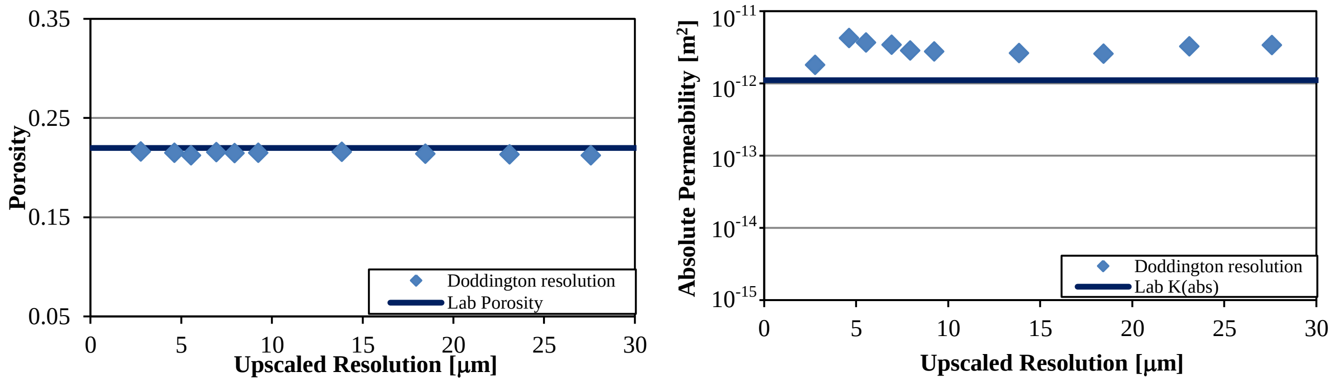

Figure 24. Porosity and absolute permeability comparison of resolution images of Doddington sandstone.

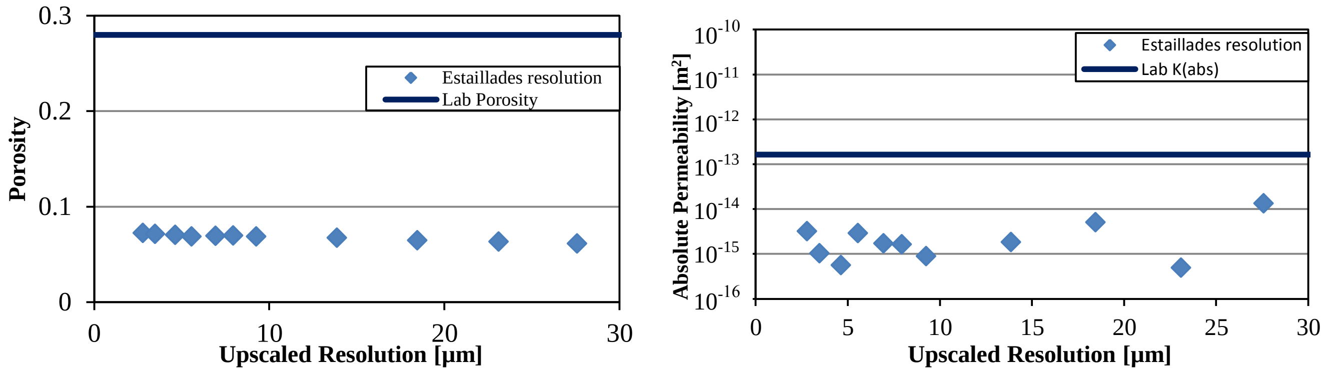

Figure 25. Porosity and absolute permeability of resolution images of Estaillades limestone

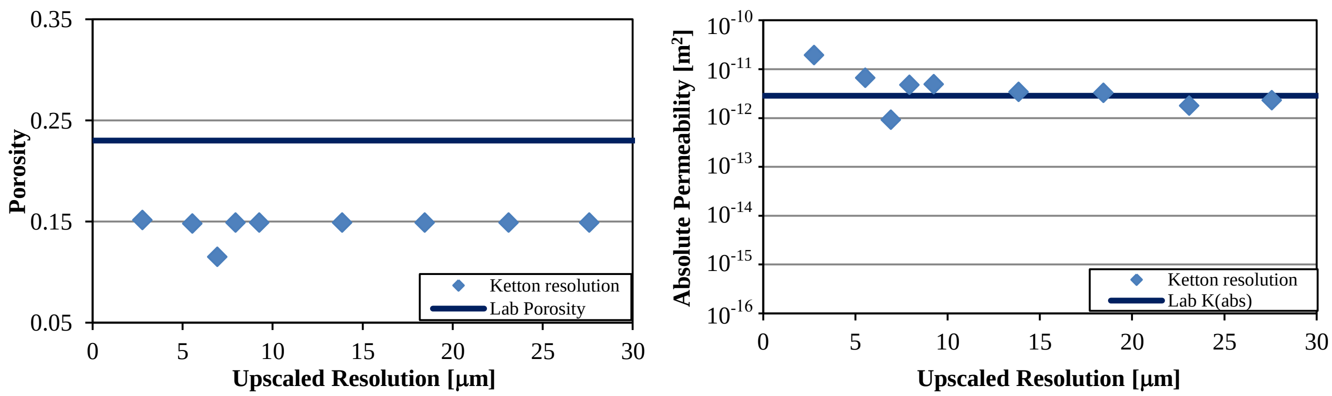

Figure 26. Porosity and absolute permeability comparison of resolution images of Ketton limestone.

In all resolution study cases, the upscaled large 1024^3 voxels image produced accurate predictions of porosity in sandstones and absolute permeability in both sandstones and Ketton limestone. All data points are close to or even matching the experimental value. One exception to this case is Estaillades for reasons explained earlier regarding the portion of undetected micro-pores. Maximum detectable porosity value of Ketton does not include the micro-pores; however, the permeability values are predicted very precisely and accurately. In sandstone, predicted porosity is almost identical to experimental value. Absolute permeability is always slightly higher than experimental values but within reasonable accuracy.

Conclusions and recommendations

Cores are the only parts of the reservoir we can measure in the lab and a good representation of the reservoir scale is required to trust the experimental results. Similarly, a µ-CT image stack out of a part of a core needs to be representative of its core and its reservoir as well. As a result, understanding the effects of different sub-volumes of µ-CT images and scan resolutions will play a major rule in simulation results.

At the network level, sandstone pore and pore throat radii histograms are homogenous at large and small sub-volumes. In limestone, reducing the sub-volume has significant effects due to increased heterogeneity at below 200 $voxel^3$ as in Estaillades, or large grain size as in Ketton. Coarsening the scan resolution systematically increases the pore and pore-throat radii by lumping pores and throats together through interpolation process. Surprisingly, the larger pores and throats did not have significant effects on the basic petrophysical properties because the connectivity characteristics were restored. The major effect was on relative permeability and capillary pressure curves (appendix V, and VI).

At 2.7 µm, Berea sample, medium permeability sandstone, shows convergence toward both porosity and permeability experimental values at sample volumes between 400 and 1024 $voxel^3$ (1.11 and 2.80 mm^3). In Doddington, high permeability sandstone, porosity estimates are better at volumes between 400-1024 $voxel^3$. However, permeability values were closer to the experimental values in very small samples between 100-200 $voxel^3$ (0.3-0.6 mm^3) and in the largest sample of 1024 $voxel^3$. Limestone behaves differently because of the presence of micro-pores. It affects all simulation results. In Estaillades and Ketton, micro pores represent 2/3 and 1/3 of total porosity respectively. It is impossible to get an REV for porosity from µ-CT images and the fact that a sub-volume segmented image porosity is close to helium porosity is merely a coincidence of including more macro-pore space in the sample. At finest resolution of 2.7 µm, the permeability of Estaillades and Ketton was close to the experimental value at 800 voxels (2.15 mm^3) and above 600 $voxel^3$ (1.6 mm^3) respectively.

In the resolution study, where the input is a larger image of 1024 $voxel^3$ at 2.7 µm (2.80 mm^3) that is interpolated to coarser resolutions, simulation shows that the inclusion of more sample volume increased the ability to model basic properties accurately. In Berea sandstone, porosity is estimated accurately at up to 23 µm whereas Doddington porosity estimate is accurate at 27 µm. Permeability on the other hand was estimated accurately at up to 18 µm in Berea and between 8-27 µm in Doddington. At resolutions finer than 8 µm in Doddington permeability was overestimated. Resolution coarsening had minor effect on permeability prediction because the overall connectivity is well captured. In carbonates such as Ketton where micro-porosity is only about 1/3 of the total porosity, an excellent match between simulation and experimental permeability value was achieved at all coarsened resolutions because the flow is dominated by macro-pores. Estaillades sample results, where 2/3 of pore space is in the micro-pores, on the contrary, poorly underestimated permeability.

There is still potential for future research to study larger samples, beyond 1024 $voxel^3$. Also, studying and comparing wide variety of rock samples will enable us to get a clear picture on sub-volume and resolution effects on network simulation. Another is comparing the sub-volume and resolution effects on different prediction methods like direct simulation on µ-CT images. In addition, the effects on multi-phase flow properties need to be studied as they are important and have impact understanding reservoir behavior. This study covered porosity and absolute permeability. Other parameters are compared against each other in appendices V, VI, and VII.

Nomenclature

K	Absolute permeability [m^2]	μ-CT	High-resolution x-ray tomography, micro–computed tomography
≈	Approximately	K_r	Oil or water relative permeability
P_c	Capillary pressure [Pa]	p.u.	Porosity units
ϕ_{Helium}	Core helium porosity.	REV	Representative elementary volume

References

Al-Ansi, N. (2012). Sandstone and carbonate rock samples scanned dry using Xradia Versa 500 μ-CT scanner. Retrieved from [http://www3.imperial.ac.uk/earthscienceandengineering/research/perm/porescalemodelling/μ-CT images and networks].

Al-Ansi, N., Gharbi, O., Qaseminejad Raeini, A., Yang, J., Iglauer, S., & Blunt, M. J. (2013). Influence of Micro-Computed Tomography Image Resolution on Petrophysical Properties. International Petroleum Technology Conference, Beijing, China, 26-28 March 2013.

Al-Raoush, & Papadopoulos. (2010). Representative elementary volume analysis of porous media using X-ray computed tomography, Powder Technology, 200(1-2), 69-77, ISSN 0032-5910.

Andrew, M., Bijeljic, B., & J. Blunt, M. (2014). Pore-scale contact angle measurements at reservoir conditions using X-ray microtomography. *Advances in Water Resources,* 68(June 2014), 24-31.

Azevedo C., & Marques E. (2010). Three-dimensional analysis of fracture, corrosion and wear surfaces. *Engineering Failure Analysis*, 17(1), 286-300, ISSN 1350-6307.

Bara, B., Mitra, S., & Vick, D. (2010). Understanding the micro structure of Berea Sandstone by the simultaneous use of micro-computed tomography (μ-CT) and focused ion beam-scanning electron microscopy (FIB-SEM). *Micron, 42*(5), 412-418.

Bear, J. (1972). *Dynamics of fluids in porous media*. New York, NY, USA: Dover.

Bejeljic, B., Mostaghimi, P., & Blunt, M. J. (2013). Insights into non-Fickian solute transport in carbonates. *Water Resources Research, 49*(5), 2714-2728.

Berea Sandstone™ Petroleum Cores. (2014). Website: [www.bereasandstonecores.com].

Blunt, M. J., Bijeljic, B., Dong, H., Gharbi, O., Iglauer, S., Mostaghimi, P., Paluszny, A., & Pentland, C. (2012). Pore-scale imaging and modelling. *Advances in Water Resources*, Volume 51, January 2013, 197-216, ISSN 0309-1708.

Blunt, Martin J. (2009). *Two hundred barrels left: An analysis of population growth, oil reserves and carbon dioxide emissions*. London, United Kingdom: Imperial College London.

Cnudde, V., & Boone, M.N. (2013). High-resolution X-ray computed tomography in geosciences: A review of the current technology and applications, *Earth-Science Reviews*, 123(August 2013), 1-17, ISSN 0012-8252.

Dong, H., & Blunt, M. (2009). Pore-network extraction from micro-computerized-tomography images. *Physical Review E*, 80(3), 036307-11.

Gland, N., Dautriat, J., Vizika, O., & Dimanov, A. (2009). Stress path dependent hydromechanical properties of carbonates: Impact of heterogeneities and use of effective medium theory for critical state scaling. *IPTC*-13756.

Judd, Kenneth L. (1998). *Numerical Methods in Economics*. Page 225. MIT Press. ISBN 978-0-262-10071-7.

Kanit, T., Forest, S., Galliet, I., Mounoury, V., & Jeulin, D. (2003). Determination of the size of the representative volume element for random composites: statistical and numerical approach, *International Journal of Solids and Structures*, 40(13-14), 3647-3679, ISSN 0020-7683.

Keehm, Y., & Mukerji, T. (2004). Permeability And Relative Permeability From Digital Rocks: Issues On Grid Resolution And Representative Elementary Volume. Society of Exploration Geophysicists.

Li, J.H., & Zhang, L.M. (2010). Geometric parameters and REV of a crack network in soil, *Computers and Geotechnics*, 37(4), 466-475, ISSN 0266-352X.

Mittal, R., & Arora, G. (2010). Quintic B-spline collocation method for numerical solution of the Kuramoto–Sivashinsky equation. *Commun Nonlinear Sci Numer Simulat*, *15*(10), 2798-2808, ISSN 1007-5704.

Salmi, M., Auslender, F., Bornert, M., Fogli, M. (2012). Various estimates of Representative Volume Element sizes based on a statistical analysis of the apparent behaviour of random linear composites, *Comptes Rendus Mécanique*, 340(4-5), 230-246, ISSN 1631-0721.

Mostaghimi P, Blunt MJ, Bijeljic B. (2013). Computations of Absolute Permeability on μ-CT Images, *Mathematical Geosciences,* 45(1), 103-125. ISSN: 1874-8961.

O'Donnell, T. K., Goyne, K., Randall, W., Miles, J., Baffaut, C., Anderson, S. H., Sudduth, K. (2010). Determination of representative elementary areas for soil redoximorphic features identified by digital image processing, *Geoderma*, 161(3-4), 138-146, ISSN 0016-7061.

OPEC. (2013). Chapter 1: Wold oil trends: Overview of the reference case. *2013 World Oil Outlook* (ISBN 978-3-9502722-6-0, pp. 26-69). Vienna, Austria: Organization of Petroleum Exporting Countries Secretariat.

Otsu, N. (1979). A Threshold Selection Method from Grey-Level Histograms. *IEEE Transactions on Systems, Man, and Cyberneteics, 9*(1), 69-66.

Peng, Hu, Dultz, and Zhang. (2012). Using X-ray computed tomography in pore structure characterization for a Berea sandstone: Resolution effect, *Journal of Hydrology*, 472–473, Pages 254-261, ISSN: 0022-1694.

Pepper, J., Witt, Jr., W., & Demarest, D. (1954). Geology of the Bedford Shale and Berea Sandstone in the Appalachian Basin. United States Geological Survey Paper 259: United States Government Printing Office, Washington, DC, USA.

Renard, F., Bernard, D., Desrues, J., & Ougier-Simonin, A. (2006). Characterisation of hydraulic fractures in limestone using X-ray microtomography. *2006 GeoX Conference.*

Schoenberg, Contributions to the problem of approximation of equidistant data by analytic functions. (1946). *Quart. Appl. Math*., 4, pp. 45–99 and 112–141.

Tanino, Y., & Blunt, M. (2012). Capillary trapping in sandstones and carbonates: Dependence on pore structure. *Water Resources Research, 48*(8).

Valvatne, P. (2004). *Predictive pore-scale modelling of multiphase flow*. PhD thesis. London, United Kingdom: Imperial College London.

Valvatne, P. H., and M. J. Blunt (2004), Predictive pore-scale modelling of two-phase flow in mixed wet media, *Water Resources Research*, 40(7).

Varslot, T., Kingston, A., Latham, S., Middleton, J., Knackstedt, M., & Sheppard, A. (2011). Combining High-Fidelity Helical Micro-Tomography with region-of-interest scanning for improved core characterisation. *Society of Core Analysts (2011-26)*.

Vik B., Bastesen E., Skauge A. (2013). Evaluation of representative elementary volume for a vuggy carbonate rock—Part: Porosity, permeability, and dispersivity, *Journal of Petroleum Science and Engineering*, 112(December 2013), 36-47, ISSN 0920-4105.

Wang, M, Kulatilake, P. Um, W, Narvaiz, J. (2002). Estimation of REV size and three-dimensional hydraulic conductivity tensor for a fractured rock mass through a single well packer test and discrete fracture fluid flow modelling, *International Journal of Rock Mechanics and Mining Sciences*, 39(7), 887-904, ISSN 1365-1609.

Yu, Y. (2013). *Pore Volume Measurement. An experimental method to measure porosity from cuttings: Evaluation and error analysis*. MSc thesis. Lubbock, TX, USA: Texas Tech University.

Appendix-I: Literature Review

#	Paper	Year	Title	Authors	Contribution
1	International Journal of Rock Mechanics & Mining Sciences 39 (2002) 887–904	2002	**Estimation of REV size and three-dimensional hydraulic conductivity tensor for a fractured rock mass through a single well packer test and discrete fracture fluid flow modelling**	Wang, Kulatilake, Um, and Narvaiz	A new methodology to determine REV and 3D hydraulic conductivity tensor for a fractured rock mass.
2	International Journal of Solids and Structures 40 (2003) 3647–3679	2003	**Determination of the size of the RVE for random composites: statistical and numerical approach**	Kanit, Forest, Galliet, Mounoury, Jeulin	propose and illustrate a more quantitative definition of the RVE, which is based on statistical arguments.
3	Wat. Resources Research 10.1029/2004	2004	**Predictive pore-scale modelling of two-phase flow in mixed wet media**	Per H. Valvatne, Martin J. Blunt	Demonstrate that easily acquired data can be used to predict hard to measure flow properties.
4	SEG Int'l Exposition and 74th Annual Meeting	2004	**Permeability and Relative Permeability from Digital Rocks: Issues on Grid Resolution and Representative Elementary Volume**	Youngseuk Keehm and Tapan Mukerji	Found an REV for absolute and relative permeability with Lattice-Boltzmann fluid simulations.
5	Physical Review E 80, 036307	2009	**Pore-network extraction from micro-computerized-tomography image**	Hu Dong and Martin Blunt	Build on the work already done by Silin and Patzek, (Physica A 371,336 2006) with good correlation to most rock types.
6	Powder Technology 200 (2010) 69–77	2010	**Representative elementary volume analysis of porous media using X-ray computed tomography**	Al-Raoush, Papadopoulos	The author suggest that the REV of porosity cannot be considered as REV for other parameters [detailed study].
7	Computers and Geotechnics 37 (2010) 466–475	2010	**Geometric parameters and REV of a crack network in soil**	Li and Zhang	A well-structured paper on finding REV on cracked soil with high focus on statistical methods.
8	Geoderma 161 (2011) 138–146	2010	**Determination of representative elementary areas for soil redoximorphic features identified by digital image processing**	O'Donnel, Goyne, Miles, Baffaut, et al	The author's methodology identified an REA of two distinctive features and his findings will standardize and optimize the way of soil testing required by the government.
9	SCA 2011-26	2011	**Combining High-Fidelity Helical Micro-Tomography with region-of-interest scanning for improved core characterisation**	Varslot, Kingston, Latham, et al.	The method greatly enhances the ability to characterize difficult-to-work-with cores or highly uncertain analysis.
10	Mathematical Geosciences. 45(1), 103-125	2012	**Computations of Absolute Permeability on μ-CT Images**	Mostaghimi, Blunt, Bijeljic.	Compares different methods to calculate absolute permeability. Also, studies the existence and magnitude of REV for different rock types.
11	Journal of Hydrology; 472-473 (2012) 254-261	2012	**Using X-ray computed tomography in pore structure characterization for a Berea sandstone: Resolution effect**	Peng, Hu, Dultz, Zhang	Obtained REV of 2.8 mm for large-pore porosity/large-pore connectivity form MCT study.

12	Advances in water resources 51 (2013) 197-216	2012	**Pore-scale imaging and modelling**	Blunt, Bijeljic, Dong, Gharbi, Iglauer, et. al.	Provides a thorough overview of pore-scale imaging and modelling including limitations are areas of future research.
13	C. R. Mecanique 340 (2012) 230–246	2012	**Various estimates of Representative Volume Element sizes based on a statistical analysis of the apparent behavior of random linear composites**	Salmi, Auslender, Bornert, Fogli	Excellent approach to the problem. Statistical approach to the no RVE. Otherwise, very similar to other papers.
14	Earth Science Reviews 123 (2013)	2013	**High-resolution x-ray computed tomography in geoscience: A review of current technology and application**	V. Cnudde, M N Boone	Limited contribution but it is a great overview of high resolution x-ray technology.
15	IPTC 16600	2013	**Influence of Micro-Computed Tomography Image Resolution on the Predictions of Petrophysical Properties**	Al-Ansi, Gharbi, Raeini, Yang, Iglauer, and Blunt	Various effects of high and low resolution have been successfully identified and correlated.
16	Journal of Petroleum Science and Engineering 112 (2013) 36–47	2013	**Evaluation of representative elementary volume for a vuggy carbonate rock-part: Porosity, permeability, and dispersivity**	Vik n, Bastesen, Skaug	Experimental study that investigates the variation of porosity-permeability ratio with sample size to determine REV.

Source	International Journal of Rock Mechanics & Mining Sciences 39 (2002) 887–904
Year	2002
Title	**Estimation of REV size and three-dimensional hydraulic conductivity tensor for a fractured rock mass through a single well packer test and discrete fracture fluid flow modelling**
Authors	Wang, Kulatilake, Um, and Narvaiz
Contribution	A new methodology to determine REV and 3D hydraulic conductivity tensor for a fractured rock mass.
Objective	determine the representative elementary volume (REV) size and three-dimensional (3-D) hydraulic conductivity tensor for a fractured rock mass
Methodology	3-D stochastic fracture network model is built and compared to rock mass. Then the data is compared to borehole to generate a stochastic-deterministic fracture network system in a cubic block. Then packer tests are simulated numerically applying a developed discrete fracture fluid flow model. By studying directional hydraulic conductivity behaviour of different cubic block sizes, an REV for hydraulic behaviour was estimated
Conclusion	A cubic block of size 18 meters with packer test interval of length 6.5m located at the centre of the block is found to be representative. Packer tests were numerically simulated using the block size of 18 meters and average flow rate per unit hydraulic gradient. When a relationship was developed between flow rate per unit gradients of fractures that intersect the borehole and with those which do not, and by studying directional hydraulic conductivity behaviour of different cubic sizes, REV of hydraulic behaviour of the rock mass was determined to be a block size of 15m.
Comment	Although the paper deals with finding the REV of hydraulic conductivity tensors which is not directly related to my area of research, the methodology and structure is very helpful.

Source	International Journal of Solids and Structures 40 (2003) 3647–3679
Year	2003
Title	**Determination of the size of the RVE for random composites: statistical and numerical approach**
Authors	Kanit, Forest, Galliet, Mounoury, Jeulin
Contribution	propose and illustrate a more quantitative definition of the RVE, which is based on statistical
Objective	arguments
Methodology	The RVE must ensure a given accuracy of the estimated property obtained by spatial averaging of the stress, the strain, or the energy fields in a given domain. Alternatively, the use of smaller volumes must be compensated by averaging over several realizations of the microstructure to get the same accuracy, provided no bias is introduced in the estimation by some edge effects generated by the boundary conditions
Conclusion	The author suggests that linear effective properties can be found by using mean values of apparent properties of small volumes because simulations on large volumes are prohibitive.
Comment	This paper discusses mechanical properties such as elasticity and heat transfer. It does not discuss oil field properties. However, its method sheds the light and suggests different approach.

Source	Water Resources Research doi: 10.1029/2003WR002627, 2004
Year	2004
Title	**Predictive pore-scale modelling of two-phase flow in mixed wet media**
Authors	Per H. Valvatne, Martin J. Blunt
Contribution	Easily acquired data can be used to predict hard to measure flow properties
Objective	Predict flow properties for a variety of porous media using pore-scale modelling with geologically realistic networks
Methodology	1. Network representation of sandstone. 2. Adjust pore size distribution to match capillary pressure. 3. Predict single and multiphase relative permeability
Conclusion	Reliable prediction of relative permeability with wettability changes and different pore structures.
Comment	• This paper discusses in details how fluid is moved in the pore space with respect to contact angles, wettability, capillary pressure, and transport properties. • Steady state relative permeability as benchmark • Wettability effects on experimental data

Source	SEG Int'l Exposition and 74th Annual Meeting
Year	2004
Title	**Permeability and Relative Permeability from Digital Rocks: Issues on Grid Resolution and Representative Elementary Volume**
Authors	Youngseuk Keehm and Tapan Mukerji
Contribution	Found an REV for absolution and relative permeability with Lattice-Boltzmann fluid simulations
Objective	Find an REV values for both absolution and relative permeability
Methodology	Examine the results of different Lattice-Boltzmann fluid simulations of two rocks that are random-dense sphere packing and digital Fontainebleau sandstone. Perform single and two-phase flow simulations on these digital rocks with different grid spacing
Conclusion	For absolute permeability: REV is d<=a/10 For relative permeability: REV is L>=20a - a is the length scale - d is the grid spacing
Comment	Consider the length scale of pore geometry such as (mean grain size, mean pore size, hydraulic radius, etc.) to have more meaningful REV

Source	Physical Review E 80, 036307
Year	2009
Title	**Pore-network extraction from micro-computerized-tomography image**
Authors	Hu Dong and Martin Blunt
Contribution	Build on the work already done by Silin and Patzek, (Physica A 371,336 2006) with good correlation to most rock types.
Objective	Extract simplified networks of pores and throats with parameterized geometry and interconnectivity from images of pore space.
Methodology	The parameters of the pore networks, such as coordination number, and pore and throat size distribution are computed and compared to other methods, experimental data and direct computation of permeability and formation factor.
Conclusion	Good agreement is reached in most cases allowing networks derived from a wide variety of rock types to be used for predictive modelling.
Comment	This paper examines different methodologies to extract pore networks and identifies their strengths and weaknesses. Two step searching algorithm to define a void ball then clustering process to define pores and throats.

Source	Powder Technology 200 (2010) 69–77
Year	2010
Title	**Representative elementary volume analysis of porous media using X-ray computed tomography**
Authors	Al-Raoush, Papadopoulos
Contribution	The author suggest that the REV of porosity cannot be considered as REV for other parameters [detailed study]
Objective	Investigate whether the use of a REV for porosity can be used as an REV for other parameters
Methodology	Utilize 3D algorithms to determine the REV of particle size distribution, local void ratio, and coordination number.
Conclusion	Local void ratio REV is much smaller than the REV of particle size distribution and coordination number. Also, they stressed that REV of porosity should not be considered as an REV of other properties.
Comment	Excellent graphical representations of findings

Source	Computers and Geotechnics 37 (2010) 466–475
Year	2010
Title	**Geometric parameters and REV of a crack network in soil**
Authors	Li and Zhang
Contribution	A well-structured paper on finding REV on cracked soil with high focus on statistical methods.
Objective	investigate the crack patterns and probability distributions of the geometric parameters of cracks and to determine the representative elementary volume (REV) of the crack network
Methodology	First, characterize geometric properties of desiccation crack using digital imaging method. Then study the pattern of the crack in two dimensions and obtain statistical data and probability distribution of crack properties. Finally, an REV is determined to satisfy the equivalent continuum assumption.
Conclusion	The REV size was found [statistically] to be approximately five times mean crack length.
Comment	The authors do not consider 3D properties of the cracks because they say it is difficult to quantify in-situ. He assigns different probability distributions to each property of the crack network.

Source	Geoderma 161 (2011) 138–146
Year	2010
Title	**Determination of representative elementary areas for soil redoximorphic features identified by digital image processing**
Authors	O'Donnel, Goyne, Miles, Baffaut, Anderson, Sugguth
Contribution	The author's methodology identified an REA of two distinctive features and his findings will standardize and optimize the way of soil testing required by the government.
Objective	Define and determine a representative elementary area for features that are present in the claypan soils of north eastern Missouri, USA.
Methodology	Use high quality digital cameras and image classification techniques. Three metrics were chosen to quantify heterogeneity, including percent occurrence, mean Euclidean distance and interspersion index. 16 different image sizes were tested to identify REA.
Conclusion	The study identified an area of 17.7 cm^2 as representative of the low chroma and 25.4 cm^2 of the high chroma features.

Source	Mathematical Geosciences; 45(1) pp 103-125
Year	2012
Title	Computations of Absolute Permeability on µ-CT Images
Authors	Mostaghimi, P., Blunt, M. J., and Bijeljic, B.
Contribution	Compares different methods to calculate absolute permeability. Also, studies the existence and magnitude of REV for different rock types.
Objective	Obtain an accurate absolute permeability calculation from different methods for consolidated and unconsolidated porous rocks.
Methodology	The authors solve for Stokes flow directly on binarized 3D images by imposing no-flow conditions exactly at the solid boundaries and then using algebraic multi-grid to solve the produced linear equations. Also, the results are compared with other methods such as lattice Boltzmann and the Kozeny-Carman equation. Experimental values were the benchmark of all methods.
Conclusion	1. In more heterogeneous rocks, the Kozeny—Carman equation overestimates permeability by a factor of 10. 2. Porosity's REV is a lot smaller than the REV of other properties such as absolute permeability. Larger REV is required to account for tortuosity and connectedness of the flow path. 3. REV of carbonate samples appears to be larger than the image itself. 4. Permeability of sandpacks varies by less than 10% in different directions, 25% for sandstones, and 50% in carbonates. This indicates that pore connectivity is not identical in all directions.

Source	C. R. Mecanique 340 (2012) 230–246
Year	2012
Title	**Various estimates of Representative Volume Element sizes based on a statistical analysis of the apparent behavior of random linear composites**
Authors	Salmi, Auslender, Bornert, Fogli
Contribution	Excellent approach to the problem. Statistical approach to the no RVE. Otherwise, very similar to other papers
Objective	Propose various estimates of the size of the Representative Volume Element (RVE) of random linear elastic matrix-inclusion composites
Methodology	Derives estimated RVE from the computation of the apparent behaviour of finite size volume elements.
Conclusion	The paper suggests three proposals for size of RVE:# 1. Determine a computational RVE size by a rigorous probabilistic interpretation. 2. Determine the size of RVE based on fluctuations of apparent properties through a coefficient of variation of apparent behaviours. 3. By substituting a heterogeneous material by a homogeneous equivalent in structure calculations. When there is no RVE examine when the pdfs converge toward Gaussian distribution as the variance of RVE is larger than the variance of pdf.
Comment	This paper contains very high level of math and statistical methods.

Source	Earth Science Reviews 123 (2013)
Year	2013
Title	**High-resolution x-ray computed tomography in geoscience: A review of current technology and application**
Authors	V. Cnudde, M N Boone
Contribution	Limited to the research but it gives an excellent overview of technology and applications
Objective	Review of the principle, advantages and limitations of x-ray CT itself are presented as well as its applications in geoscience.
Comment	Excellent background reading to better understand x-ray images and work with them.

Source	IPTC 16600
Year	2013
Title	**Influence of Micro-Computed Tomography Image Resolution on the Predictions of Petrophysical Properties**
Authors	Nayef Al-Ansi, Oussama Gharbi, Ali Qaseminejad Raeini, Jainhui Yang, Stefan Iglauer, and Martin Blunt
Contribution	Various effects of high and low resolution have been successfully identified
Objective	Study the effect of resolution on predicted static, dynamic and network properties
Methodology	Using experimental data as benchmark to assess the results of each voxel size.
Conclusion	1. Current extraction techniques do not appear to produce a unique network 2. Higher resolution reveals more pores and throats 3. The average throat radius is close to the image resolution (6 µm is not sufficient, even though permeability is showing good match on this low resolution) 4. Low permeability sands require larger images and higher resolution 5. 5-10 µm is sufficient for high permeability sands.
Comment	The paper suggests that resolution effect on multiphase flow properties need also a similar study.

Source	Journal of Petroleum Science and Engineering 112 (2013) 36–47
Year	2013
Title	**Evaluation of representative elementary volume for a vuggy carbonate rock-part: Porosity, permeability, and dispersivity**
Authors	Vik n, Bastesen, Skauge
Contribution	Experimental study that investigates the variation of porosity-permeability ratio with sample size.
Objective	Examine the heterogeneities and their effects on porosity, permeability and dispersivity
Methodology	In this study the authors take rocks from outcrops and cut them into various sizes to determine REV.
Conclusion	Properties show decreased variability with increasing sample size. Also, the mean values for small sample sizes are in good agreement with large rocks. It is suggested that arithmetic average would be the best in upscaling the permeability. Porosity values show the lowest variation.
Comment	Includes a literature survey of previous REV articles. Also, this study is fully experimental with no simulation of pore-network.

Appendix-II: Additional Images and 3D Reconstructions, Sub-Volume Study

This appendix visualizes the subject rock samples in the 2D and 3D space by showing multiple segmented images in 2D and the constructed 3D image for the sub-volume study. The sub-volume images shown below are the same as describe in the main body of the report.

Berea [1024 voxel^3 @ 2.7745 μm]

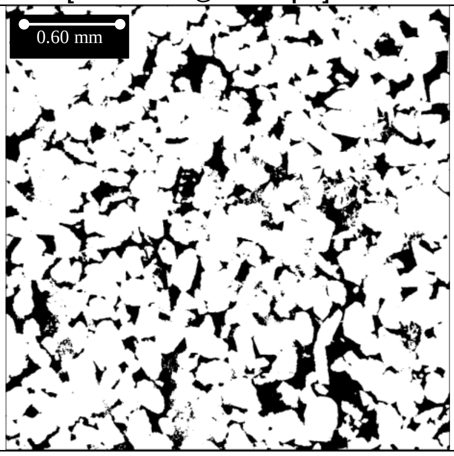	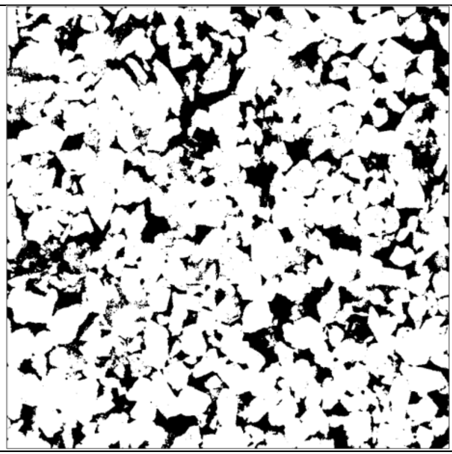	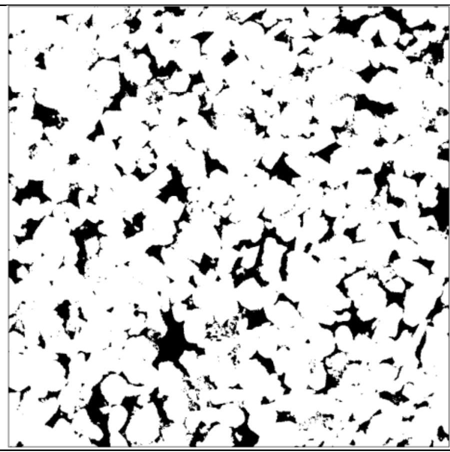
Image# 1	Image# 256	Image# 512
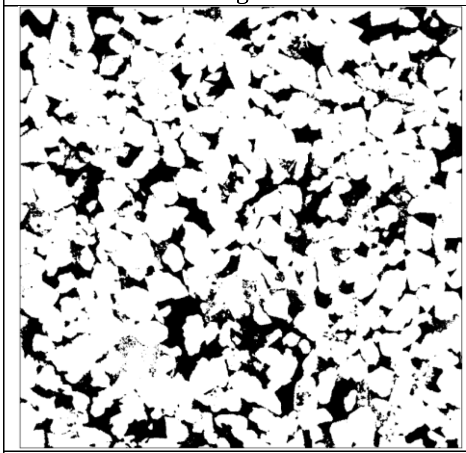	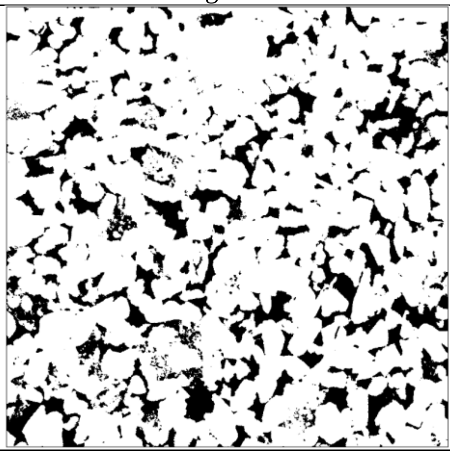	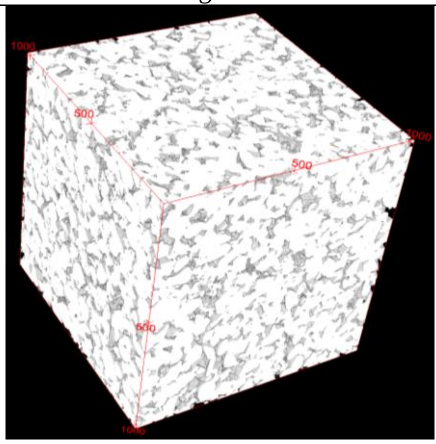
Image# 768	Image# 1024	3D image stack

Berea [800 voxel^3 @ 2.7745 μm]

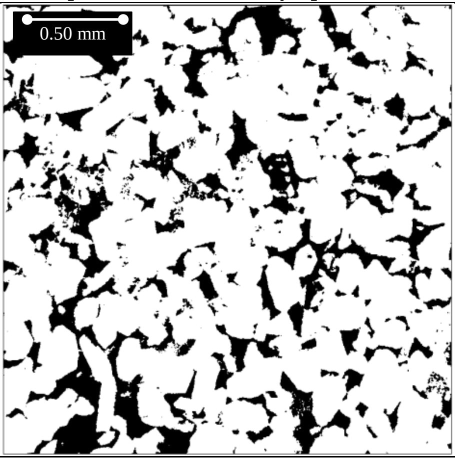	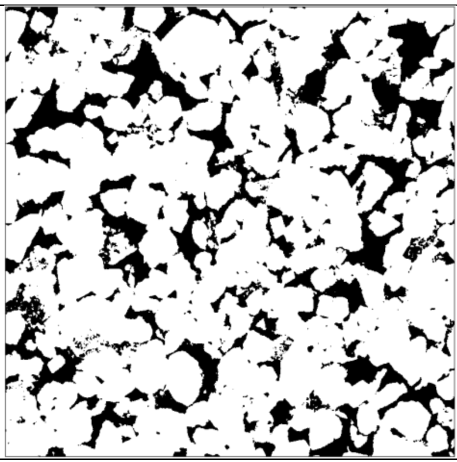	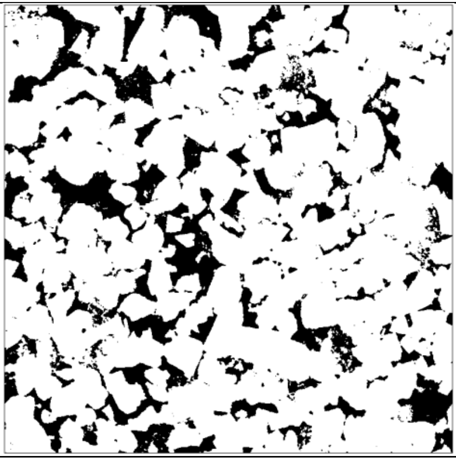
Image# 1	Image# 200	Image# 400
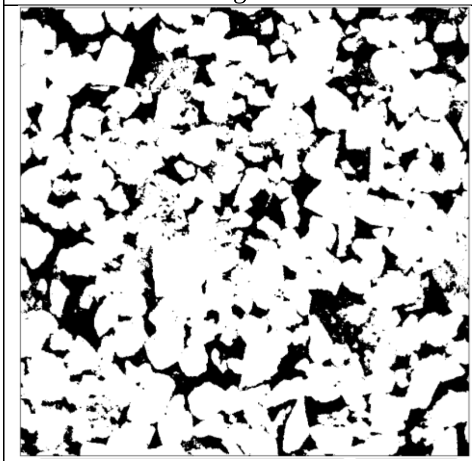	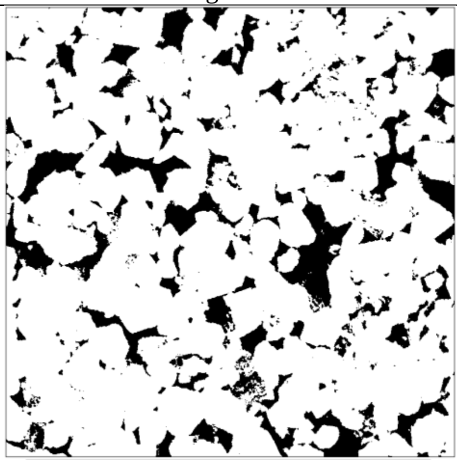	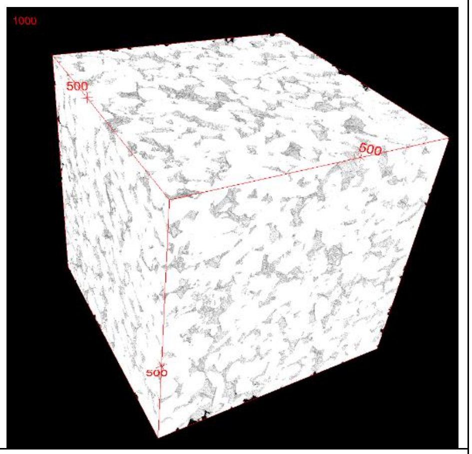
Image# 600	Image# 800	3D image stack

Berea [400 voxel^3 @ 2.7745 μm]

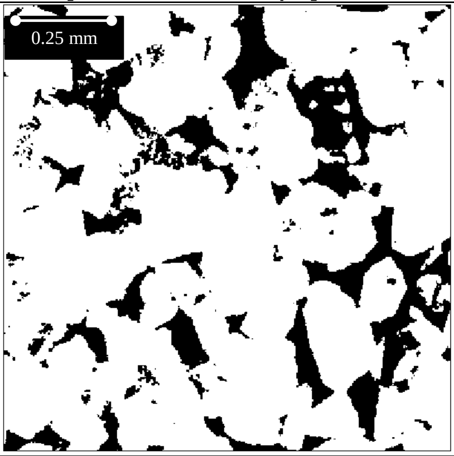

Image# 1

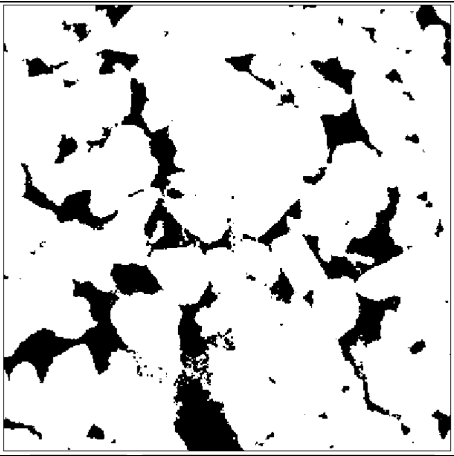

Image# 100

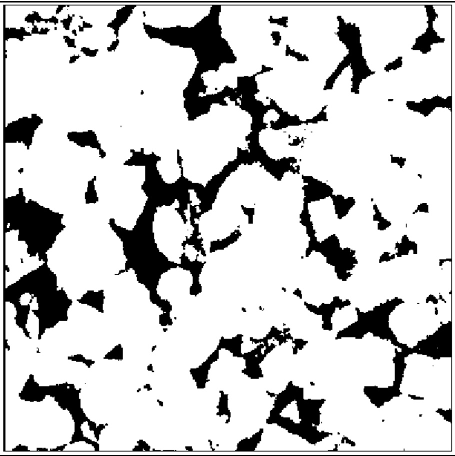

Image# 200

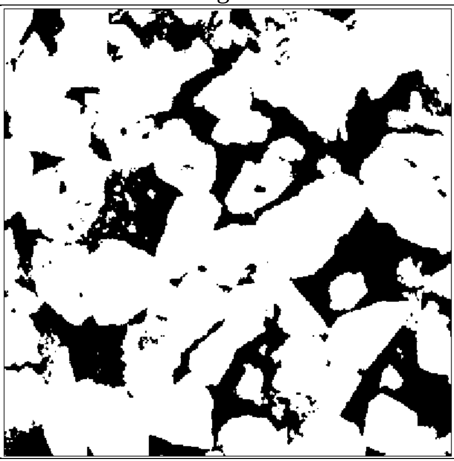

Image# 300

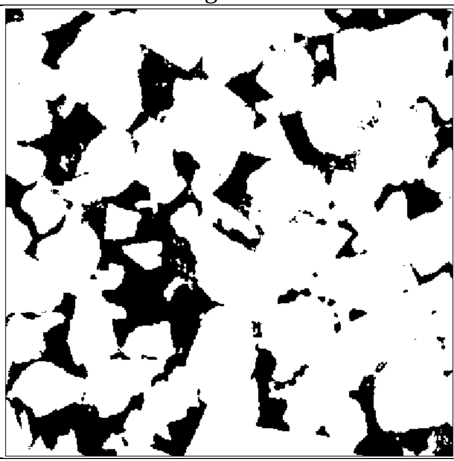

Image# 400

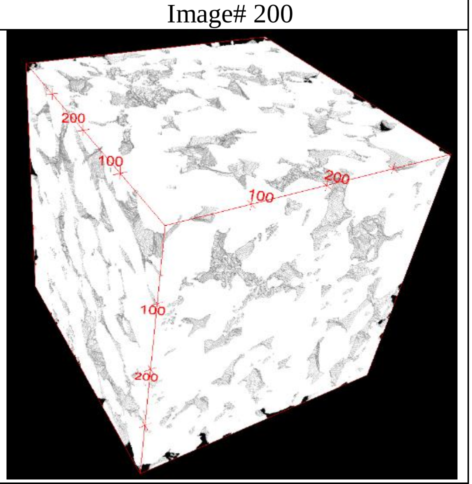

3D image stack

Berea [200 voxel^3 @ 2.7745 µm]

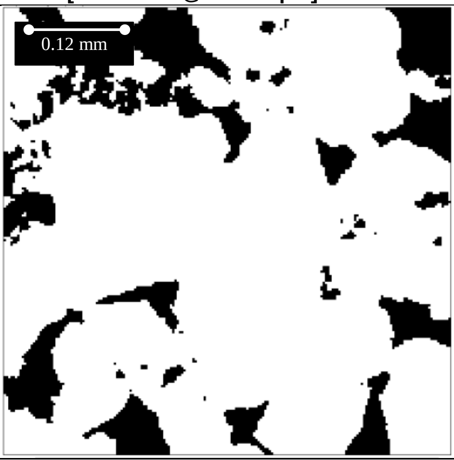		
Image# 1	Image# 50	Image# 100
	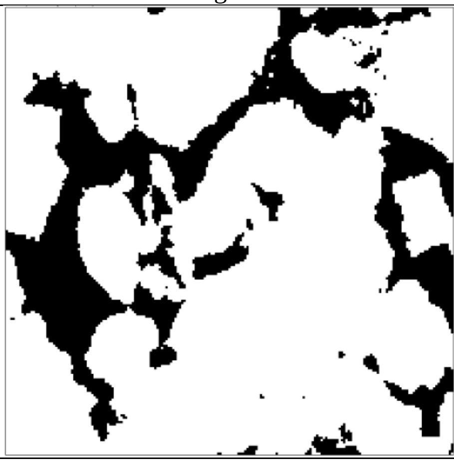	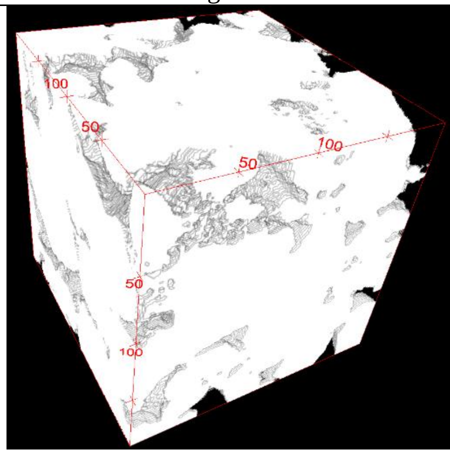
Image# 150	Image# 200	3D image stack

Berea [100 voxel^3 @ 2.7745 μm]

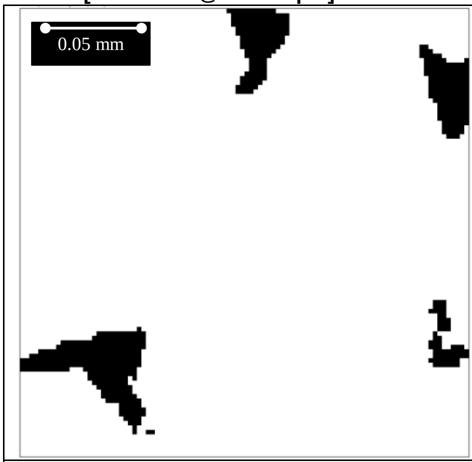

Image# 1

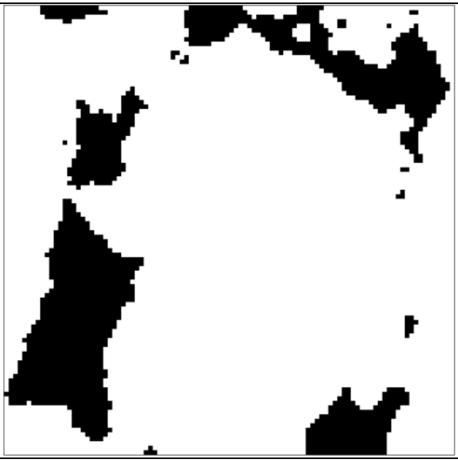
Image# 25

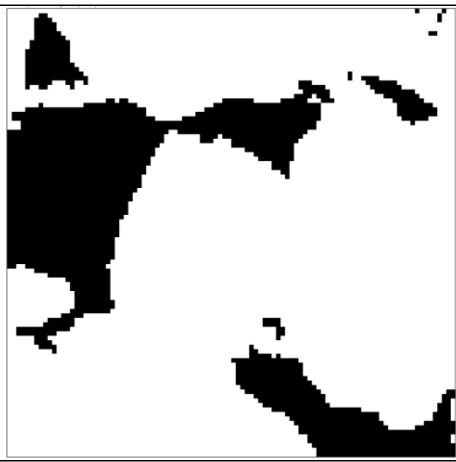
Image# 50

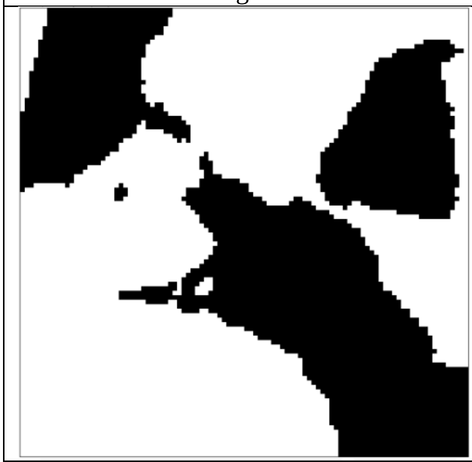
Image# 75

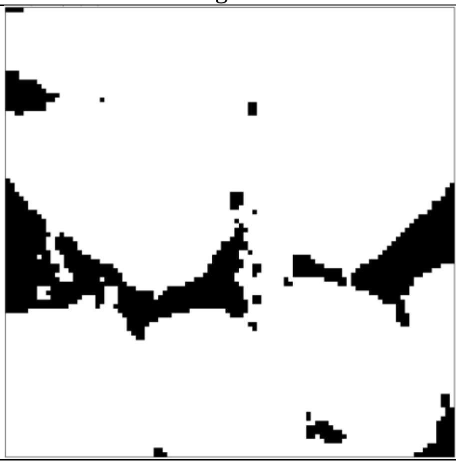
Image# 100

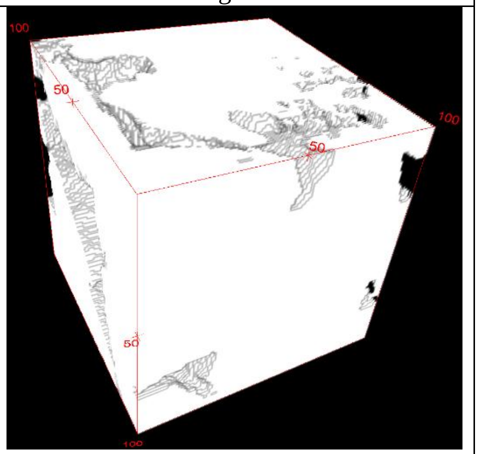

3D image stack

Doddington [1024 voxel^3 @ 2.7745 µm]

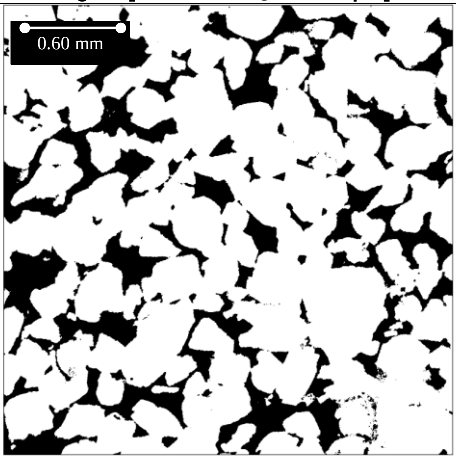	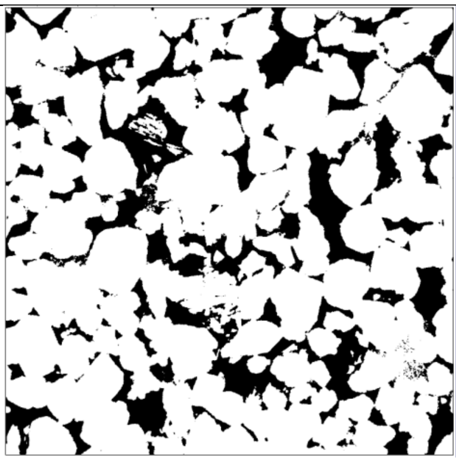	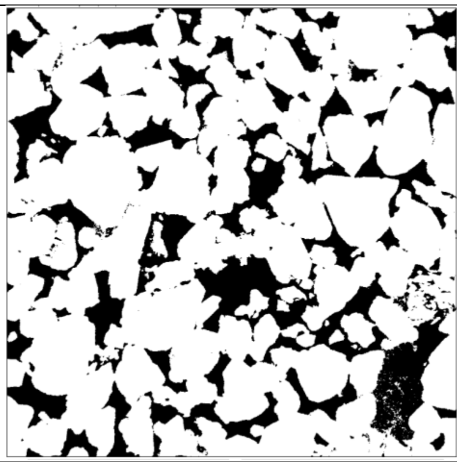
Image# 1	Image# 256	Image# 512
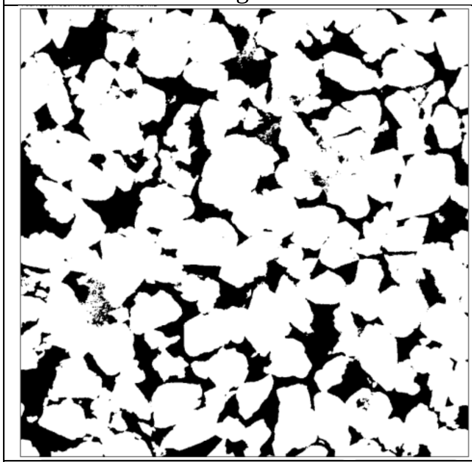	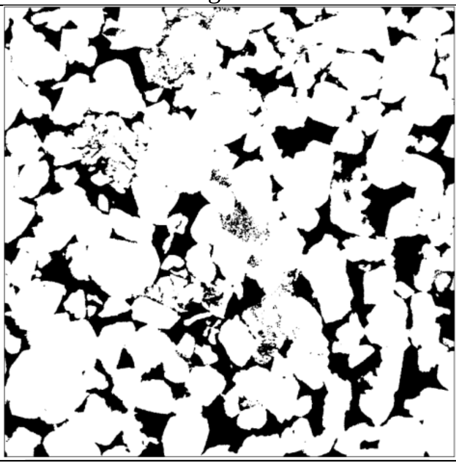	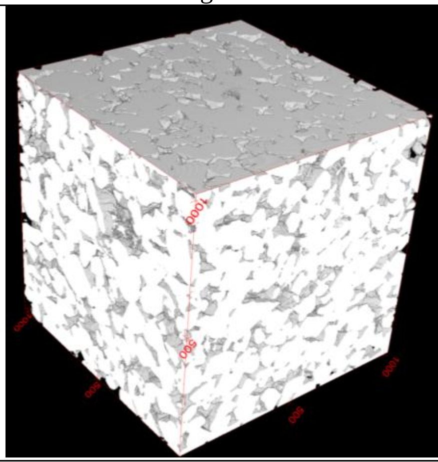
Image# 768	Image# 1024	3D image stack

Doddington [800 voxel^3 @ 2.7745 μm]

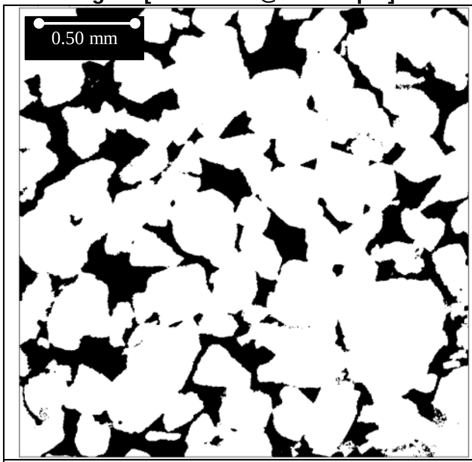	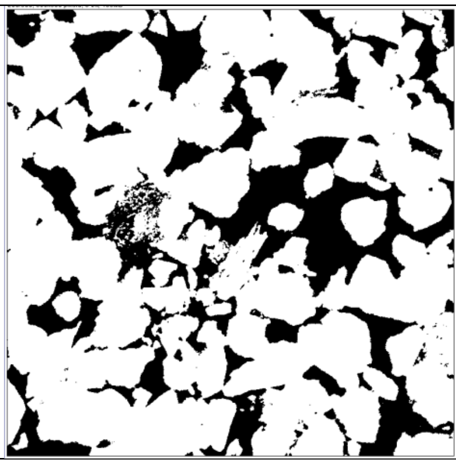	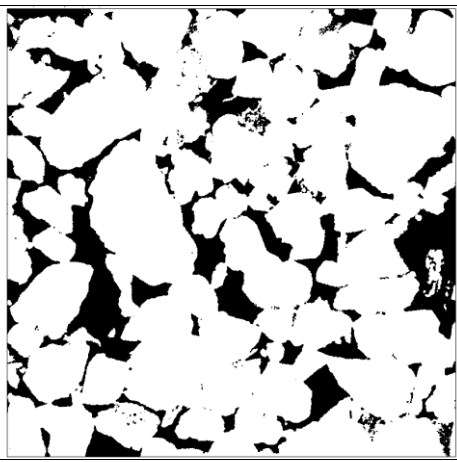
Image# 1	Image# 200	Image# 400
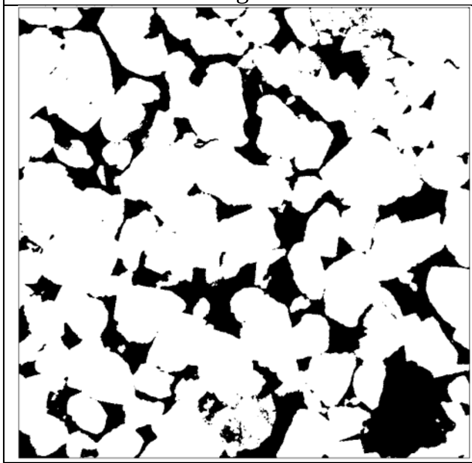	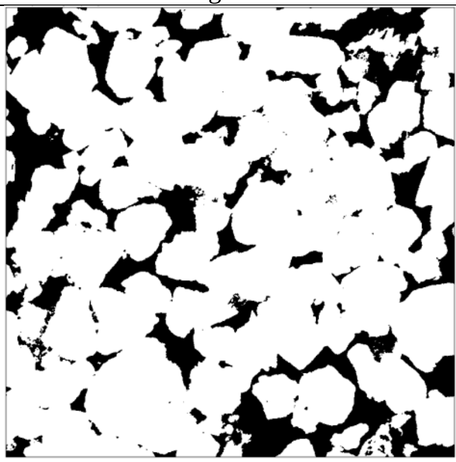	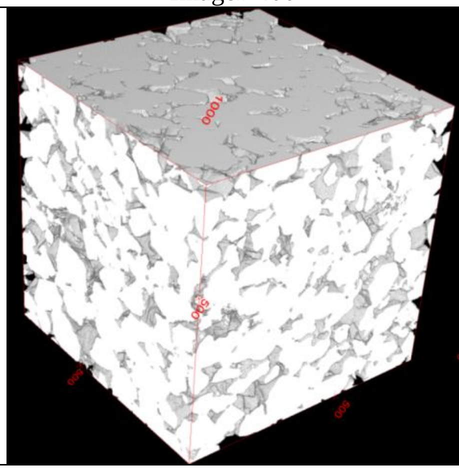
Image# 600	Image# 800	3D image stack

Doddington [400 voxel^3 @ 2.7745 μm]

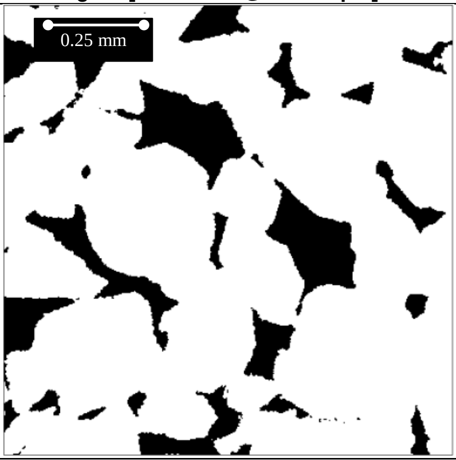

Image# 1

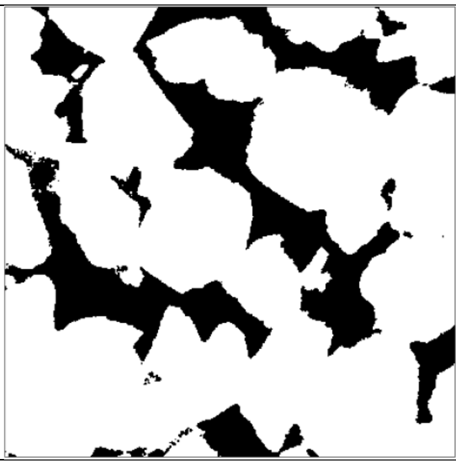

Image# 100

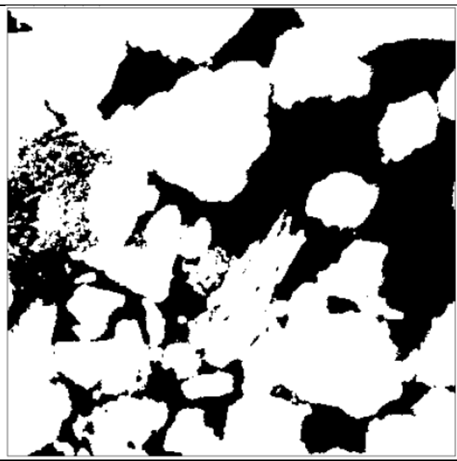

Image# 200

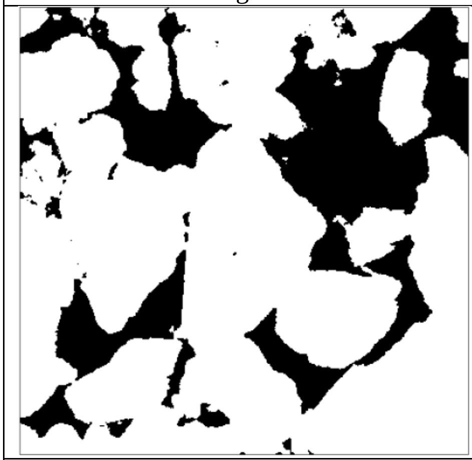

Image# 300

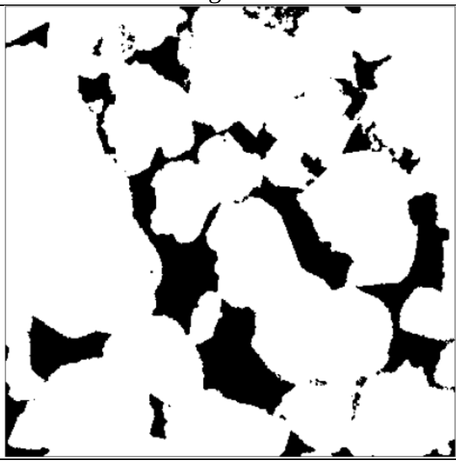

Image# 400

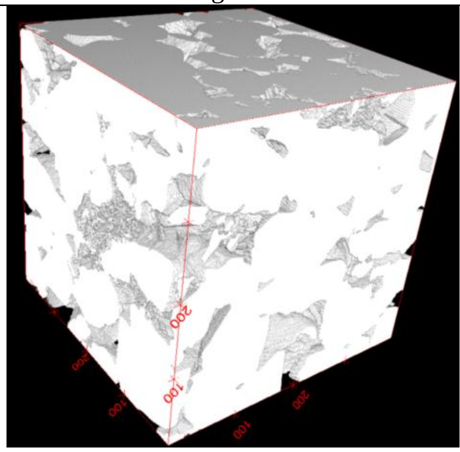

3D image stack

Doddington [200 voxel^3 @ 2.7745 µm]

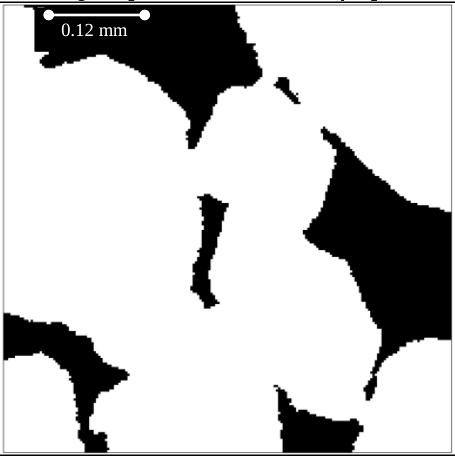		
Image# 1	Image# 50	Image# 100
		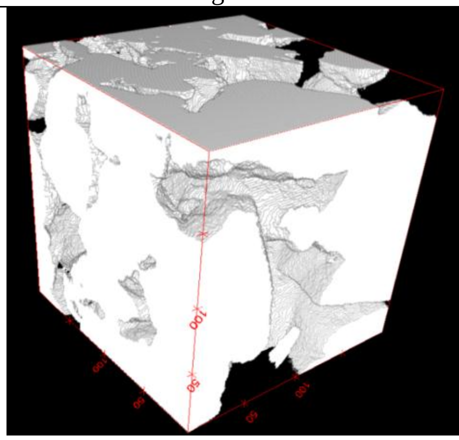
Image# 150	Image# 200	3D image stack

Doddington [100 voxel^3 @ 2.7745 µm]

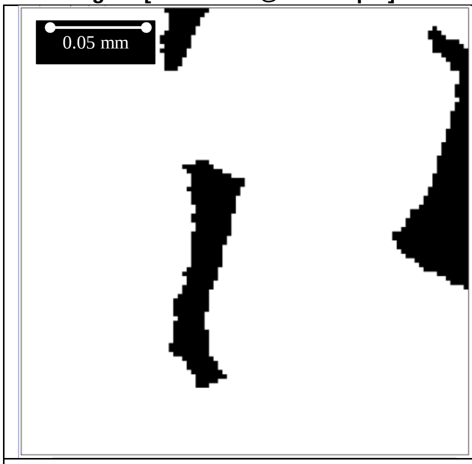

Image# 1

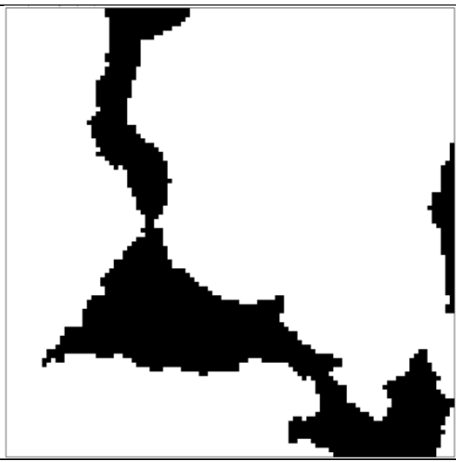

Image# 25

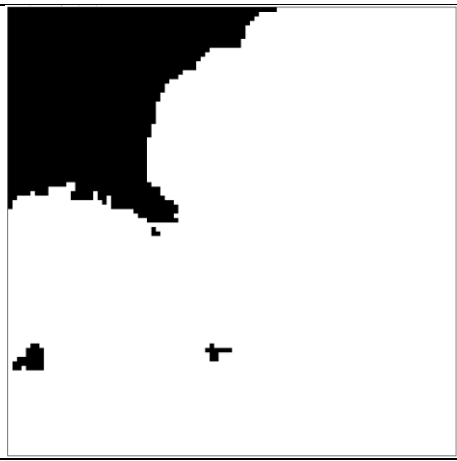

Image# 50

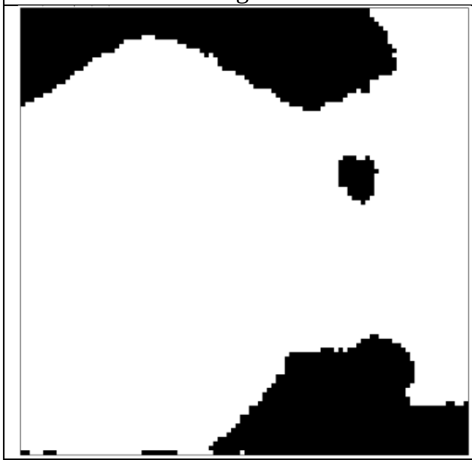

Image# 75

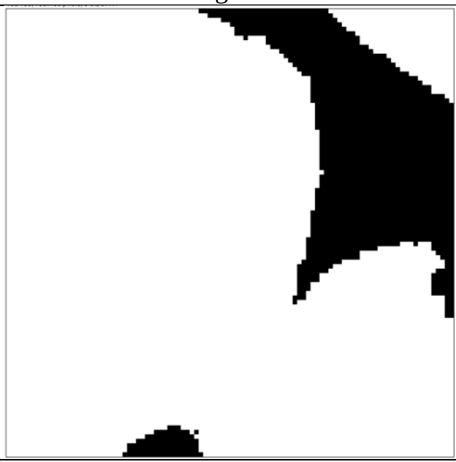

Image# 100

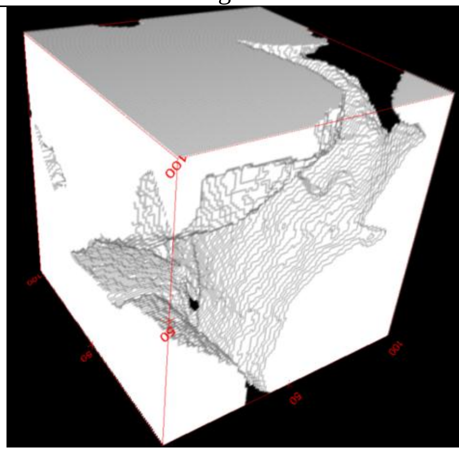

3D image stack

Estaillades [1024 voxel^3 @ 2.6824 µm]

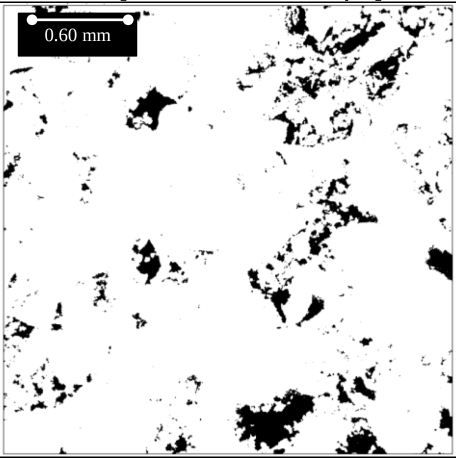

Image# 1

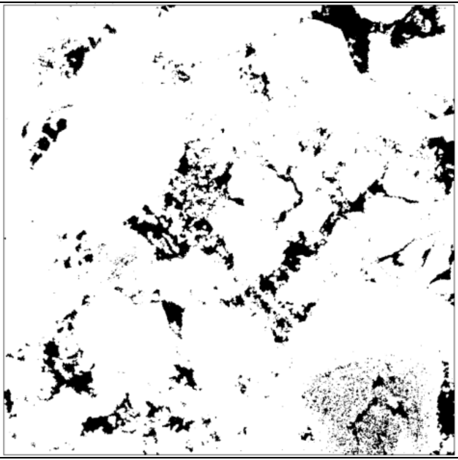

Image# 256

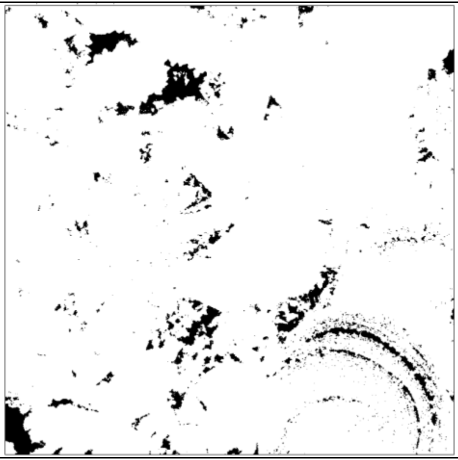

Image# 512

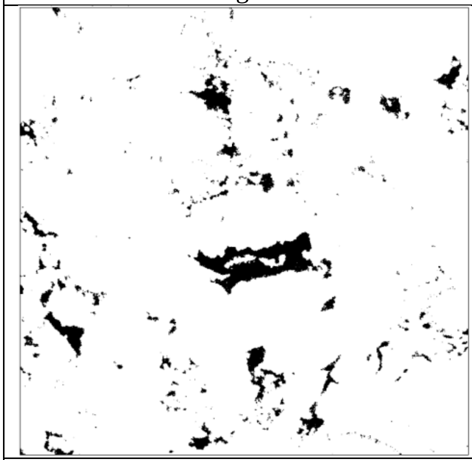

Image# 768

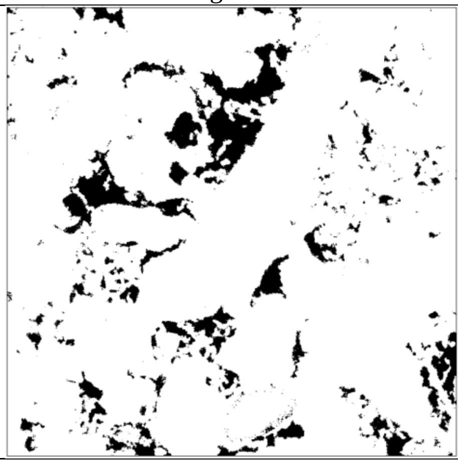

Image# 1024

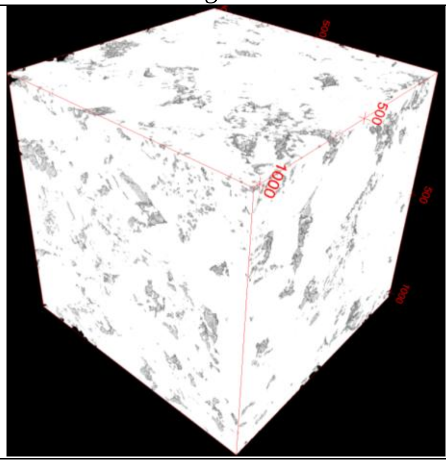

3D image stack

Estaillades [800 voxel^3 @ 2.6824 µm]

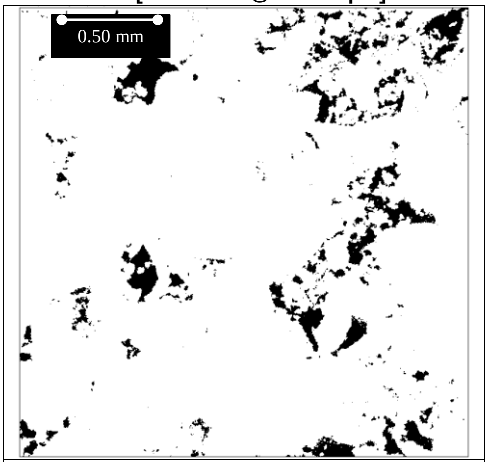

Image# 1

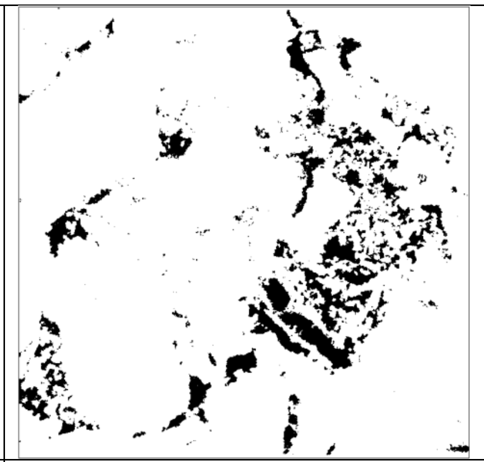

Image# 200

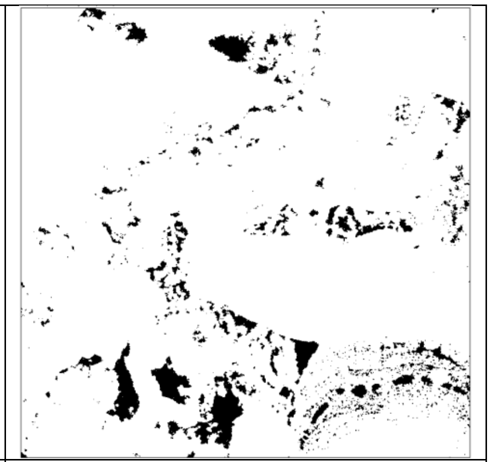

Image# 400

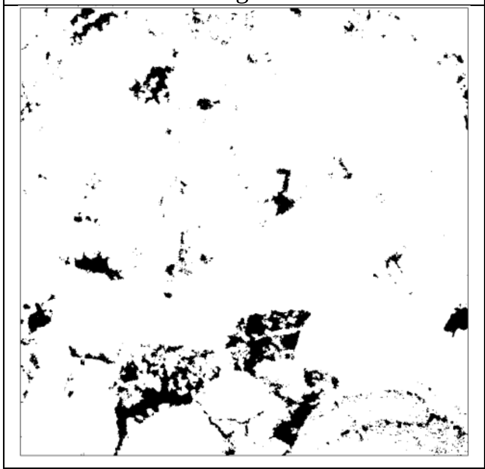

Image# 600

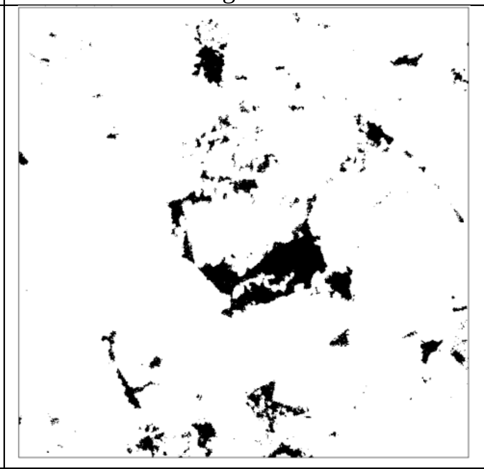

Image# 800

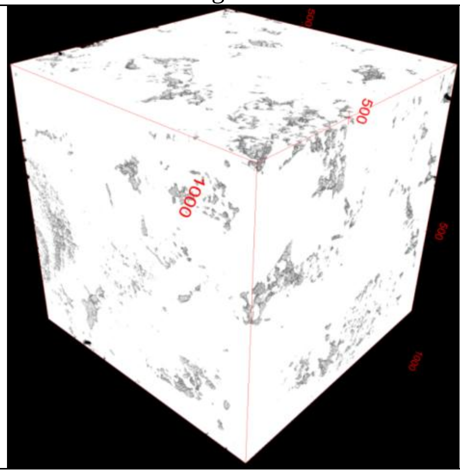

3D image stack

Estaillades [400 voxel^3 @ 2.6824 μm]

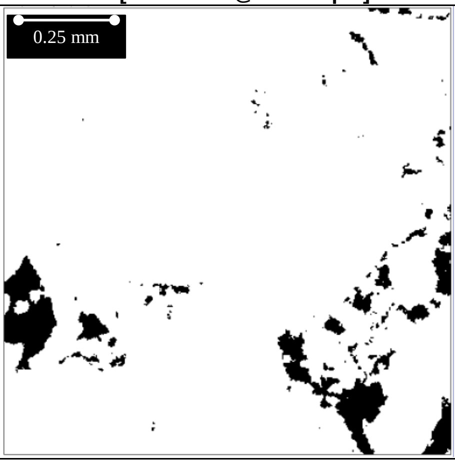	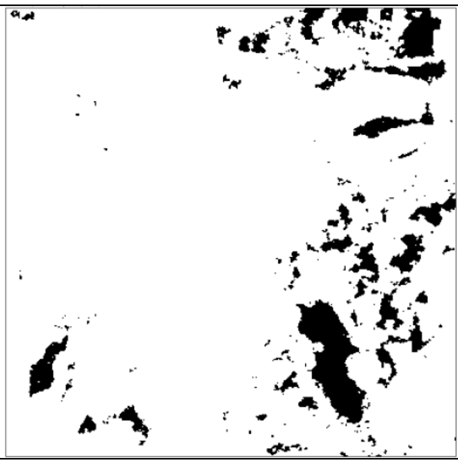	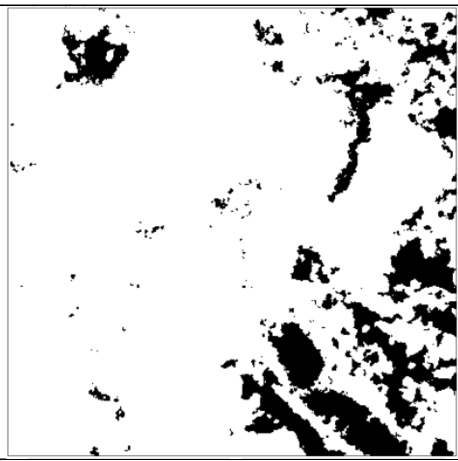
Image# 1	Image# 100	Image# 200
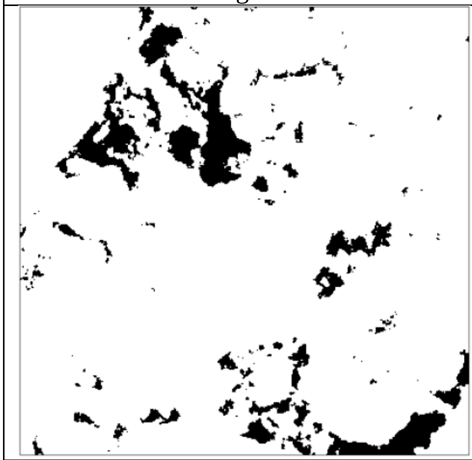		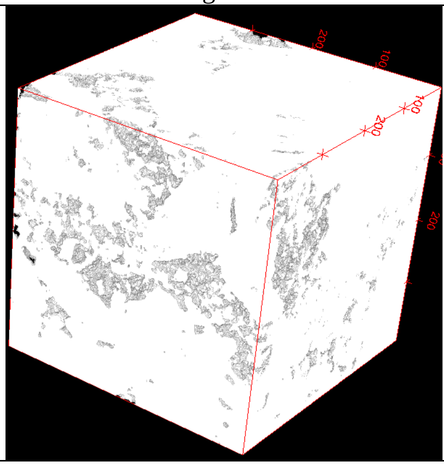
Image# 300	Image# 400	3D image stack

Estaillades [200 voxel^3 @ 2.6824 μm]

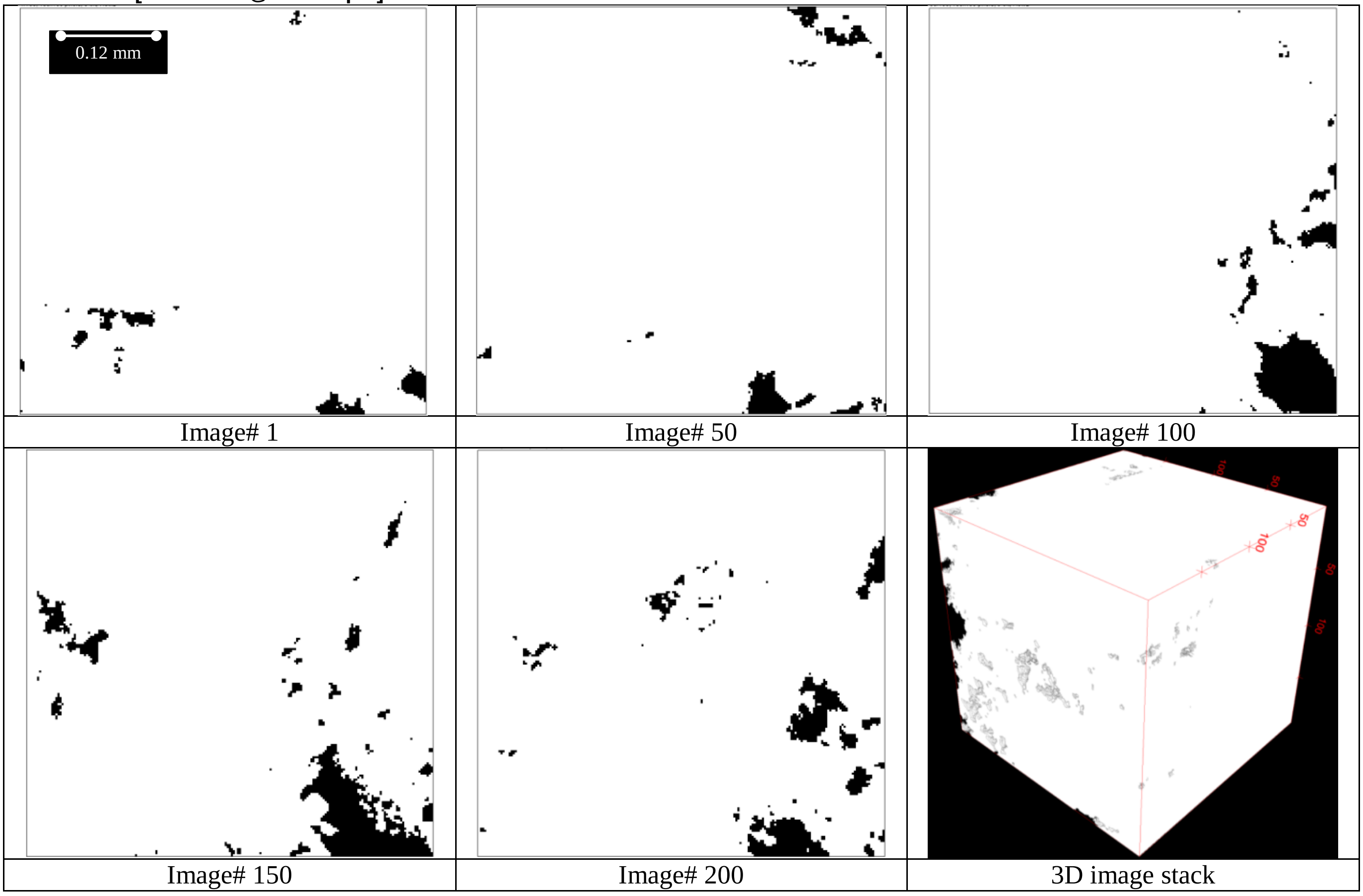

Estaillades [100 voxel^3 @ 2.6824 μm]*

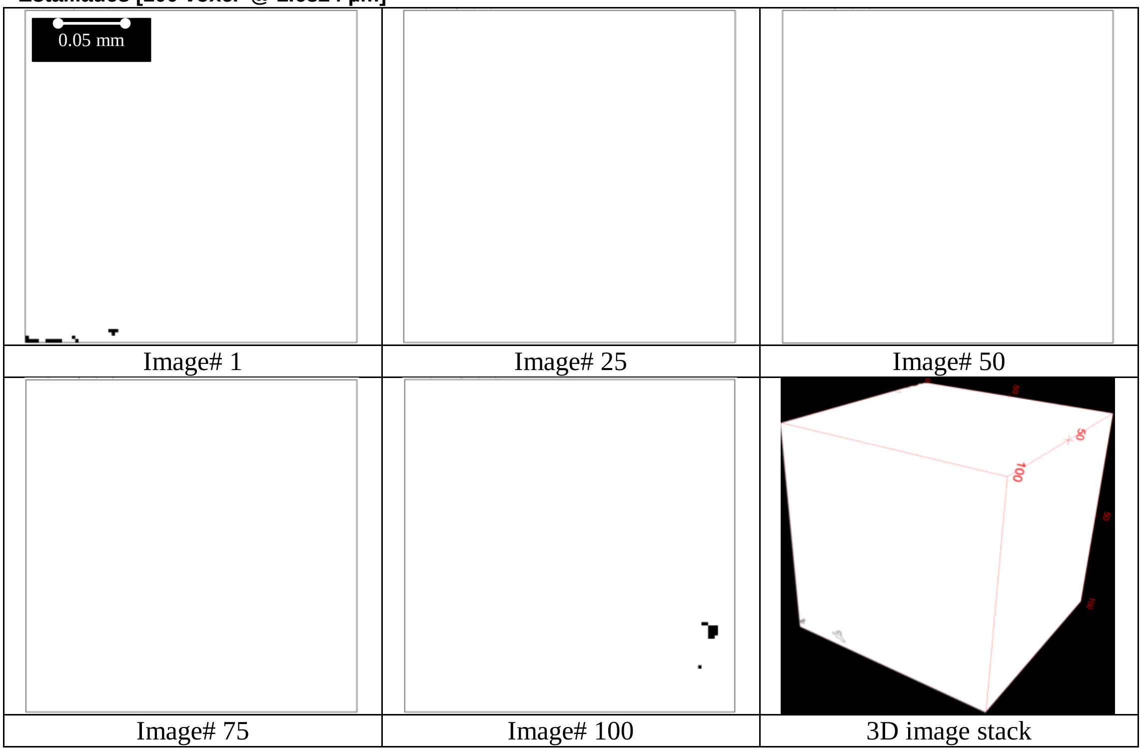

* These images are mostly blank representing ≈zero porosity. Few black voxels represent pore space that is captured at 100 voxel^3 in the center of the 1024 voxel^3 base image to be consistent in the study. If the same sub-volume was cropped out of different part of the base image, it may have more pore space.

Ketton [1024 voxel^3 @ 2.654 µm]

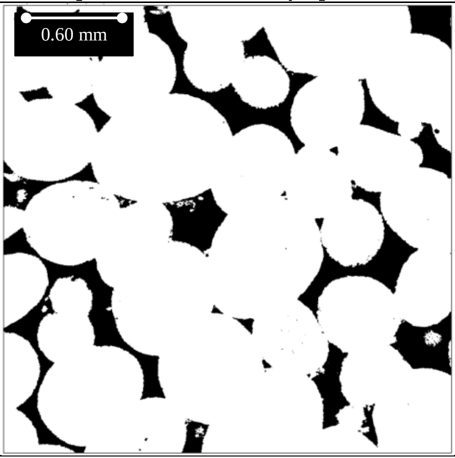	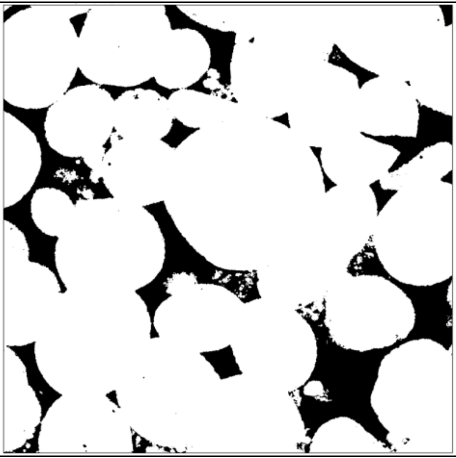	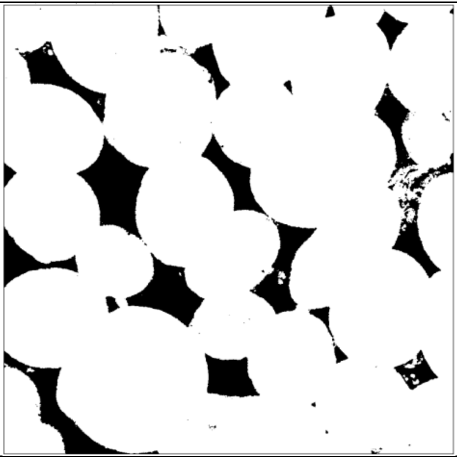
Image# 1	Image# 256	Image# 512
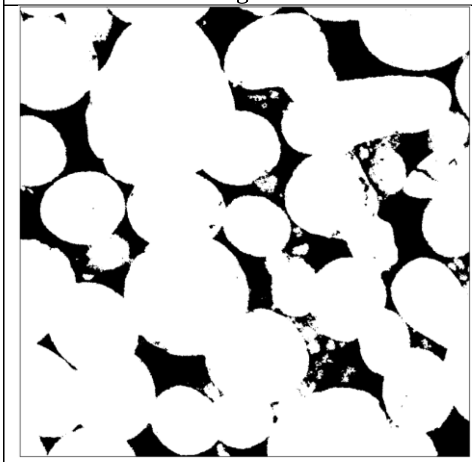	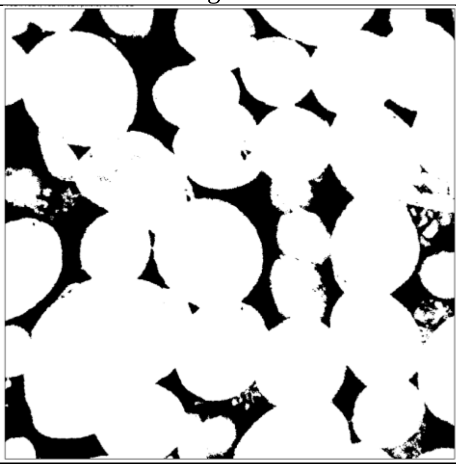	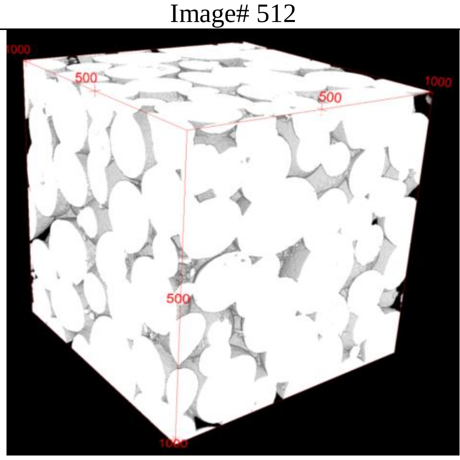
Image# 768	Image# 1024	3D image stack

Ketton [800 voxel^3 @ 2.654 µm]

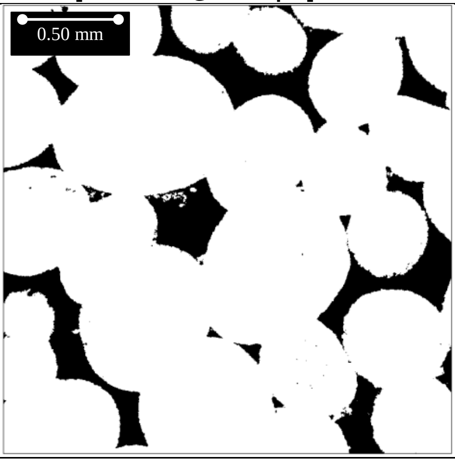

Image# 1

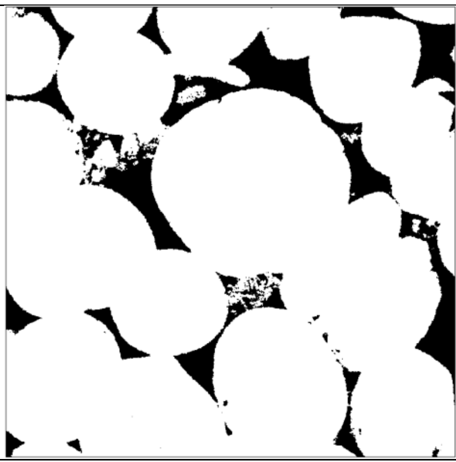

Image# 200

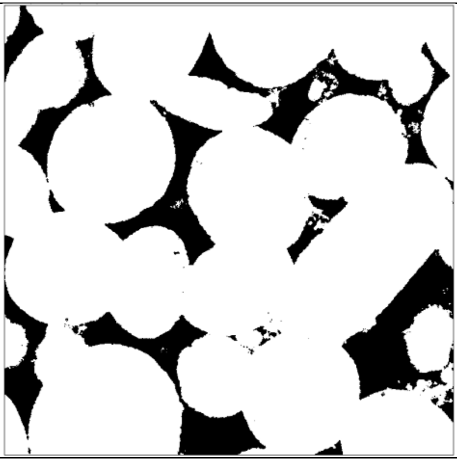

Image# 400

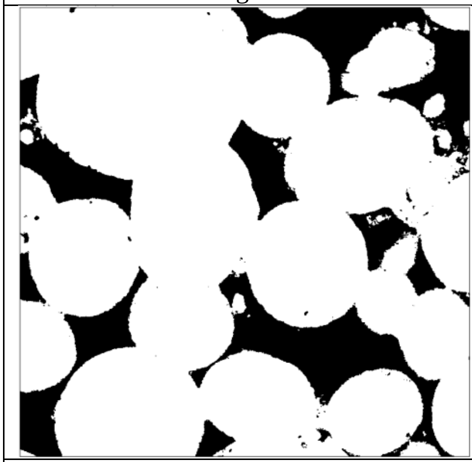

Image# 600

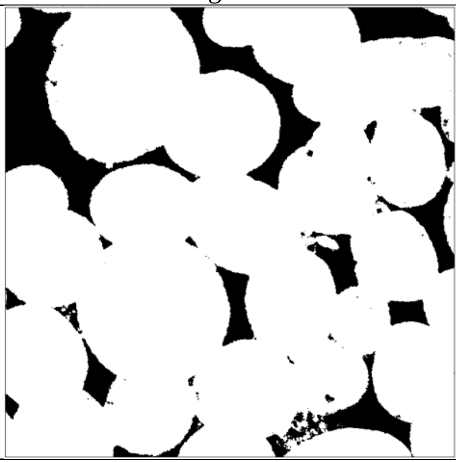

Image# 800

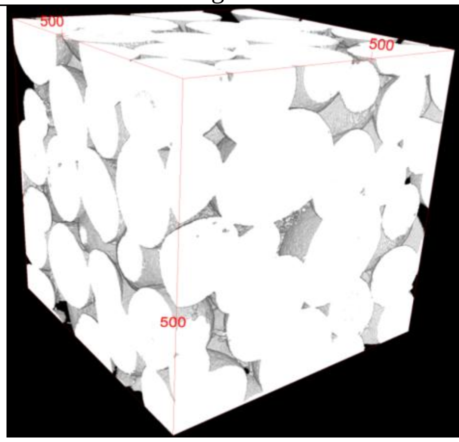

3D image stack

Ketton [400 voxel^3 @ 2.654 μm]

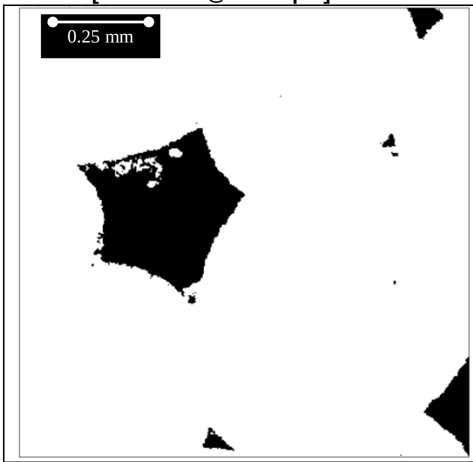

Image# 1

Image# 100

Image# 200

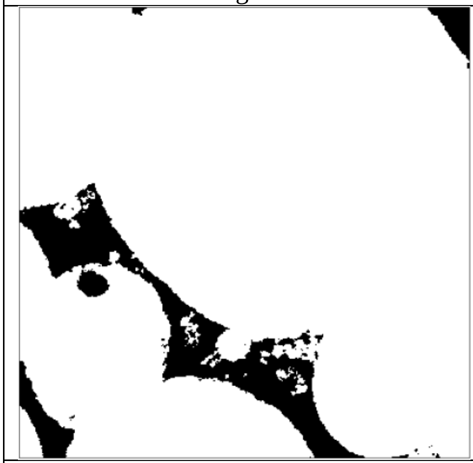

Image# 300

Image# 400

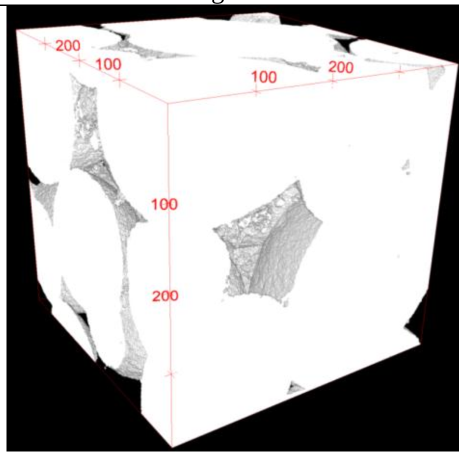

3D image stack

Ketton [200 voxel^3 @ 2.654 μm]

Image# 1

Image# 50

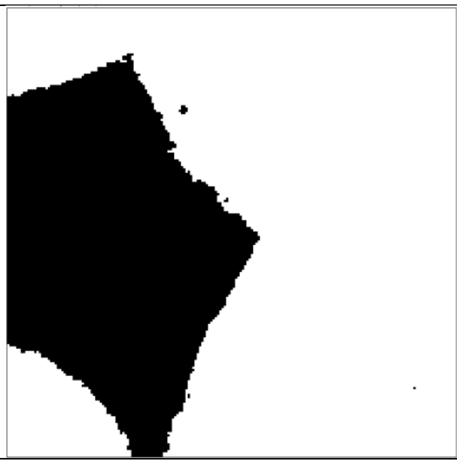

Image# 100

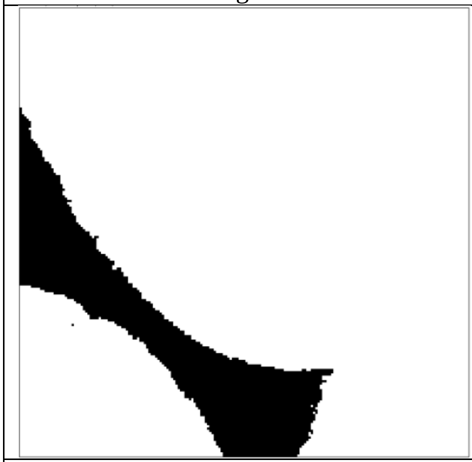

Image# 150

Image# 200

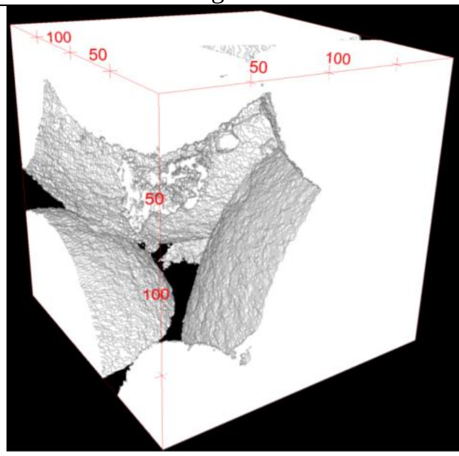

3D image stack

Ketton [100 voxel^3 @ 2.654 μm]*

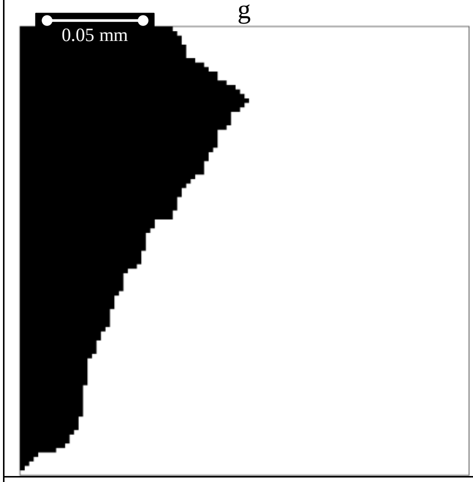	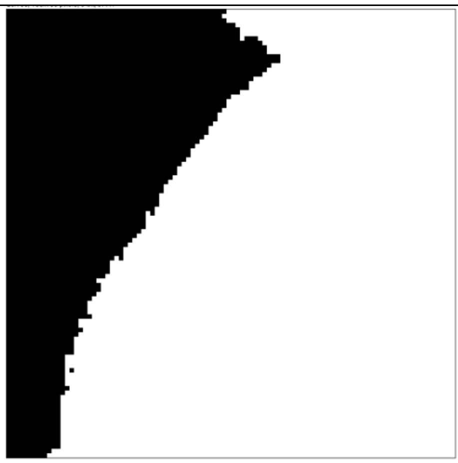	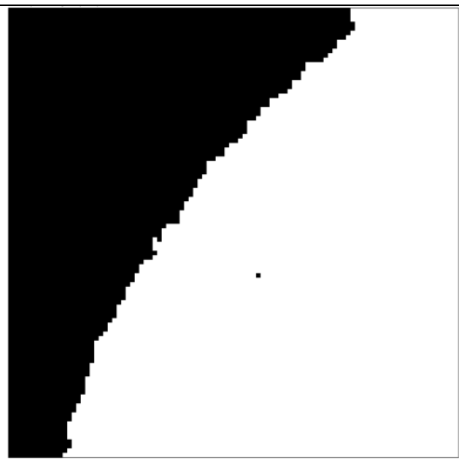
Image# 1	Image# 25	Image# 50
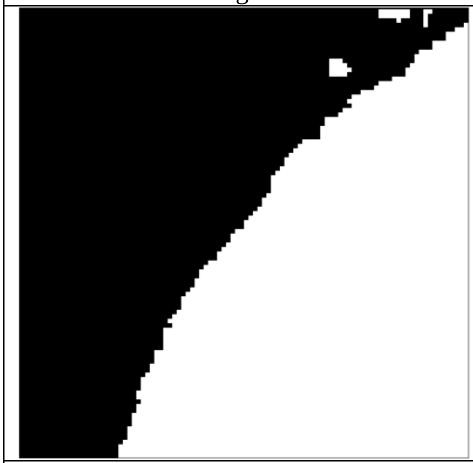	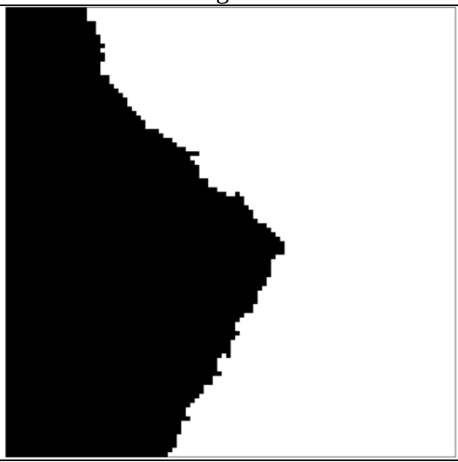	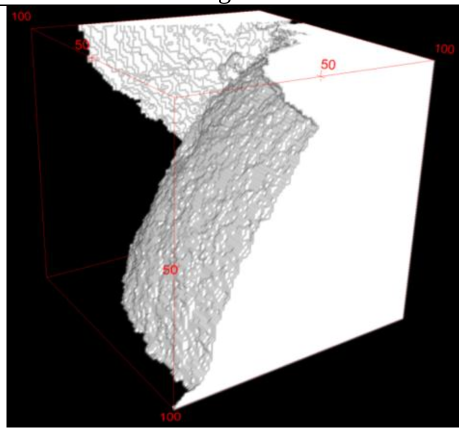
Image# 75	Image# 100	3D image stack

*The black voxels represent pore space while white voxels represent grain.

Appendix-III: Additional Images and 3D Reconstructions, Resolution Study

This appendix visualizes the subject rock samples in the 2D and 3D space by showing multiple segmented images in 2D and the constructed 3D image for the resolution study. The resolution images shown below are the same as describe in the main body of the report. The base image of all sources is the 1024 voxel^3 @ ≈2.7μm. Reduced images contain the same features but at an upscaled resolution. Only five out of ten resolutions are displayed in this appendix to emphasize the change in image features instead of the redundancy of large number of images. A recommended way to understand the effect of images is to look at the same image, for example the first one, and notice how it changes at each coarser resolution.

Berea [819 voxel^3 @ 3.469 μm]; Reduction factor=0.7998

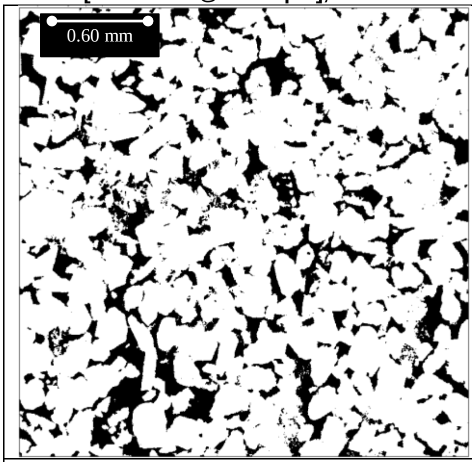

Image# 1

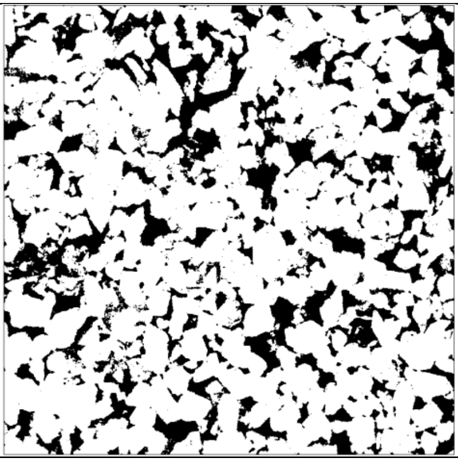
Image# 205

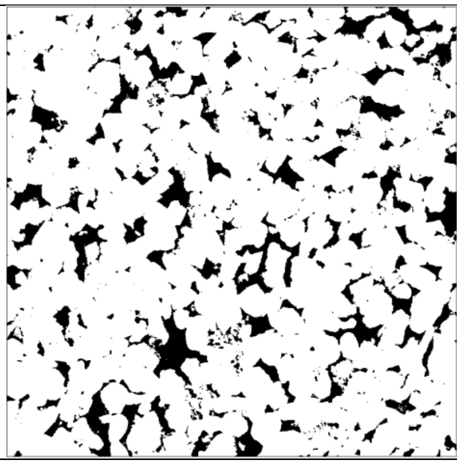
Image# 410

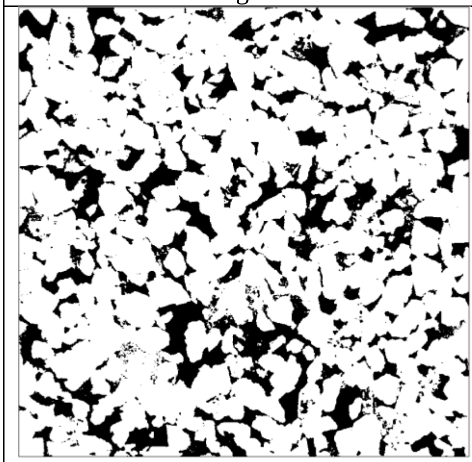
Image# 614

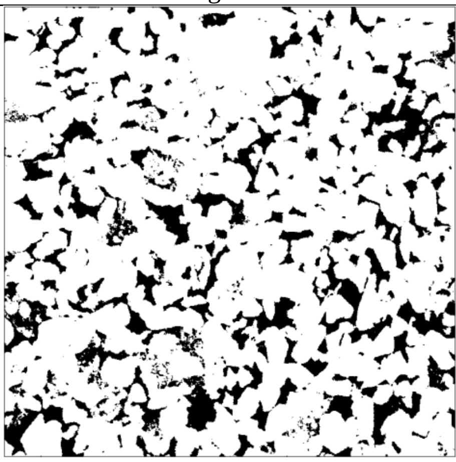
Image# 819

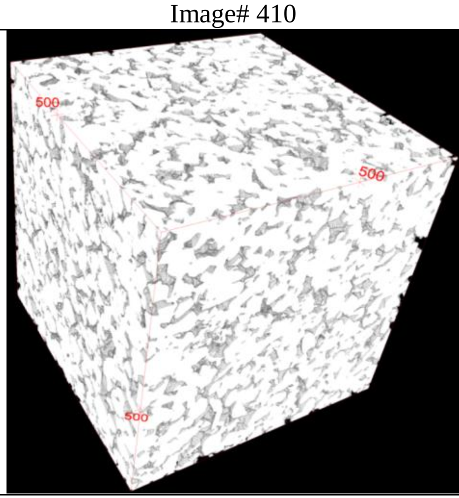

3D image stack

Berea [615 voxel^3 @ 4.620 µm]; Reduction factor=0.6006

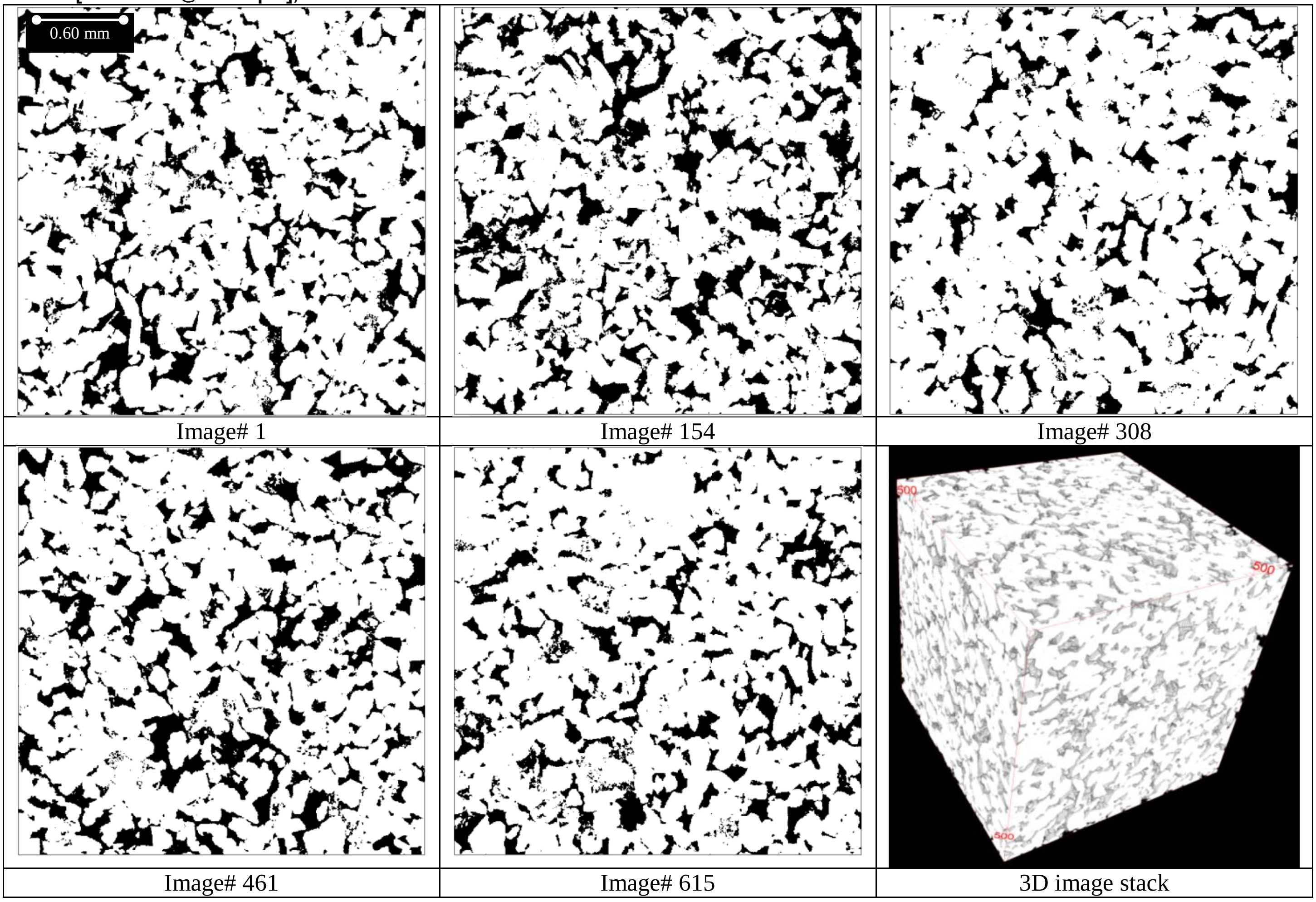

Image# 1 | Image# 154 | Image# 308

Image# 461 | Image# 615 | 3D image stack

Berea [410 voxel^3 @ 6.929 µm]; Reduction factor=0.4004

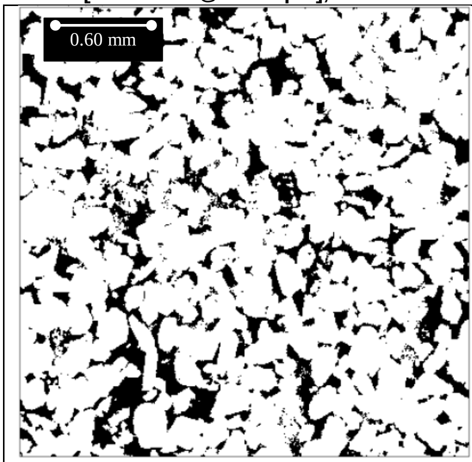

Image# 1

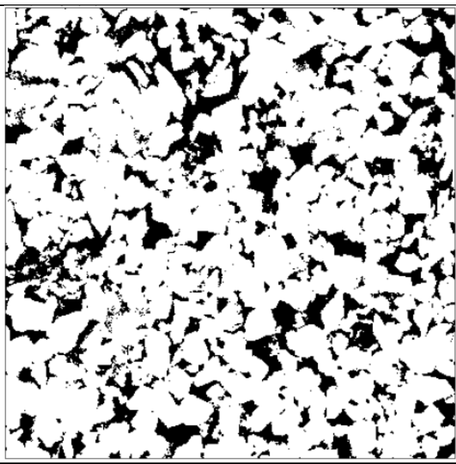

Image# 103

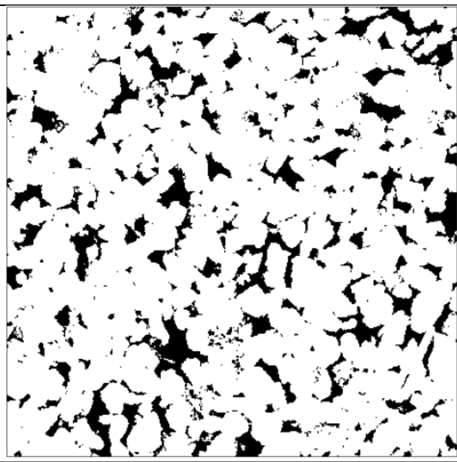

Image# 205

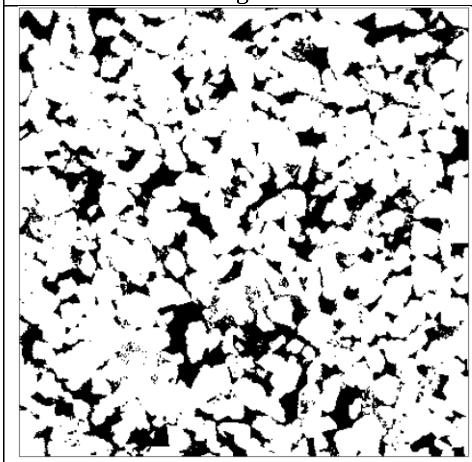

Image# 308

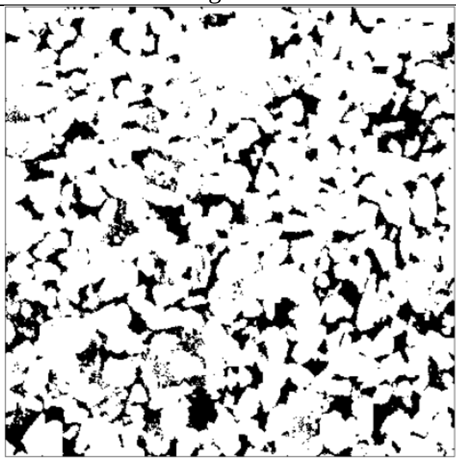

Image# 410

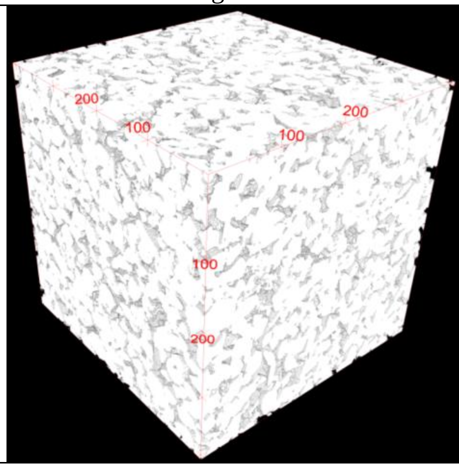

3D image stack

Berea [205 voxel^3 @ 13.859 μm]; Reduction factor=0.2002

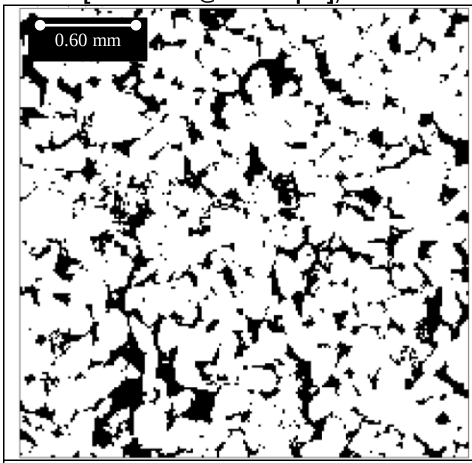	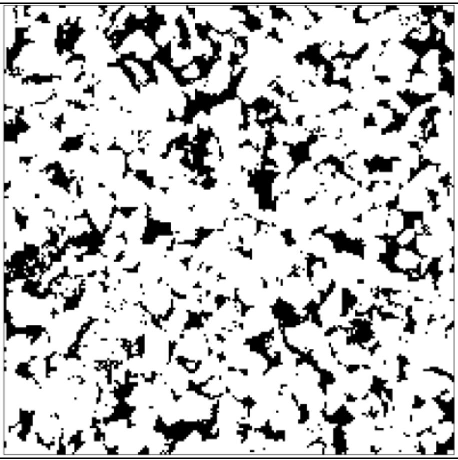	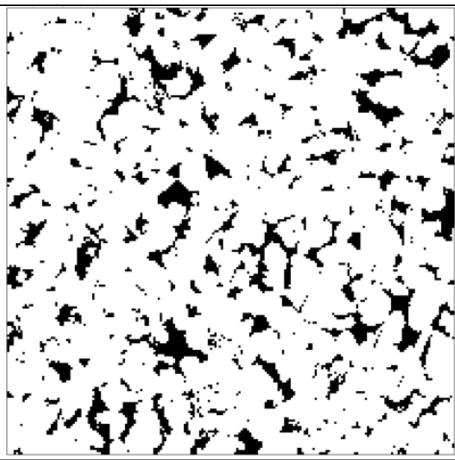
Image# 1	Image# 51	Image# 103
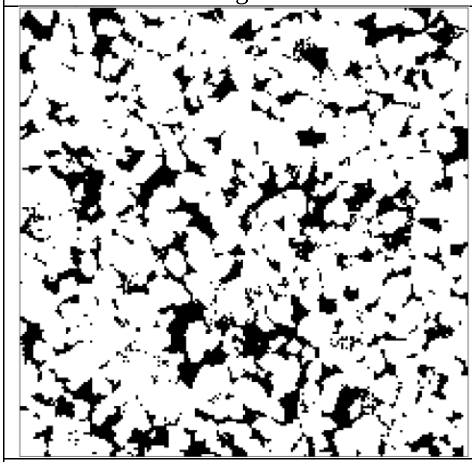	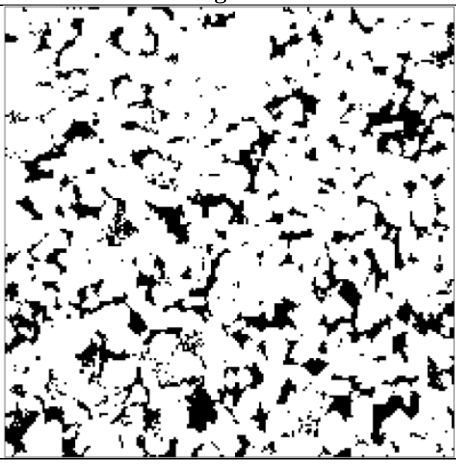	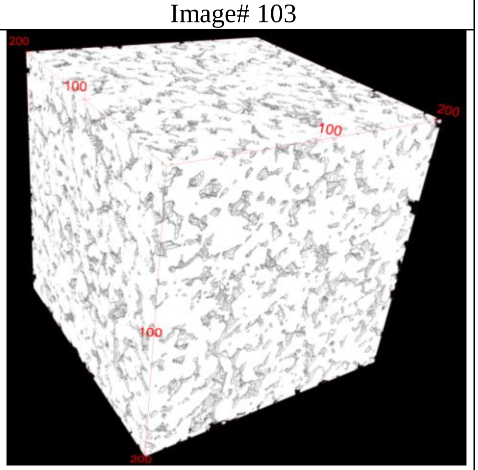
Image# 154	Image# 205	3D image stack

Berea [103 voxel^3 @ 27.583 µm]; Reduction factor=0.1006

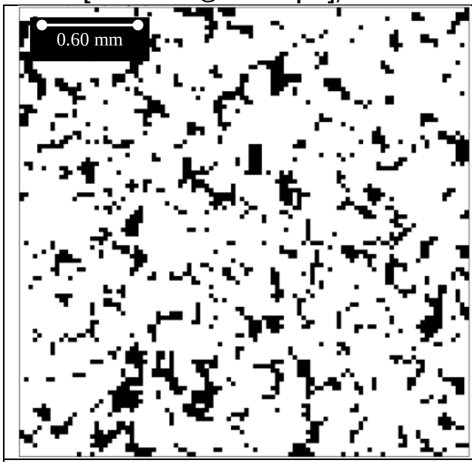	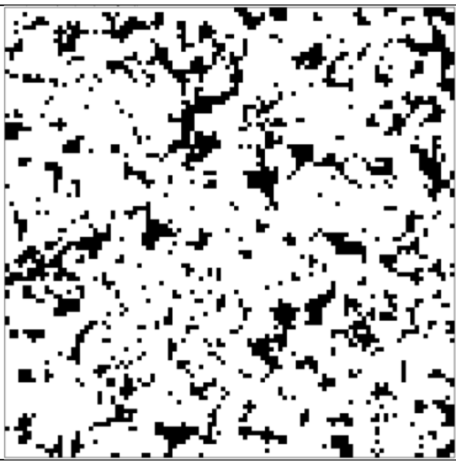	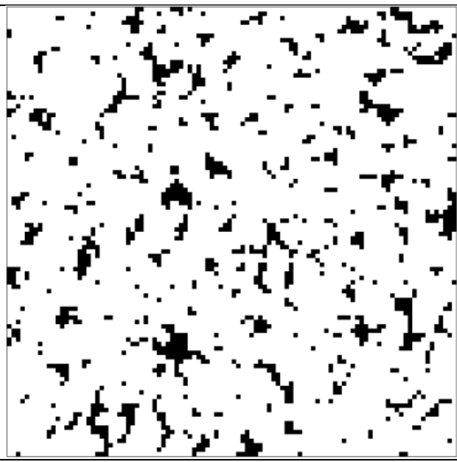
Image# 1	Image# 26	Image# 52
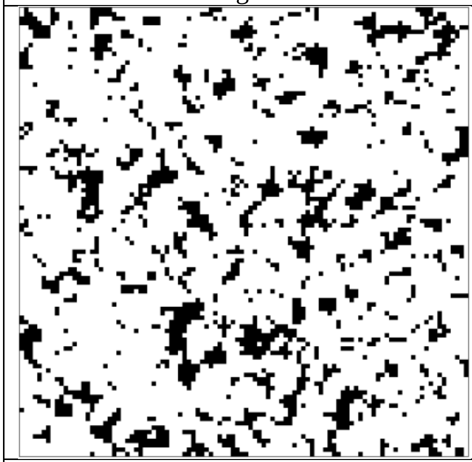	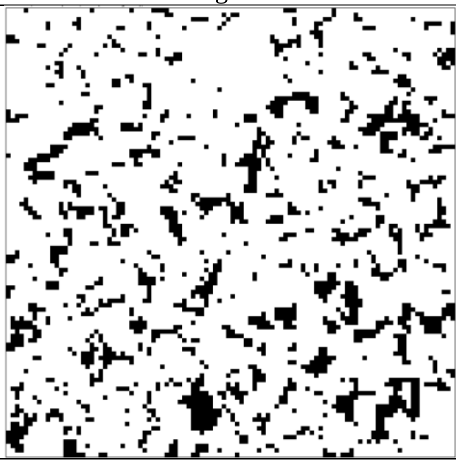	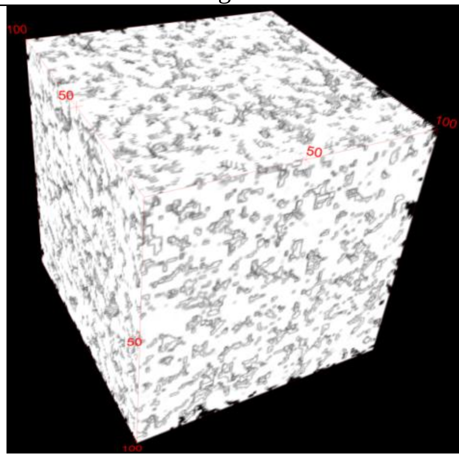
Image# 77	Image# 103	3D image stack

Doddington [819 voxel^3 @ 3.469 µm]; Reduction factor=0.7998

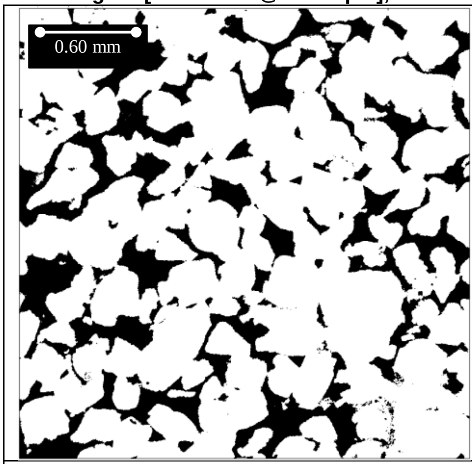	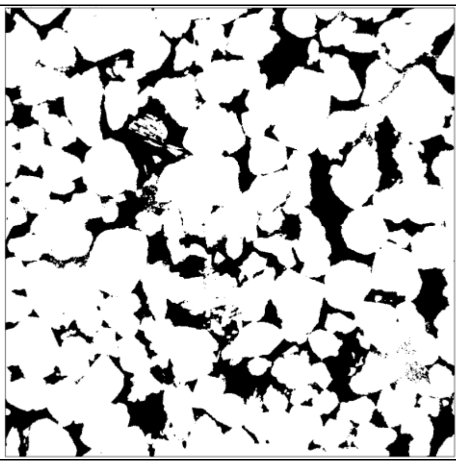	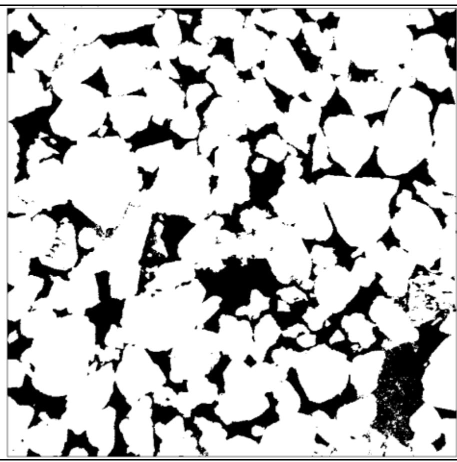
Image# 1	Image# 205	Image# 410
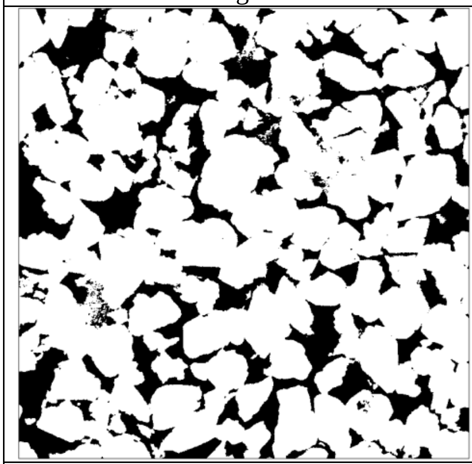	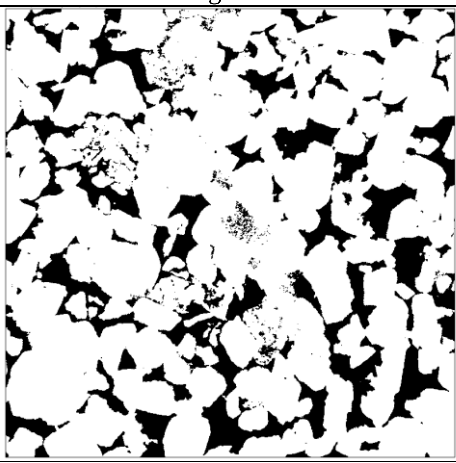	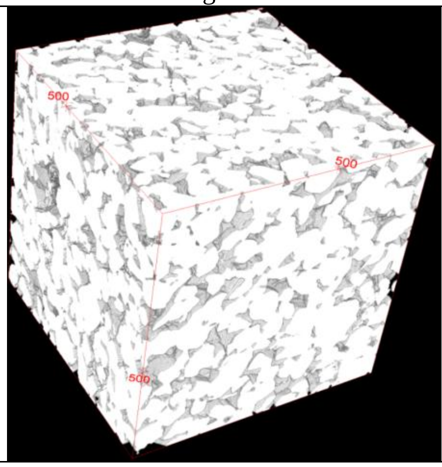
Image# 614	Image# 819	3D image stack

Doddington [615 voxel^3 @ 4.620 μm]; Reduction factor=0.6006

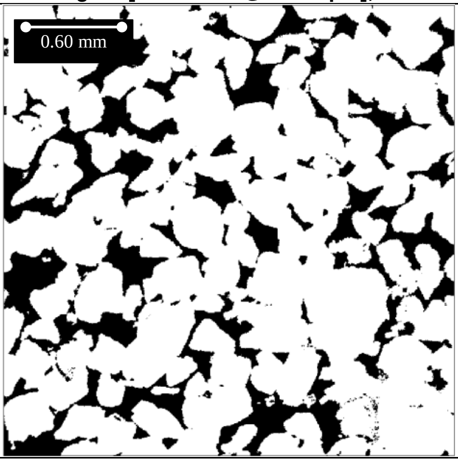	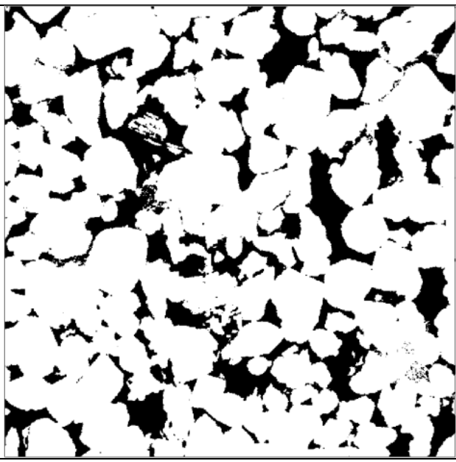	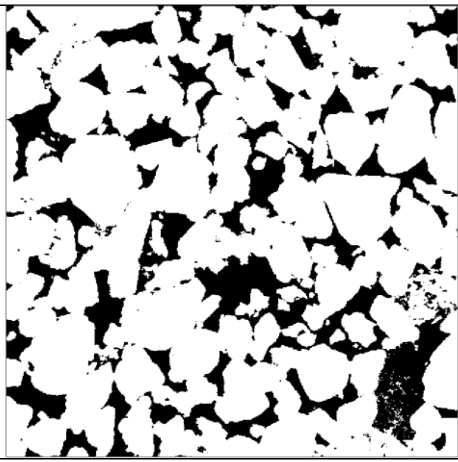
Image# 1	Image# 154	Image# 308
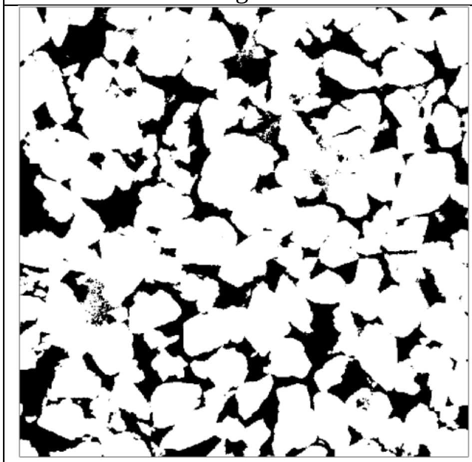	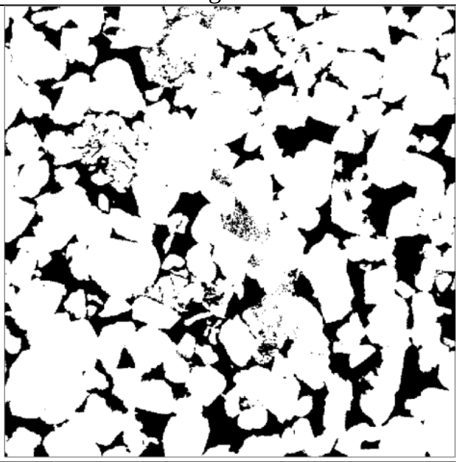	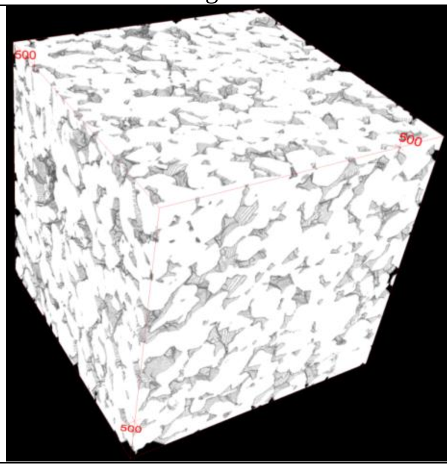
Image# 461	Image# 615	3D image stack

Doddington [410 voxel^3 @ 6.929 µm]; Reduction factor=0.4004

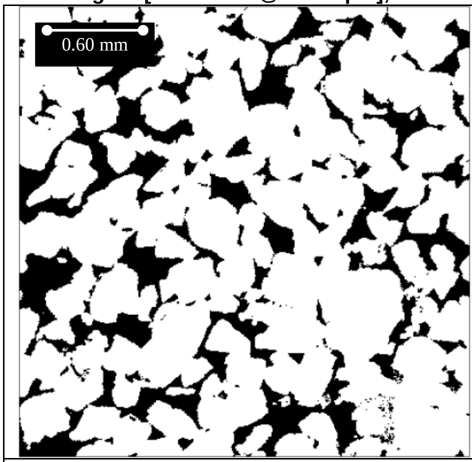	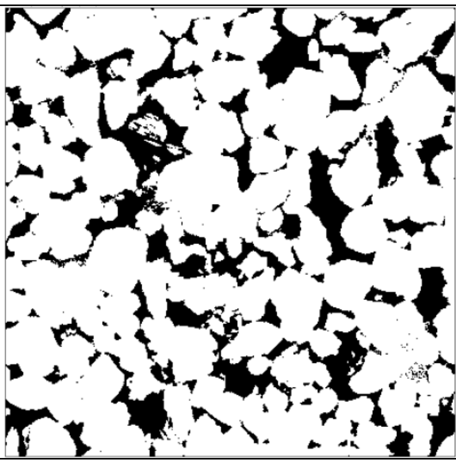	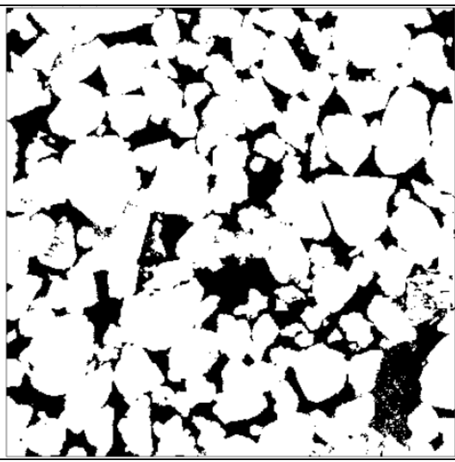
Image# 1	Image# 103	Image# 205
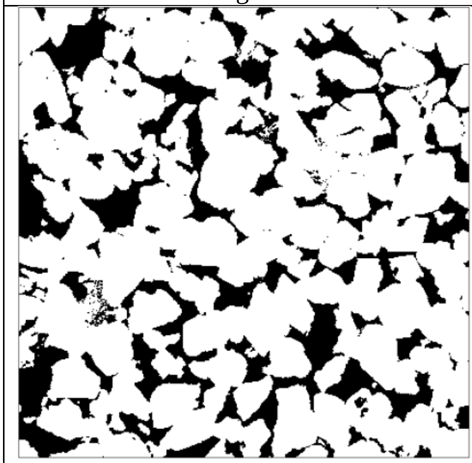	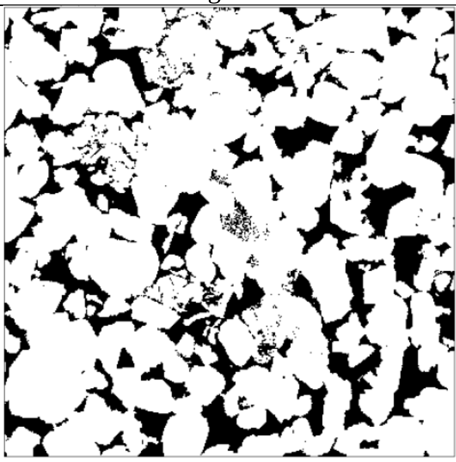	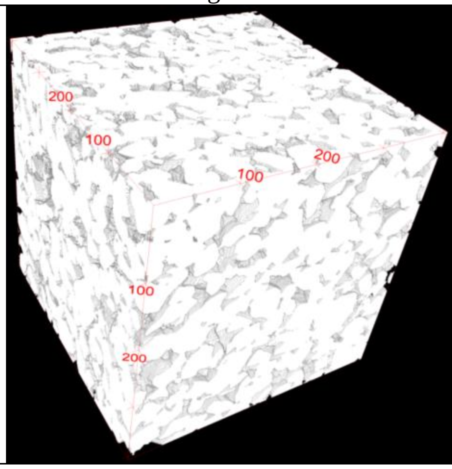
Image# 308	Image# 410	3D image stack

Doddington [205 voxel^3 @ 13.859 μm]; Reduction factor=0.2002

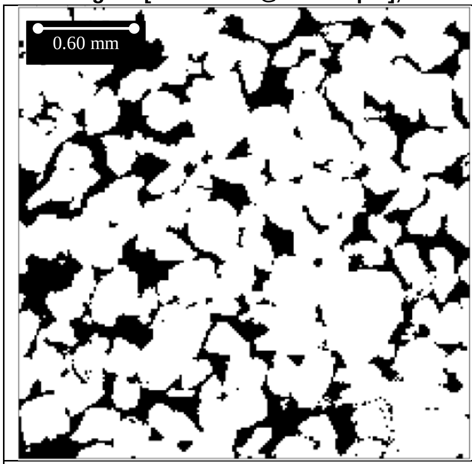	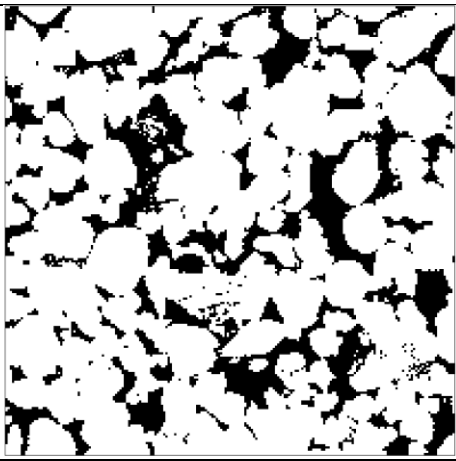	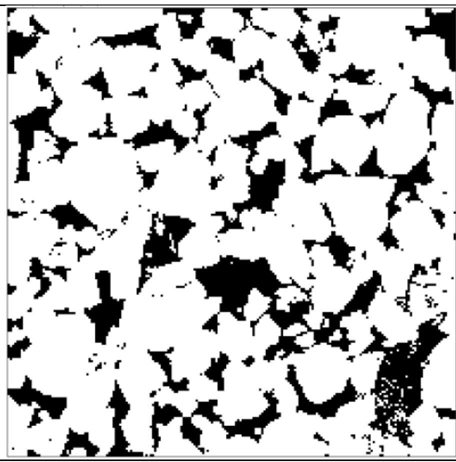
Image# 1	Image# 51	Image# 103
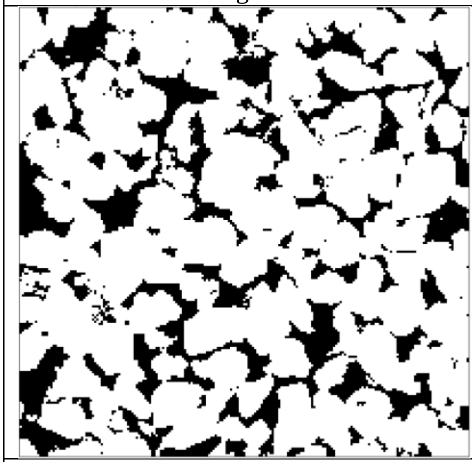	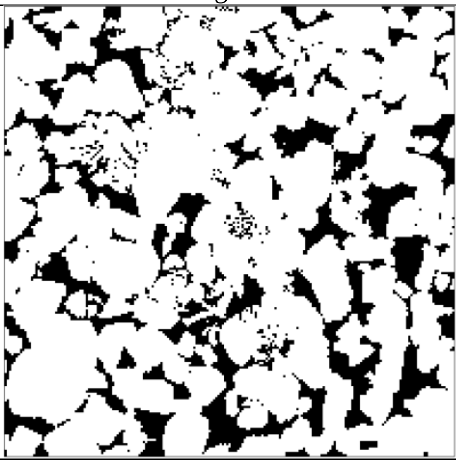	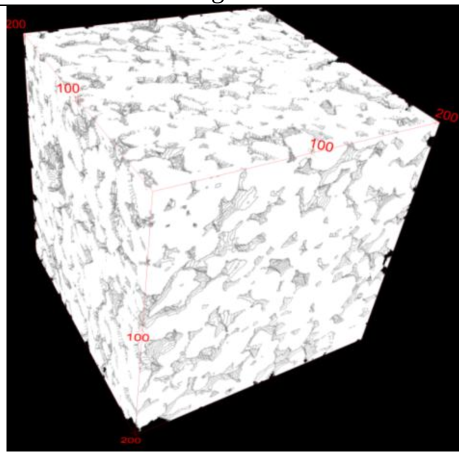
Image# 154	Image# 205	3D image stack

Doddington [103 voxel^3 @ 27.583 µm]; Reduction factor=0.1006

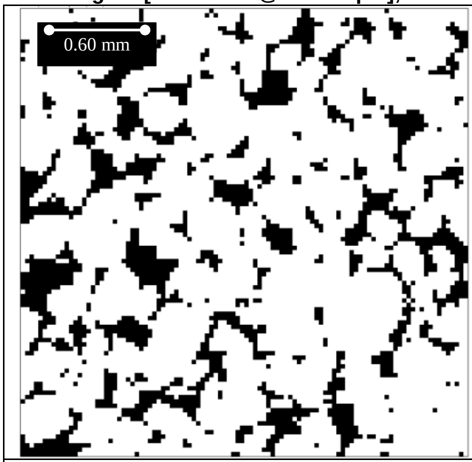	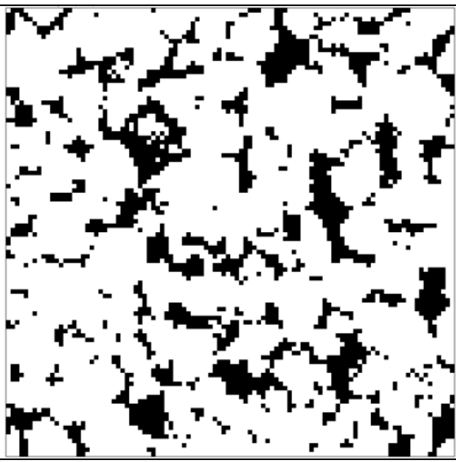	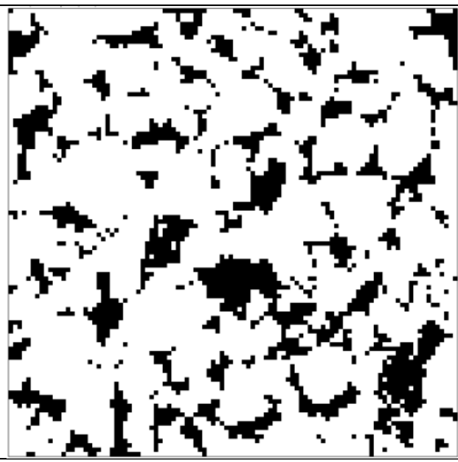
Image# 1	Image# 26	Image# 52
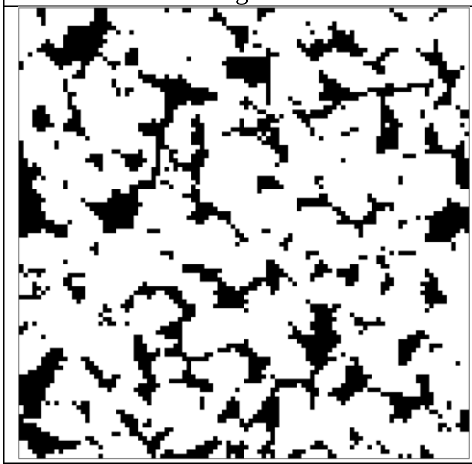	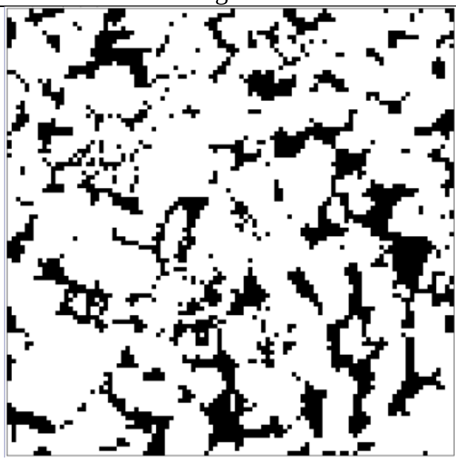	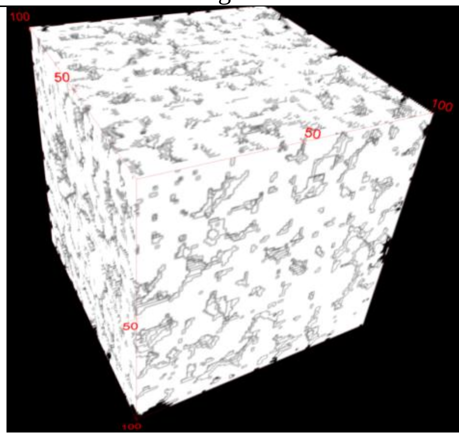
Image# 77	Image# 103	3D image stack

Estaillades [819 voxel3 @ 3.354 µm]; Reduction factor=0.7998

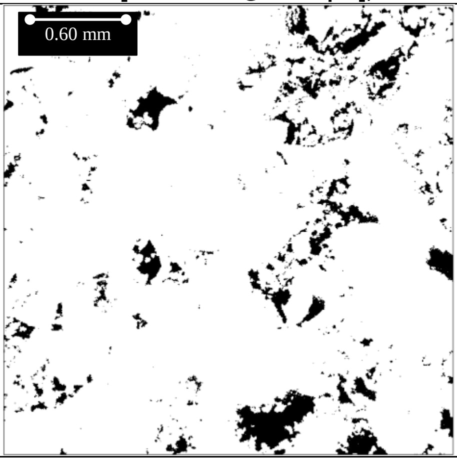

Image# 1

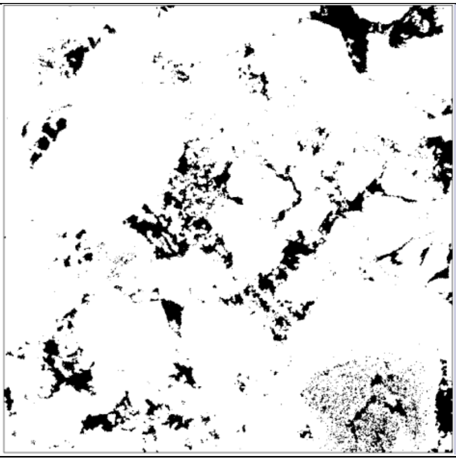

Image# 205

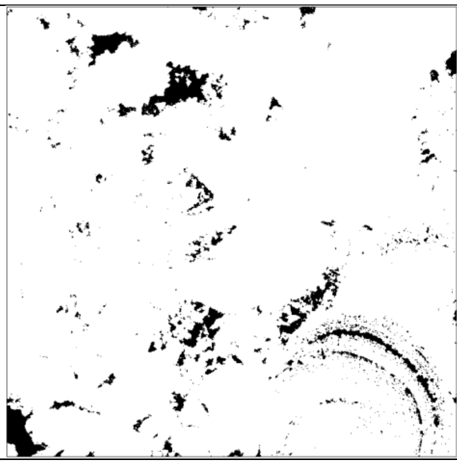

Image# 410

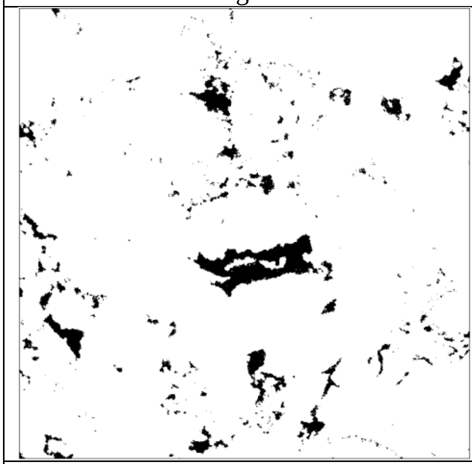

Image# 614

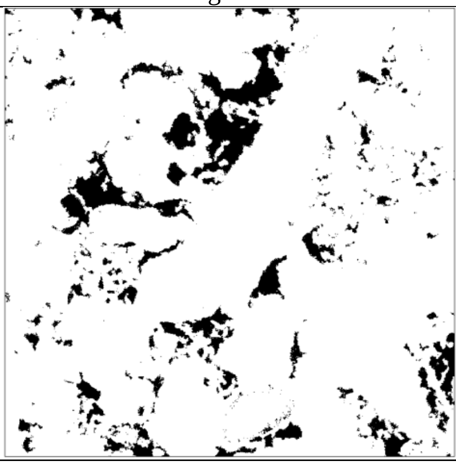

Image# 819

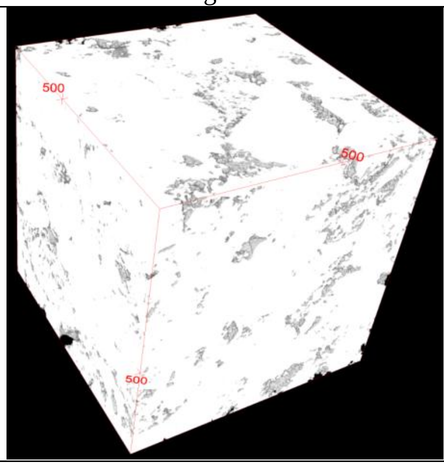

3D image stack

Estaillades [615 voxel^3 @ 4.466 μm]; Reduction factor=0.6006

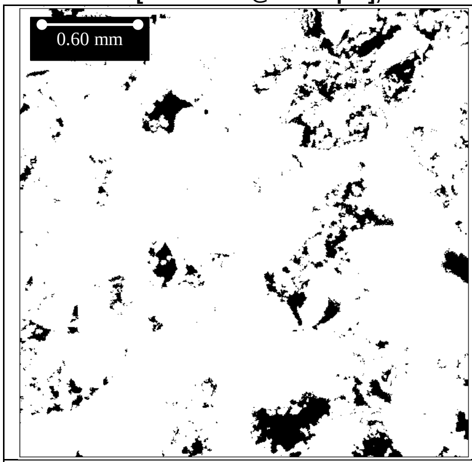	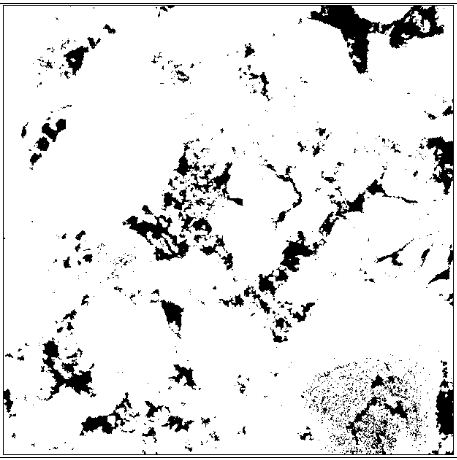	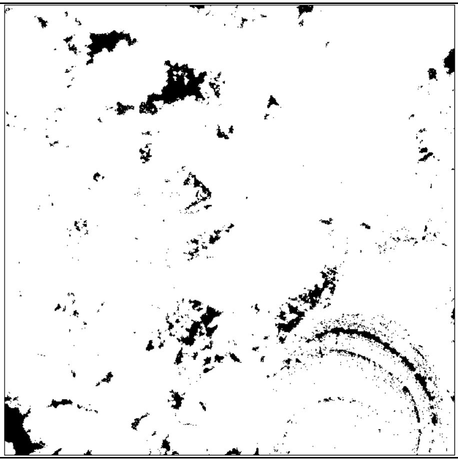
Image# 1	Image# 154	Image# 308
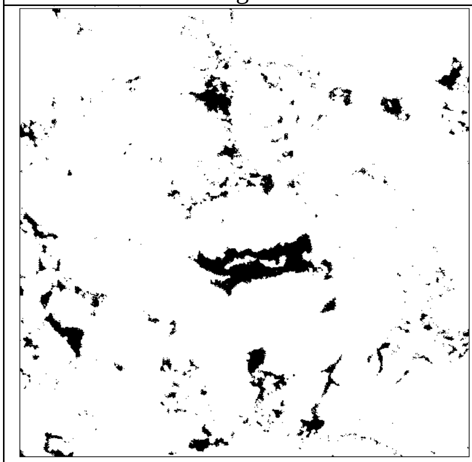	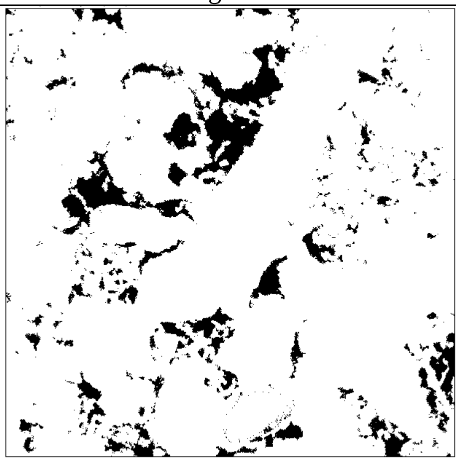	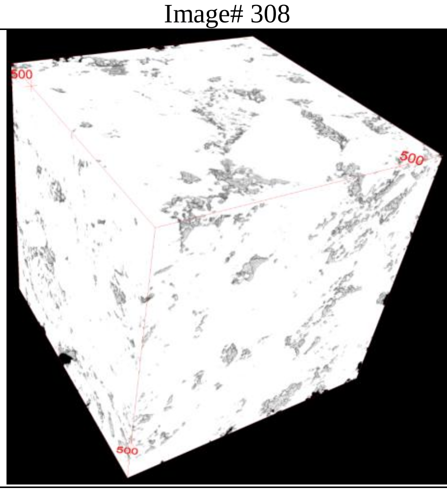
Image# 461	Image# 615	3D image stack

Estaillades [410 voxel^3 @ 6.699 μm]; Reduction factor=0.4004

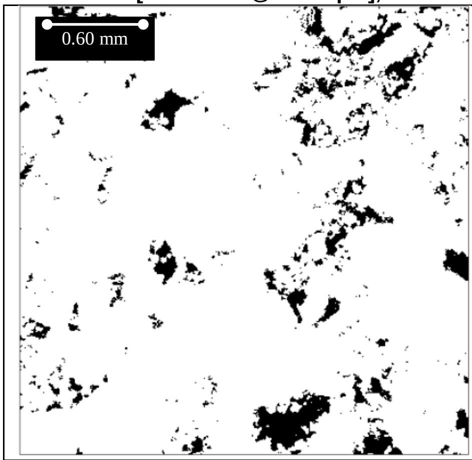

Image# 1

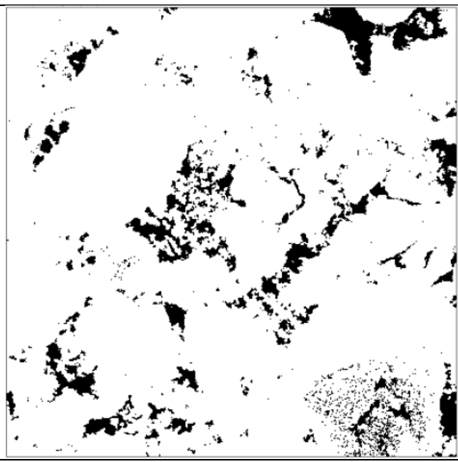

Image# 103

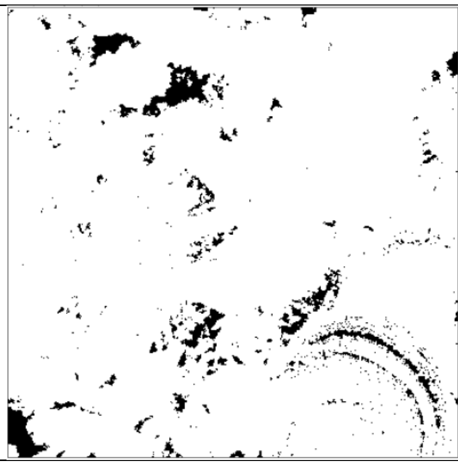

Image# 205

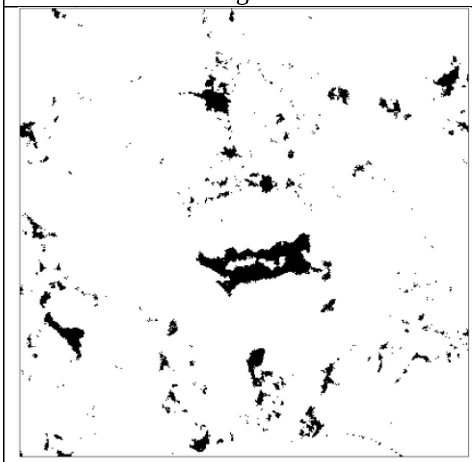

Image# 308

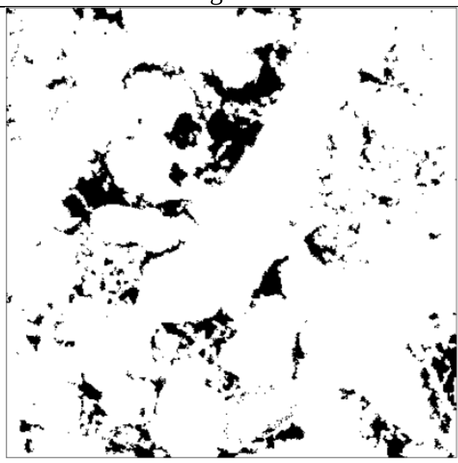

Image# 410

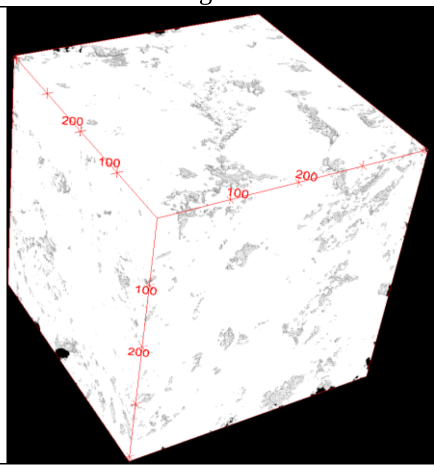

3D image stack

Estaillades [205 voxel^3 @ 13.399 μm]; Reduction factor=0.2002

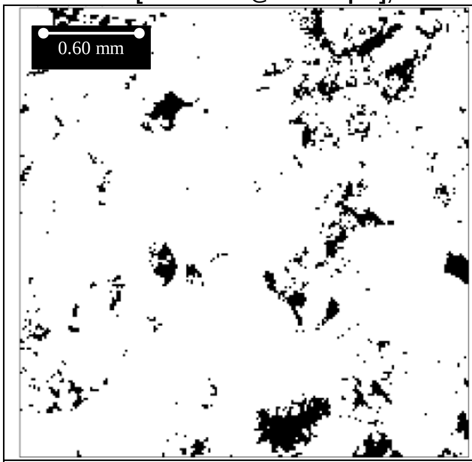

Image# 1

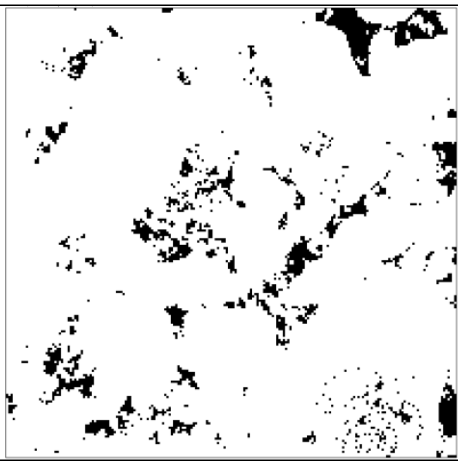

Image# 51

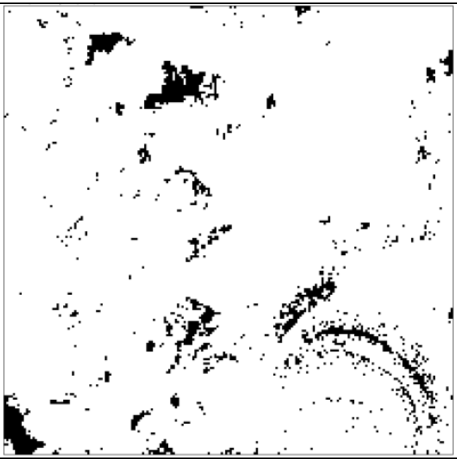

Image# 103

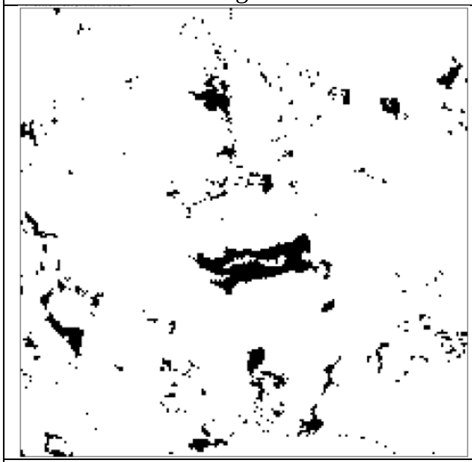

Image# 154

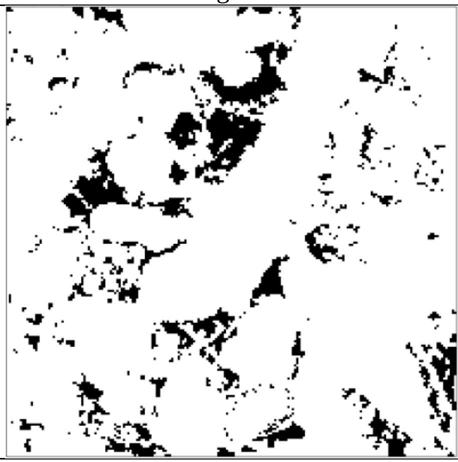

Image# 205

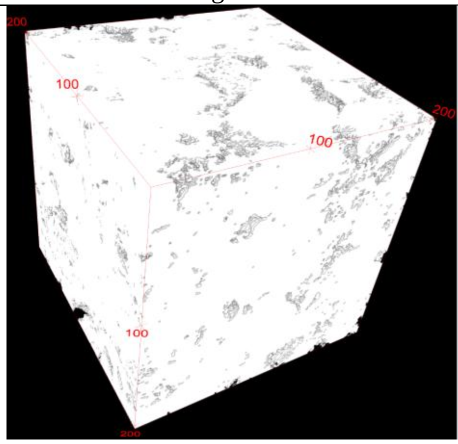

3D image stack

Estaillades [103 voxel^3 @ 26.668 μm]; Reduction factor=0.1006

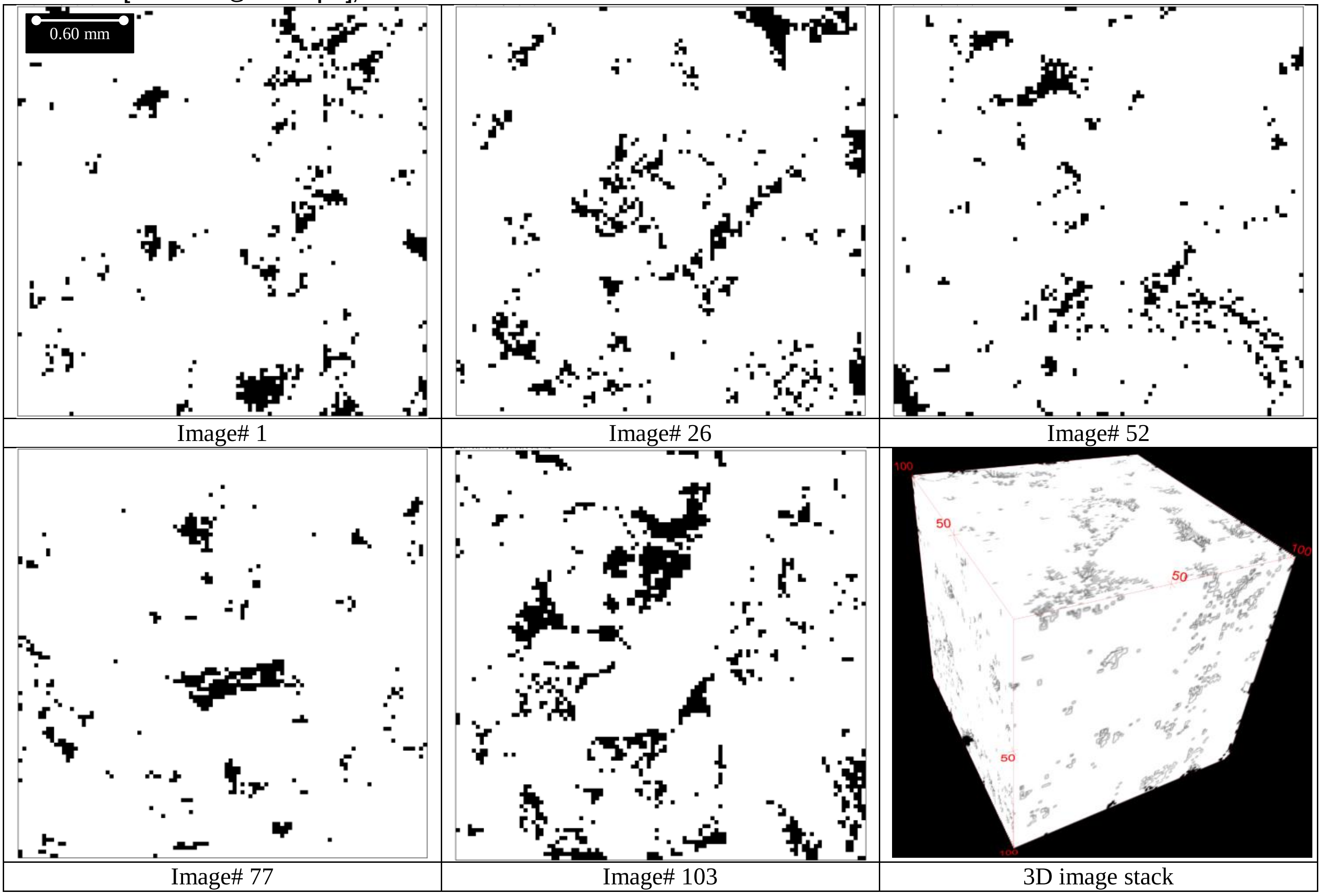

Image# 1 | Image# 26 | Image# 52

Image# 77 | Image# 103 | 3D image stack

Ketton [819 voxel^3 @ 3.318 µm]; Reduction factor=0.7998

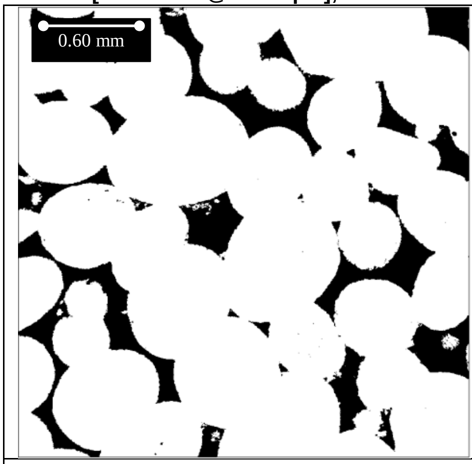	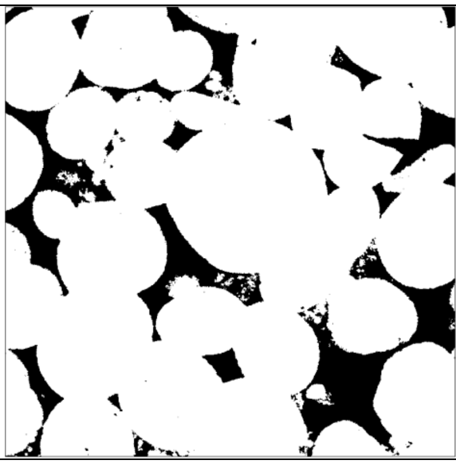	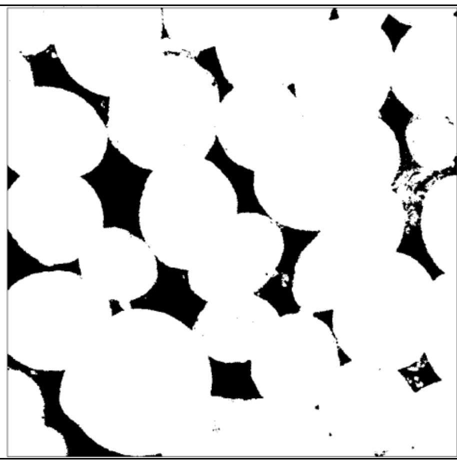
Image# 1	Image# 205	Image# 410
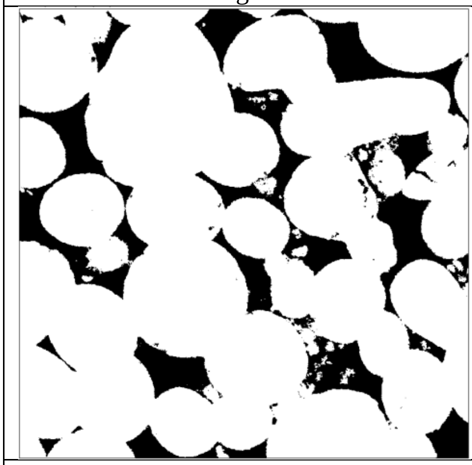	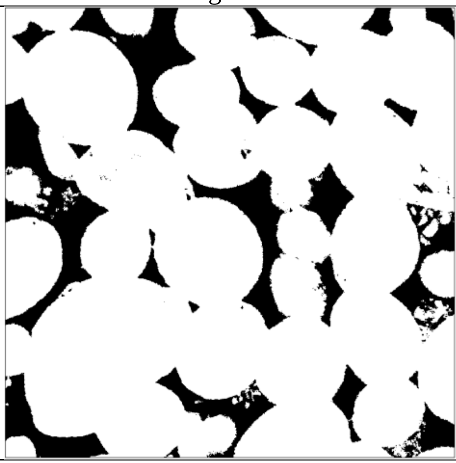	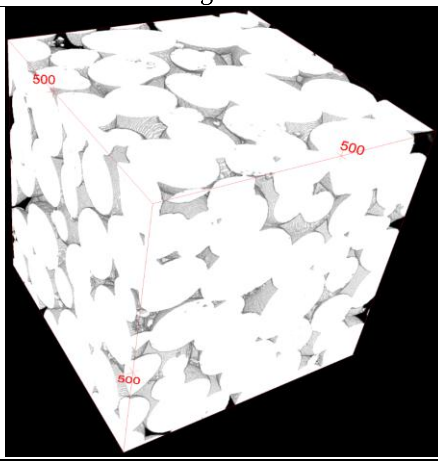
Image# 614	Image# 819	3D image stack

Ketton [615 voxel^3 @ 4.419 µm]; Reduction factor=0.6006

	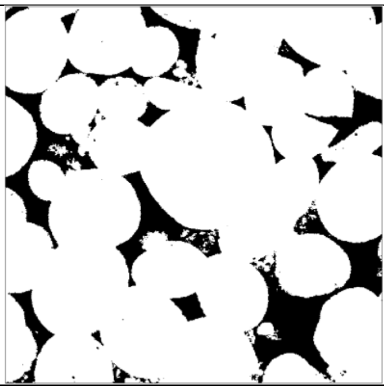	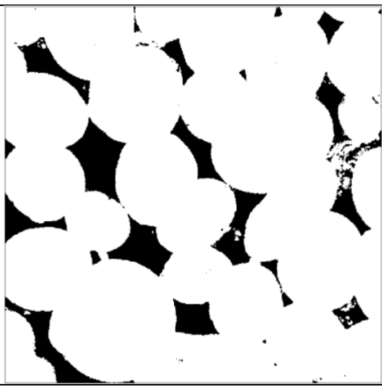
Image# 1	Image# 154	Image# 308
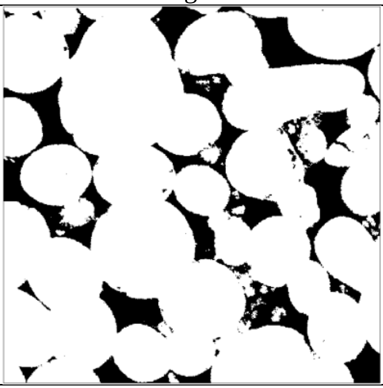	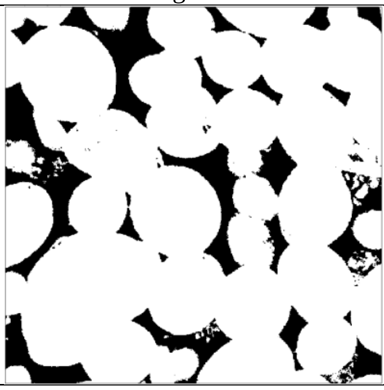	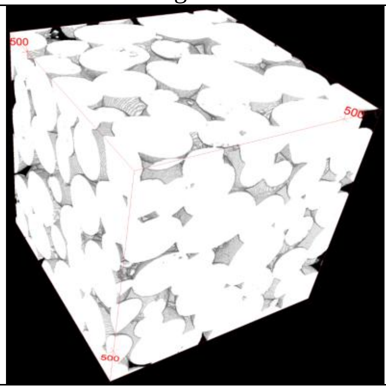
Image# 461	Image# 615	3D image stack

Ketton [410 voxel^3 @ 6.629 µm]; Reduction factor=0.4004

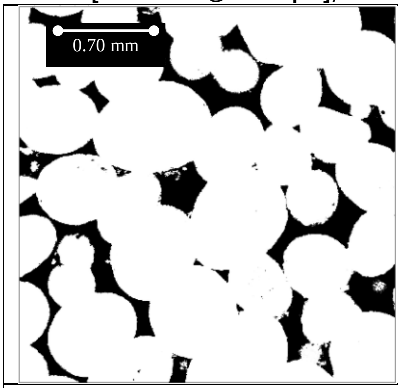	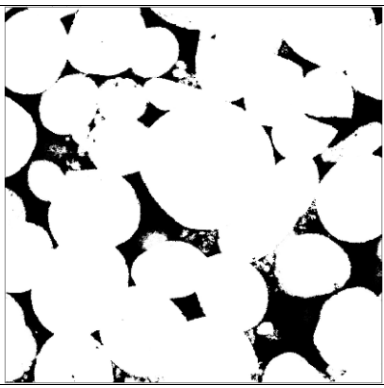	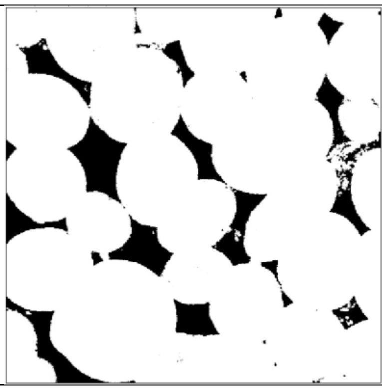
Image# 1	Image# 103	Image# 205
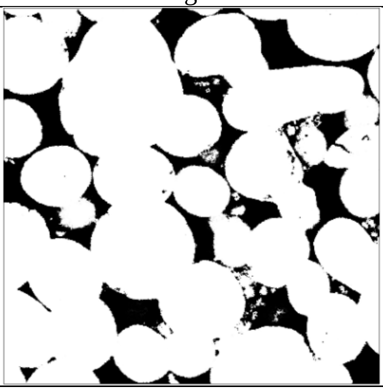	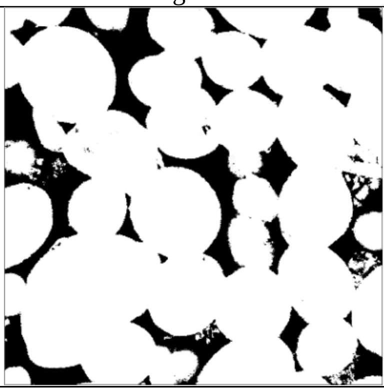	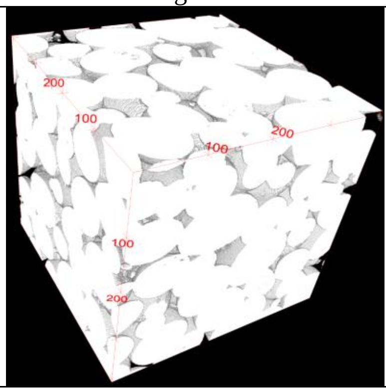
Image# 308	Image# 410	3D image stack

Ketton [205 voxel^3 @ 13.257 μm]; Reduction factor=0.2002

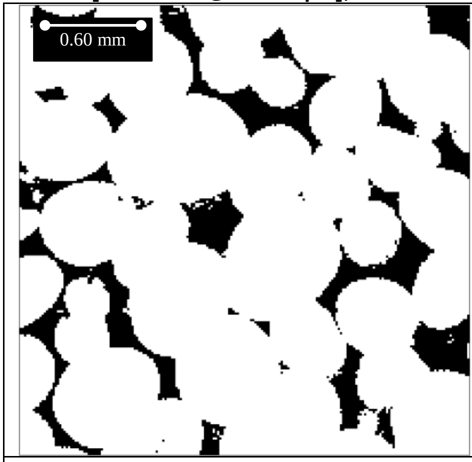	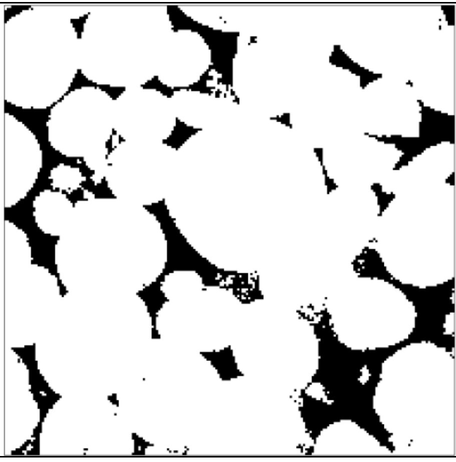	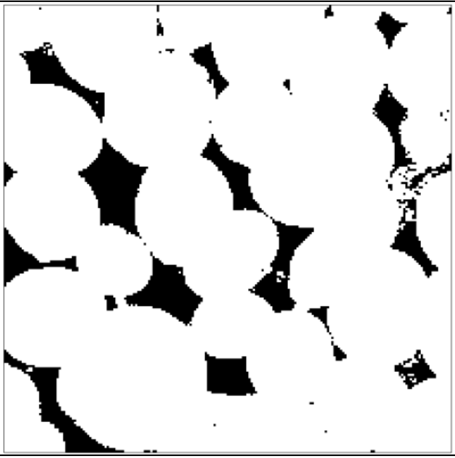
Image# 1	Image# 51	Image# 103
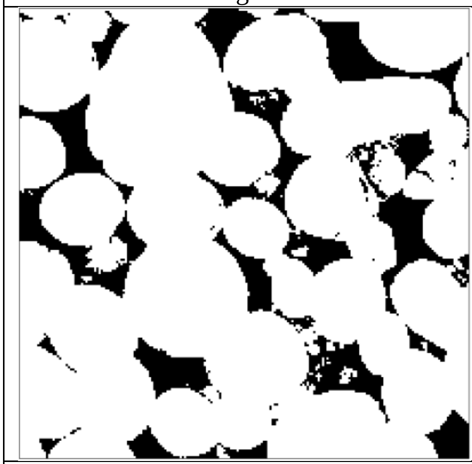	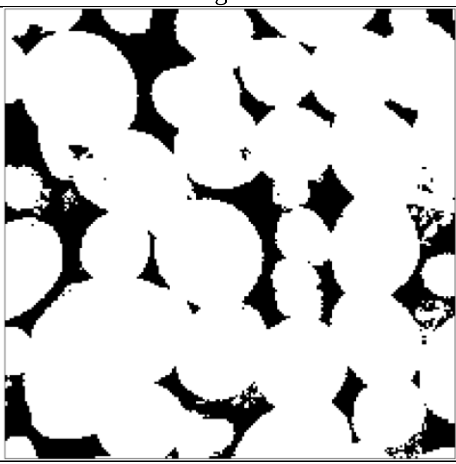	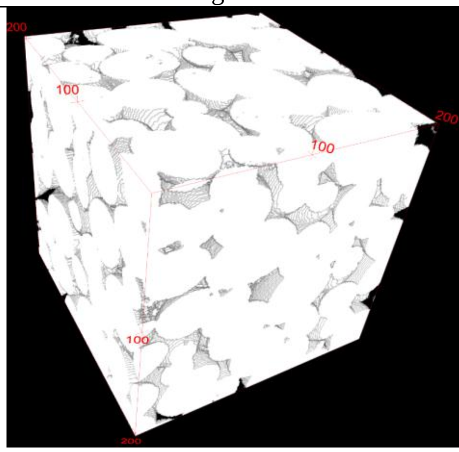
Image# 154	Image# 205	3D image stack

Ketton [103 voxel^3 @ 26.385 µm]; Reduction factor=0.1006

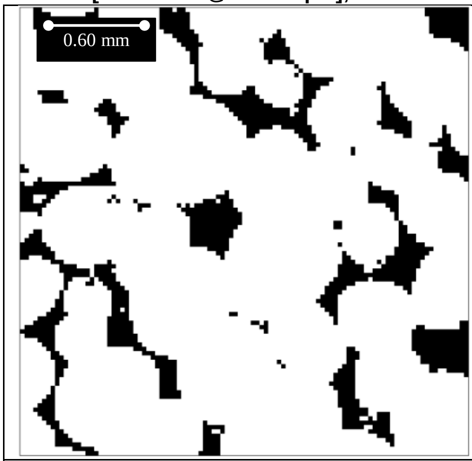	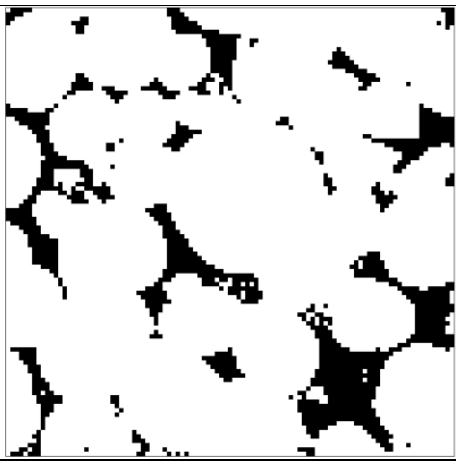	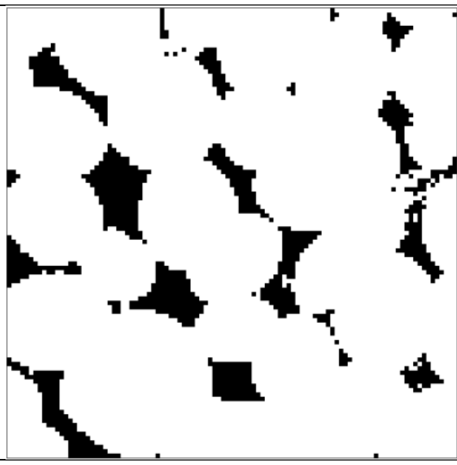
Image# 1	Image# 26	Image# 52
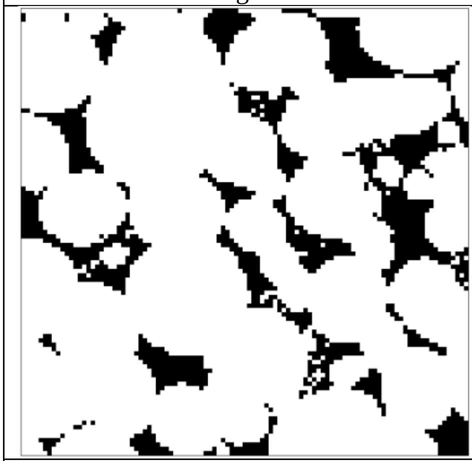	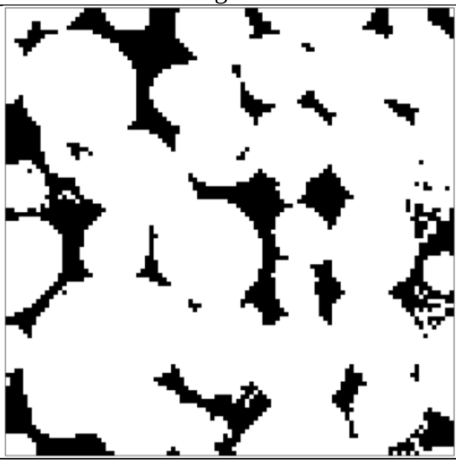	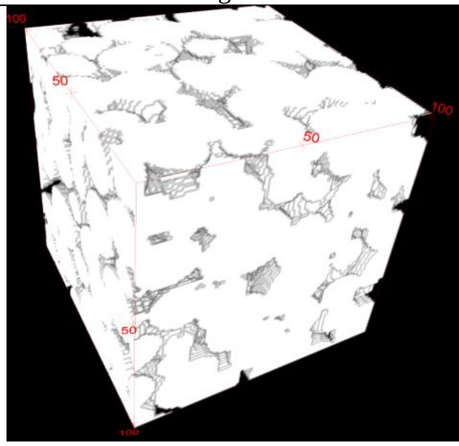
Image# 77	Image# 103	3D image stack

Appendix-IV: Two-phase simulator input code

Since the objective of this research is to examine the changes in basic petrophysical properties, an example code of the ([Per Valvatne, 2004) would serve the purpose because the basic properties output depends on the network itself rather than physical measurement like contact angels and interfacial tensions. The code below is the mixed wet sandstone example from the mentioned reference with minor edits.

```
TITLE
Ketton100SV
#

SAT_TARGET
%finalSat      maxPc      maxDeltaSw     maxDeltaPc     calcKr    calcI
  0.0     1.0E21            0.02          500000.0         T        F
  1.00    -1.0E21        0.002         500000.0         T       F
#

INIT_CON_ANG
0.0  0.0   -0.2   -3.0
#

%FRAC_CON_ANG
%0.75 T 100 160 -1 -1 rand
%#


EQUIL_CON_ANG
3  0.0  37.0   -1.0   -1.0   rand
#

RES_FORMAT
excel
#

RELPERM_DEF
residual  F
#

SAT_COMPRESS
% kr_thres maxDeltaSw OilFlood WatFlood
 0.1 0.001 T T
#

TRAPPING
%   Inject fluid from     allow drainage    water mult fact in
%      entry  exit       of dangling ends    filled circ elem
         T     F                T               0.0E-30
#

SOLVER_TUNE
%     min         Memory Scaling    Solver       Verbose     Conductance
%  tolerance         Factor         output       Solver       Cut-Off
    1.0E-30            8              0            F            0.0
#

PRS_BDRS
% calc kr using   record press    num press
%  avg press        profiles      profiles
      F                F             20
#
```

```
PORE_FILL_ALG
blunt2
#

PORE_FILL_WGT
0.0 74095 74095 74095 74095 74095
#

FLUID
% interfacial     water        oil        water          oil        water     oil
%  tension      viscosity    viscosity    resistivity    resistivity  density
density
%   (mN/m)        (cp)         (cp)        (Ohm.m)        (Ohm.m)     (kg/m3)
(kg/m3)
     52.3      1.085        0.92      0.0699           1000.0      1029.8     729.0
#

CALC_BOX
0  1
#

NETWORK
F  Ketton100SV
#

SAT_COVERGENCE
%  minNumFillings   initStepSize   cutBack   maxIncr   stable disp
       10               0.1          0.8       2.0          F
#
```

Appendix-V: Relative Permeability and Capillary Pressure data, Sub-Volume Study

Values of relative permeability and capillary pressure data are plotted in this appendix as important additional data. However, it is not compared to experimental results.

Berea [1024 voxel^3 @ 2.7745 μm]

Drainage cycle. Data points: 652

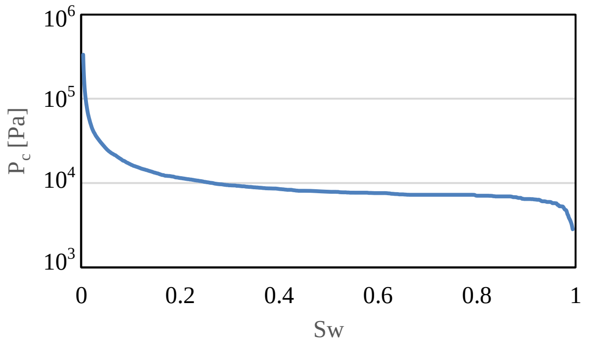

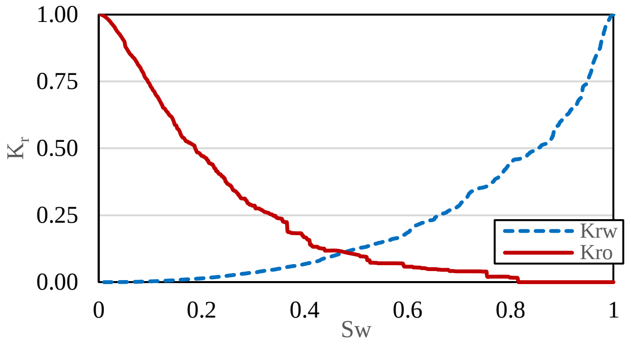

Imbibition cycle. Data points: 287

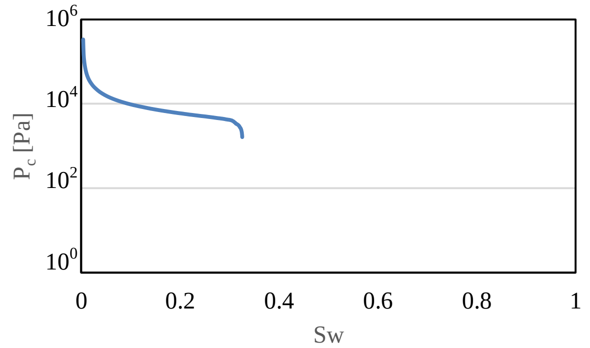

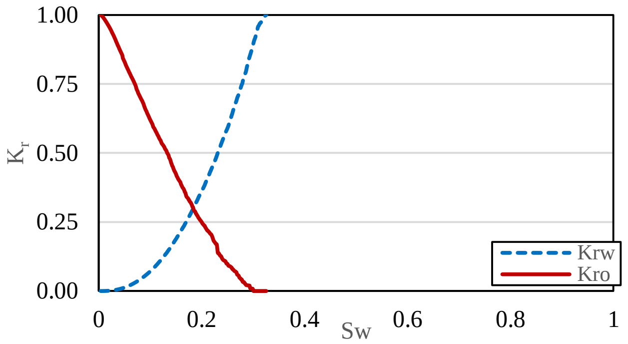

Berea [800 voxel^3 @ 2.7745 μm]

Drainage cycle. Data points: 532

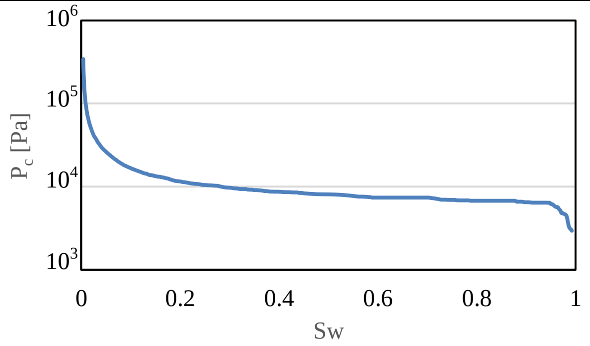

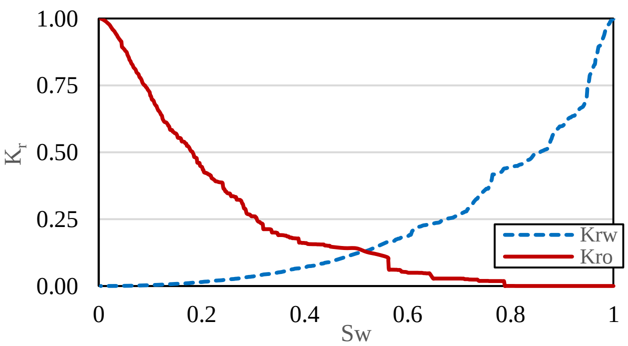

Imbibition cycle. Data points: 277

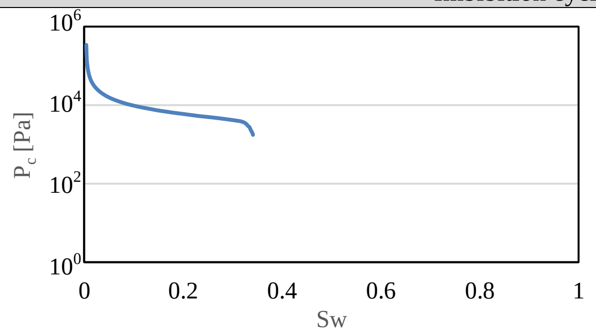

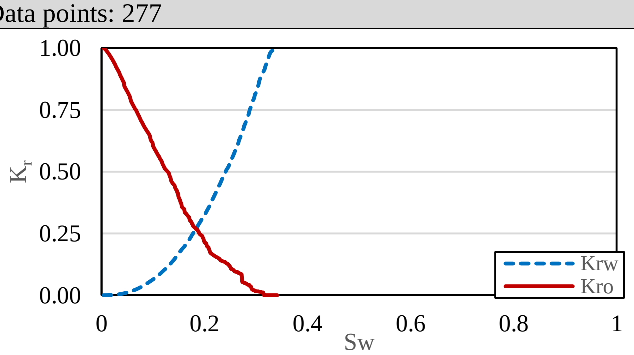

Berea [400 voxel^3 @ 2.7745 μm]

Drainage cycle. Data points: 225

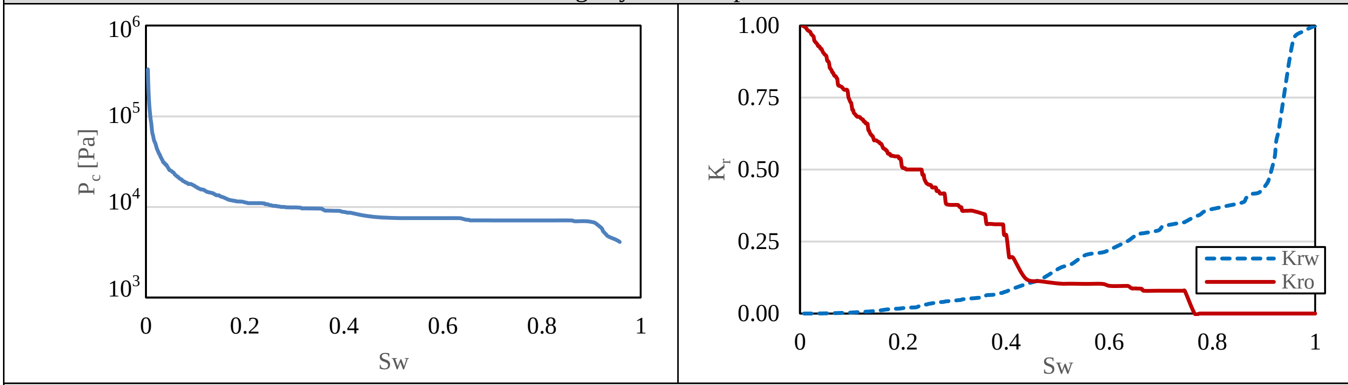

Imbibition cycle. Data points: 177

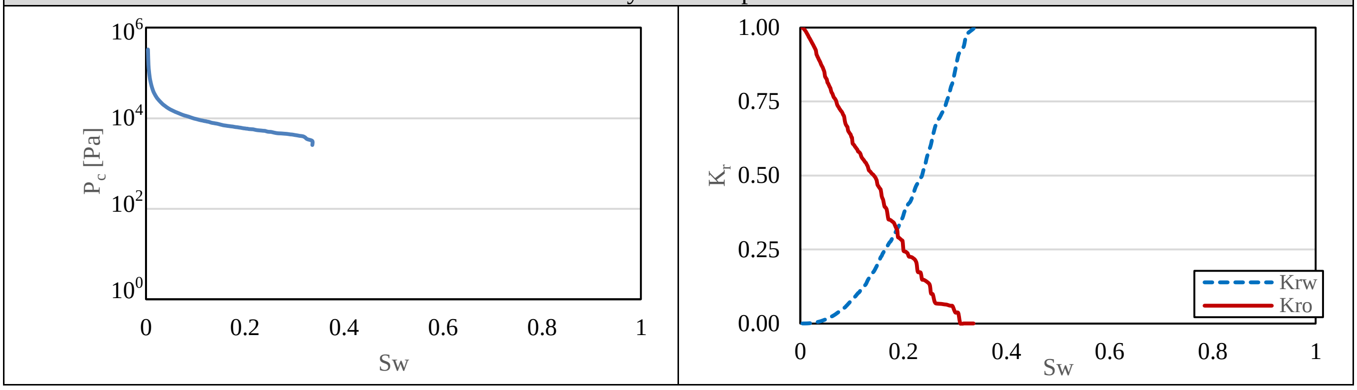

Berea [200 voxel^3 @ 2.7745 μm]

Drainage cycle. Data points: 79

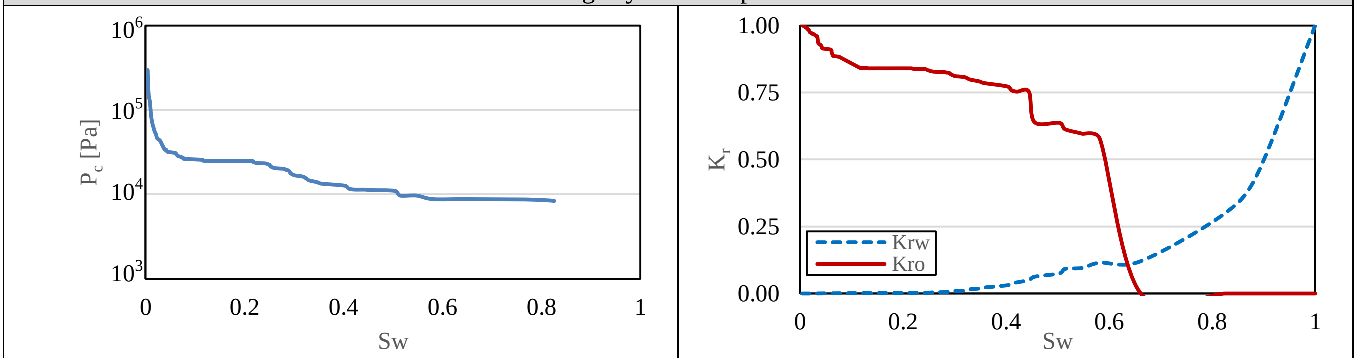

Imbibition cycle. Data points: 63

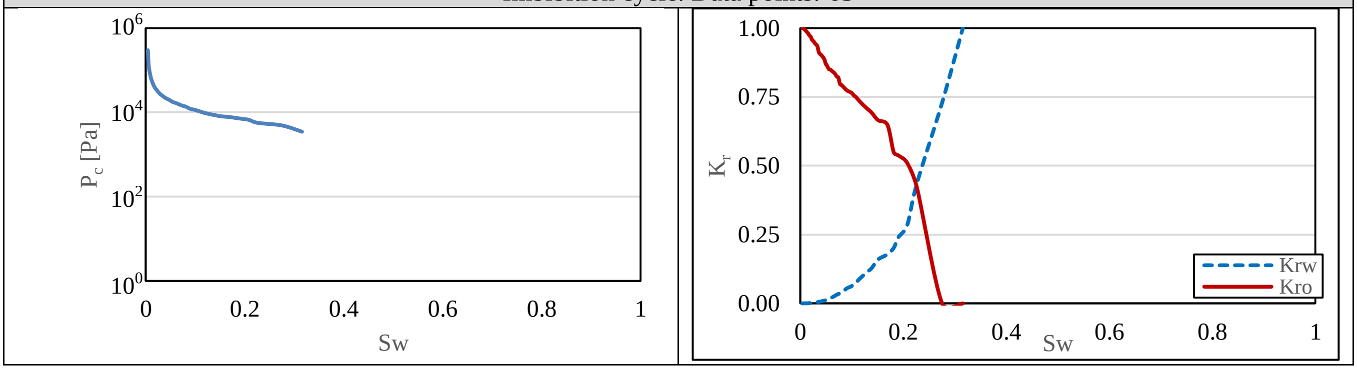

Doddington [600 voxel³ @ 2.7745 µm]

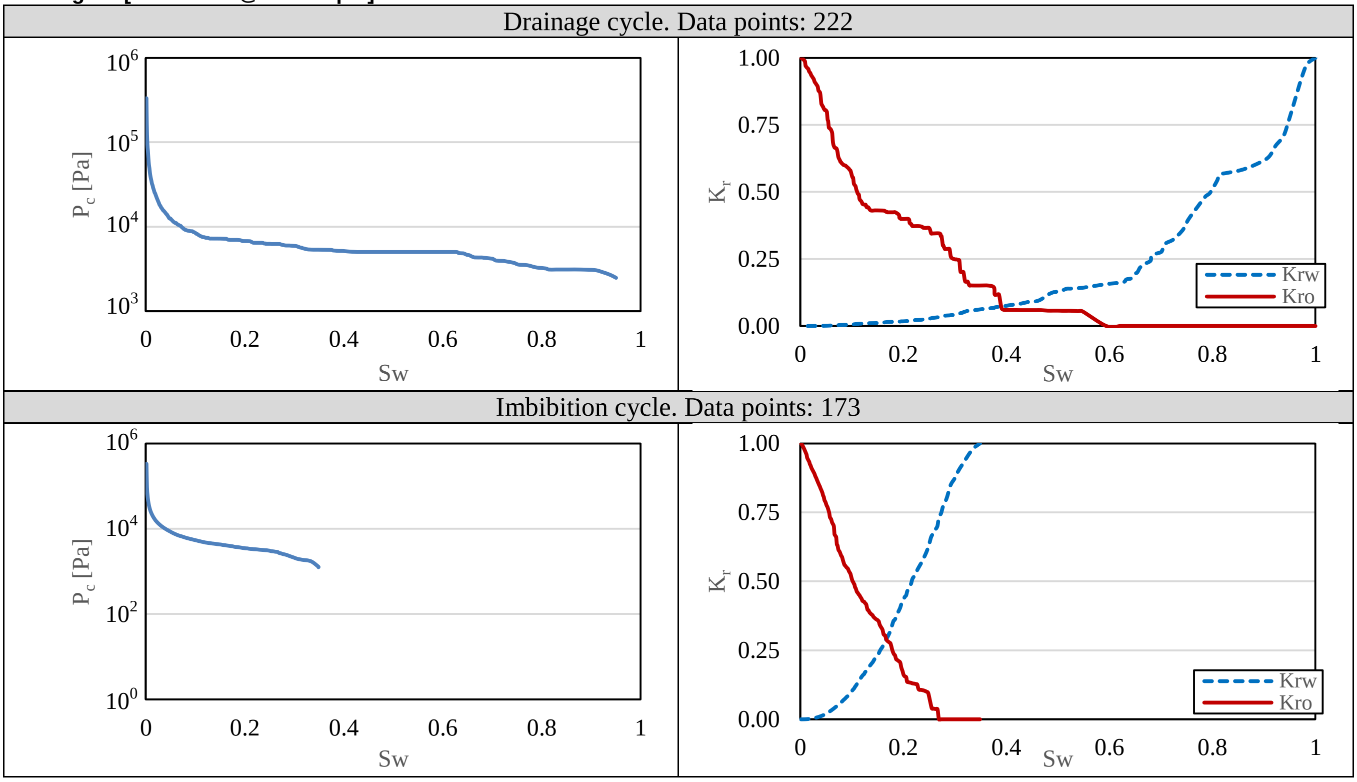

Doddington [400 voxel³ @ 2.7745 µm]

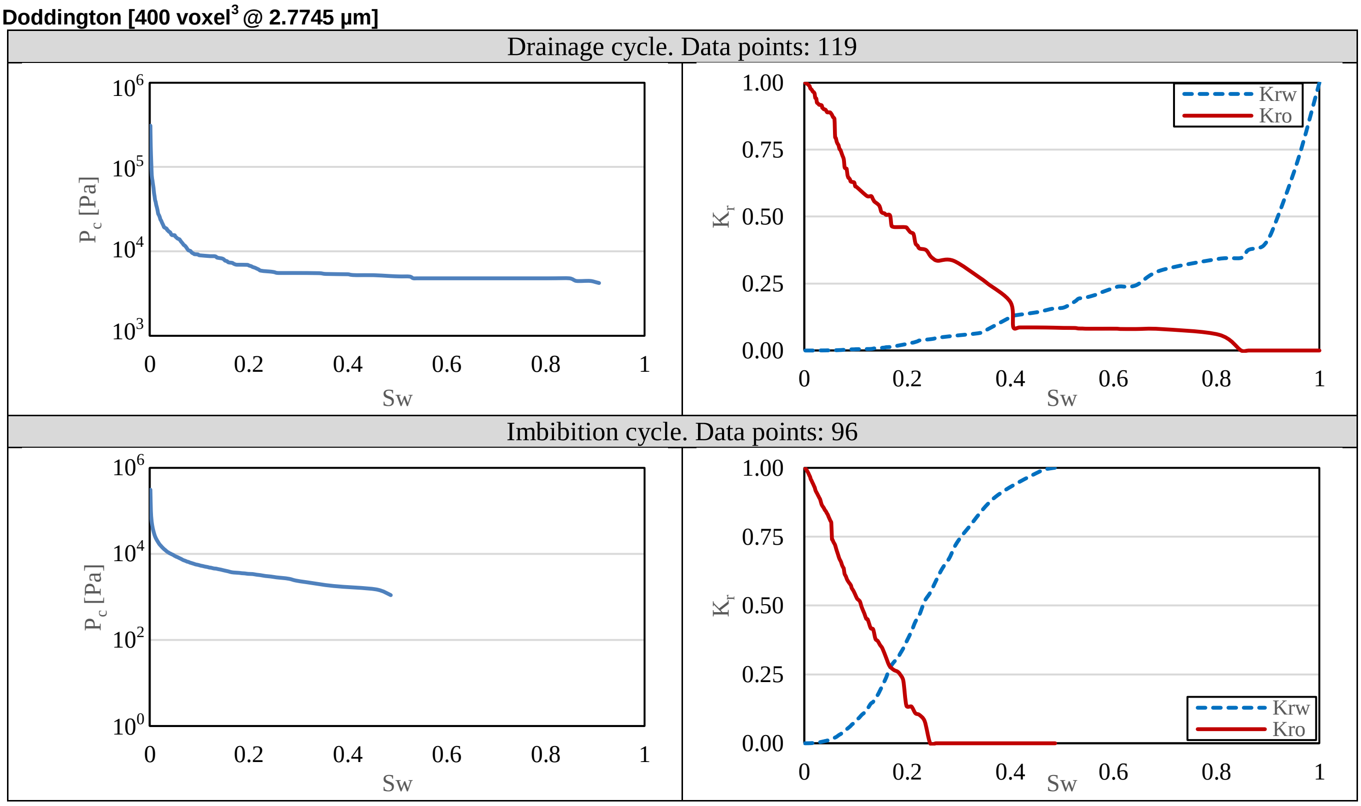

Doddington [200 voxel^3 @ 2.7745 µm]

Drainage cycle. Data points: 25

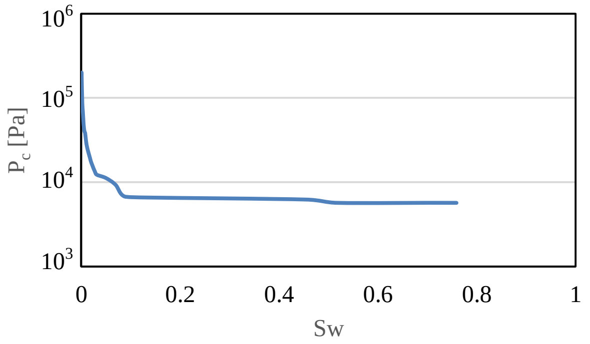

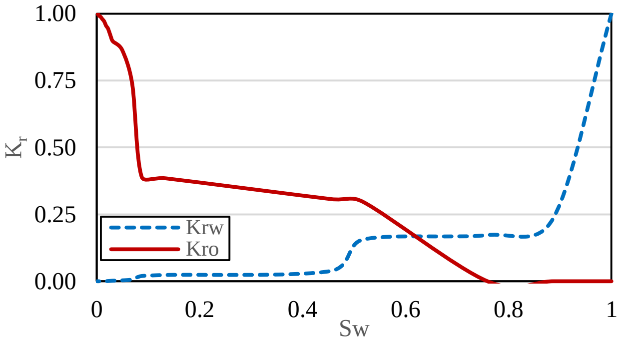

Imbibition cycle. Data points: 0
No data

Doddington [100 voxel^3 @ 2.7745 µm]

Drainage cycle. Data points: 0
No data
Imbibition cycle. Data points: 0
No data

Estaillades [1024 voxel^3 @ 2.6824 µm]

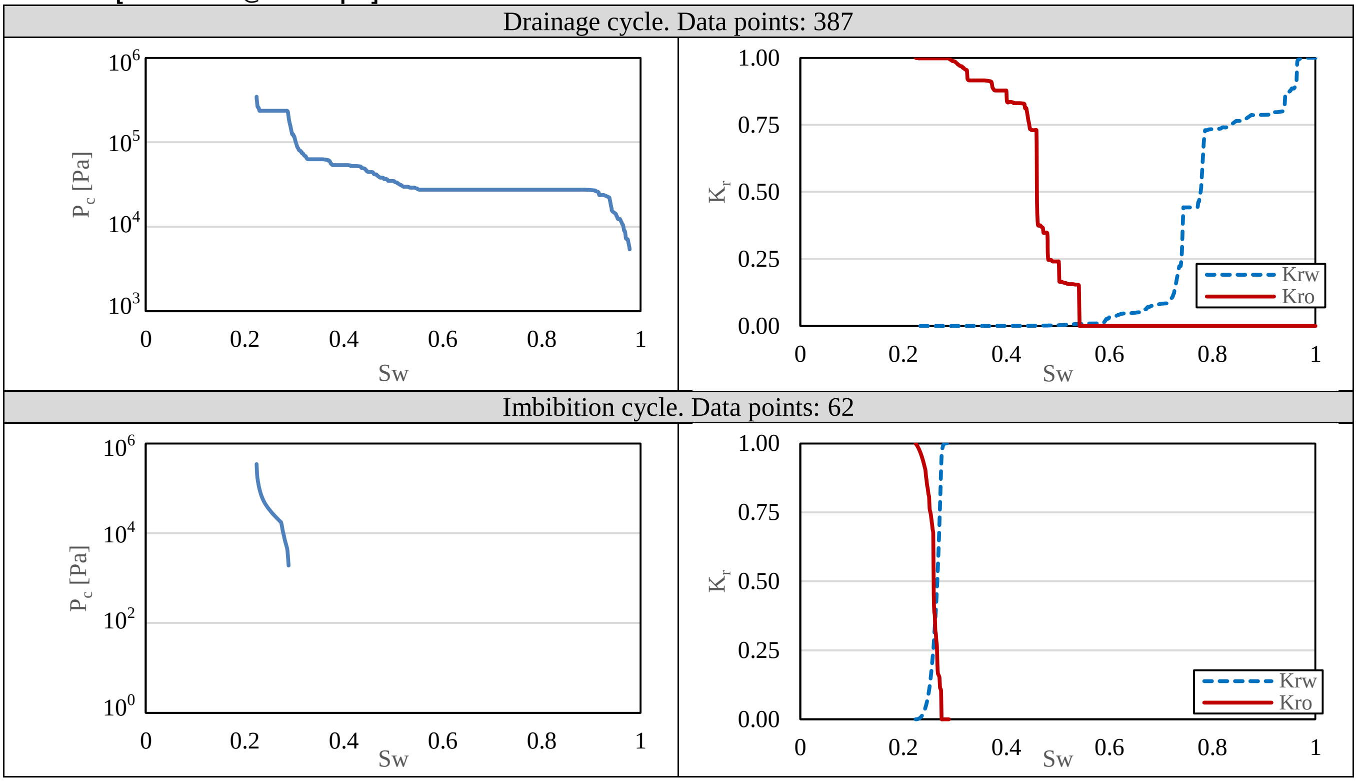

Estaillades [800 voxel^3 @ 2.6824 µm]

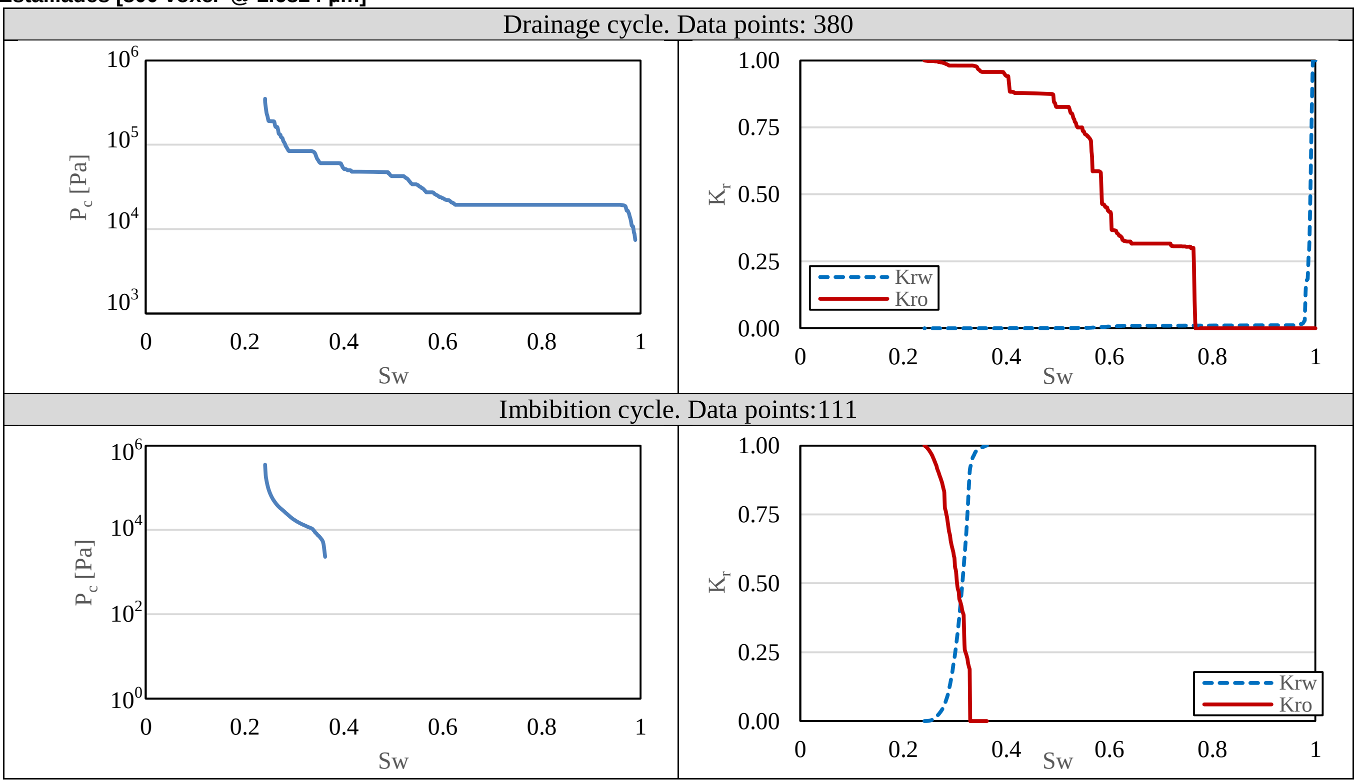

Estaillades [400 voxel^3 @ 2.6824 μm]

Drainage cycle. Data points: 290

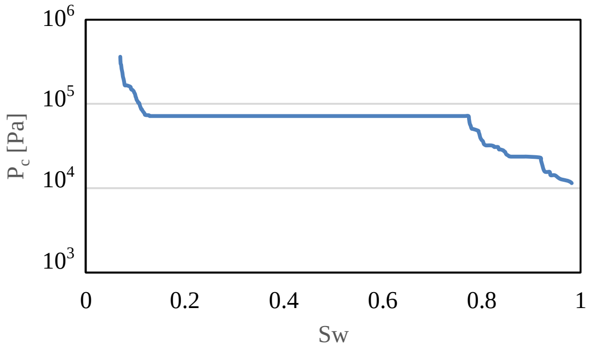

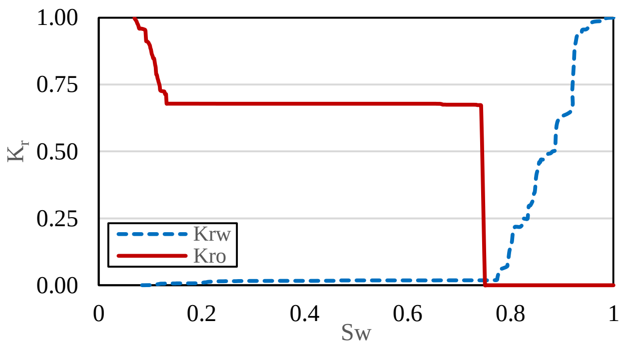

Imbibition cycle. Data points: 114

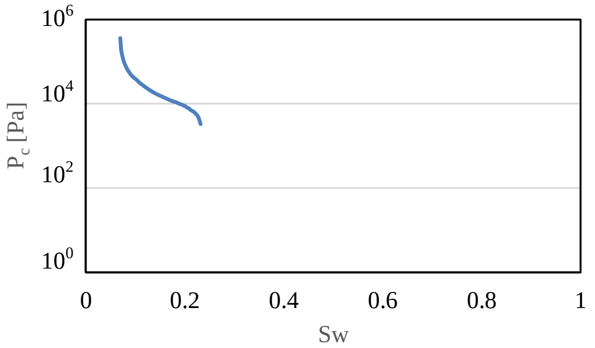

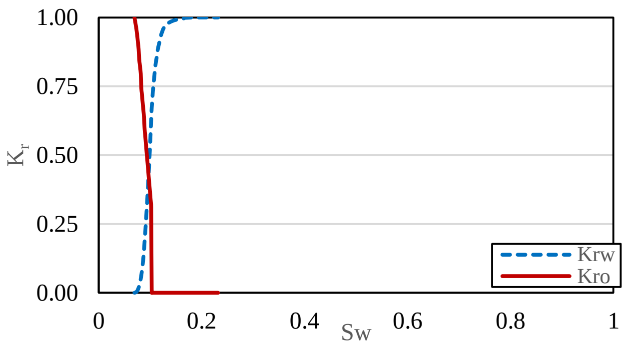

Estaillades [200 voxel^3 @ 2.6824 μm]

Drainage cycle. Data points: 10
No meaningful data
Imbibition cycle. Data points: 2
No meaningful data

Estaillades [100 voxel^3 @ 2.6824 μm]

Drainage cycle. Data points:
No data
Imbibition cycle. Data points:
No data

Ketton [600 voxel³ @ 2.6824 μm]

Drainage cycle. Data points: 69	
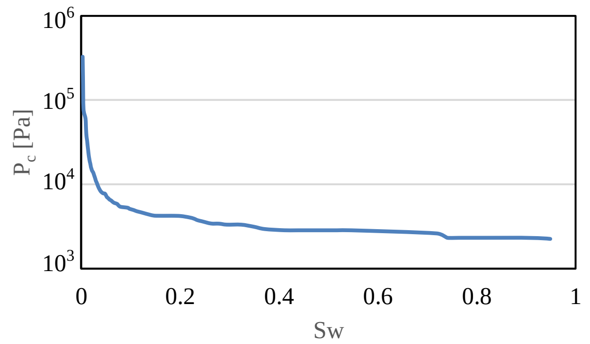	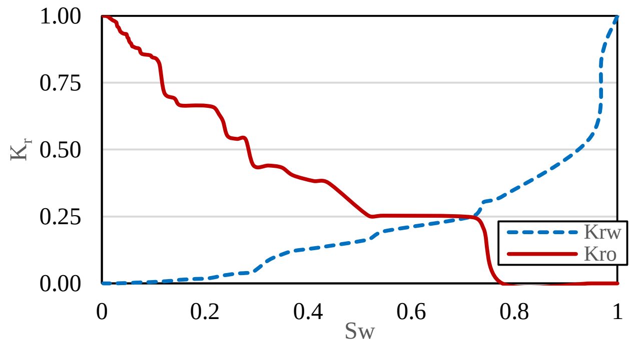

Imbibition cycle. Data points: 0
No data

Ketton [400 voxel³ @ 2.654 μm]

Drainage cycle. Data points: 41	
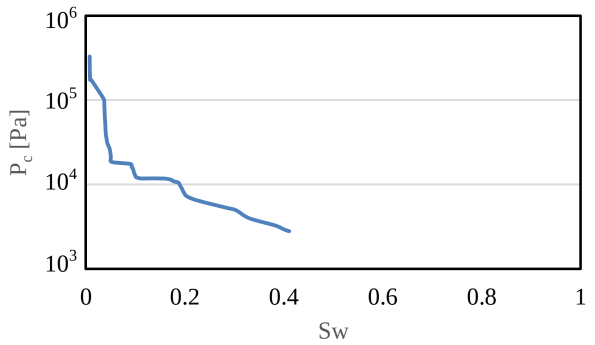	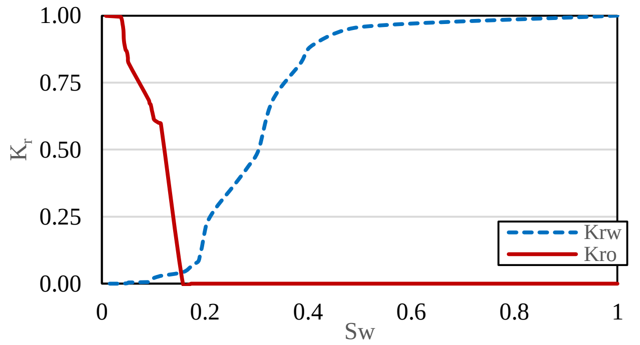

Imbibition cycle. Data points: 31	
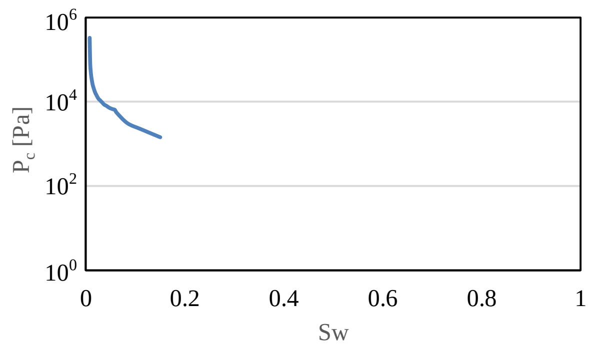	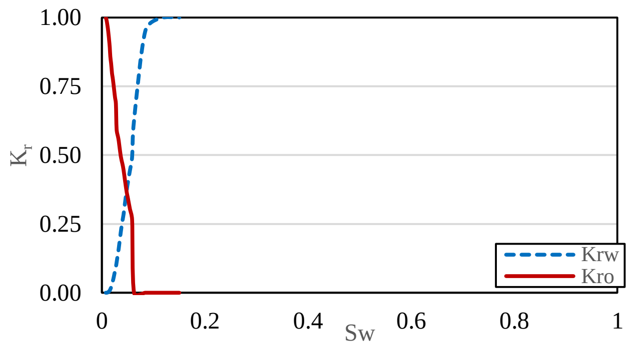

Ketton [200 voxel³ @ 2.654 μm]

Drainage cycle. Data points: 0
No data
Imbibition cycle. Data points: 0
No data

Ketton [100 voxel³ @ 2.654 μm]

Drainage cycle. Data points: 0
No data
Imbibition cycle. Data points: 0
No data

Appendix-VI: Relative Permeability and Capillary Pressure data, Resolution Study

Values of relative permeability and capillary pressure data are plotted in this appendix as important additional data. However, it is not compared to experimental results.

Berea [819 voxel^3 @ 3.469 µm]; Reduction factor=0.7998

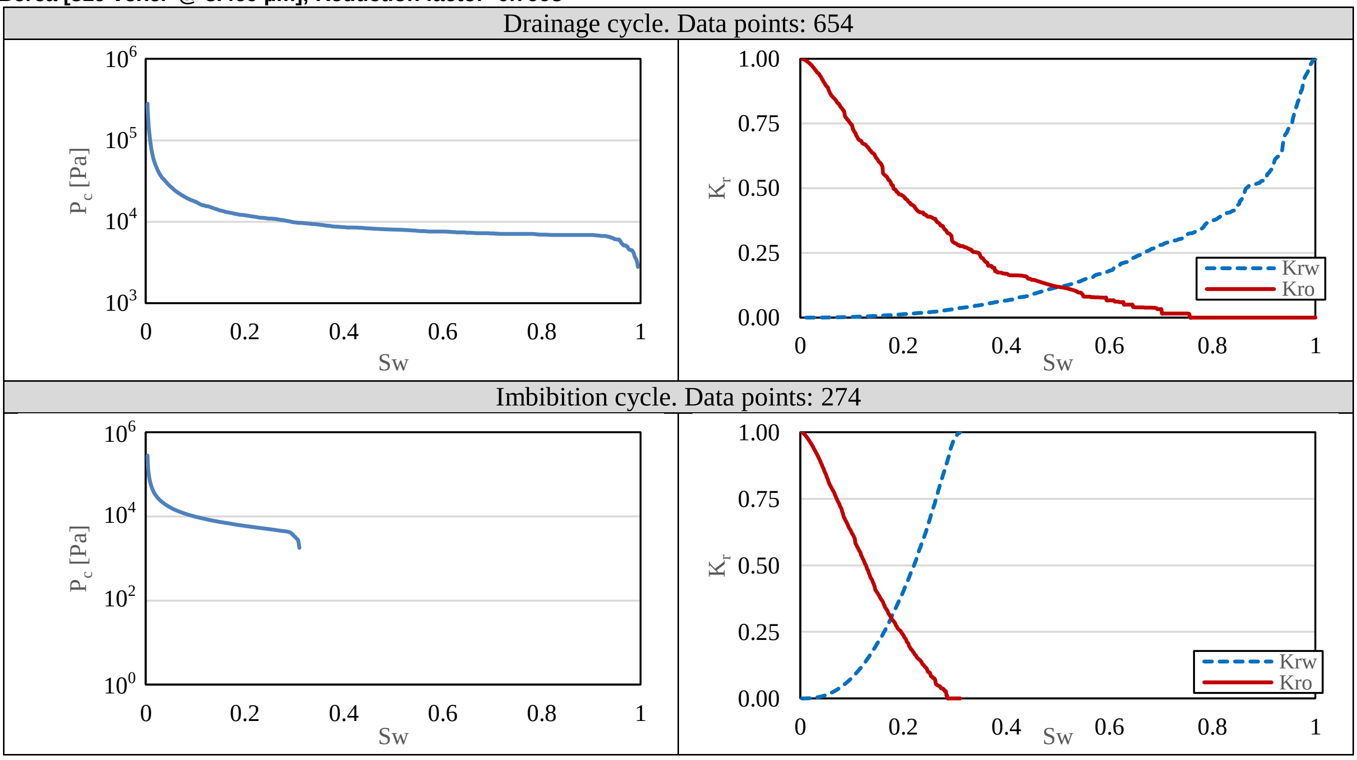

Berea [615 voxel^3 @ 4.620 µm]; Reduction factor=0.6006

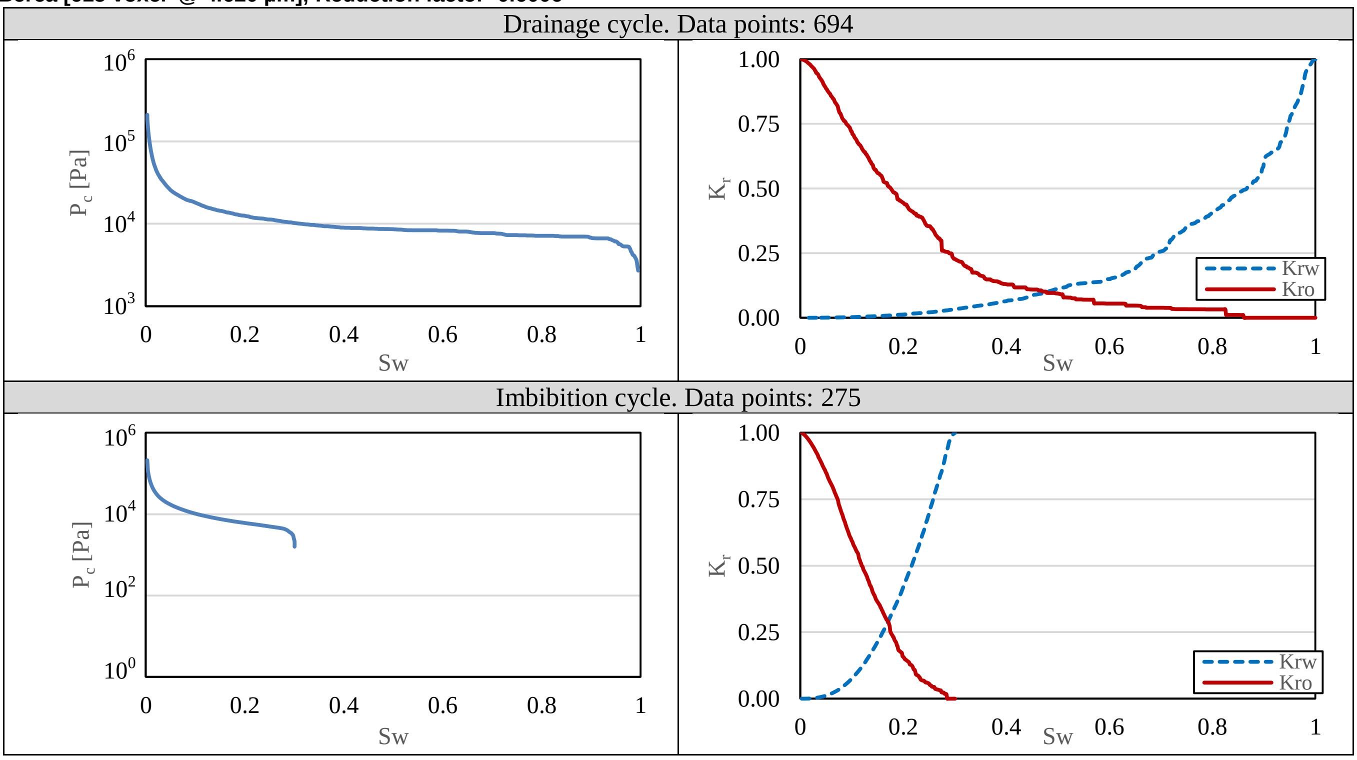

Berea [410 voxel^3 @ 6.929 µm]; Reduction factor=0.4004

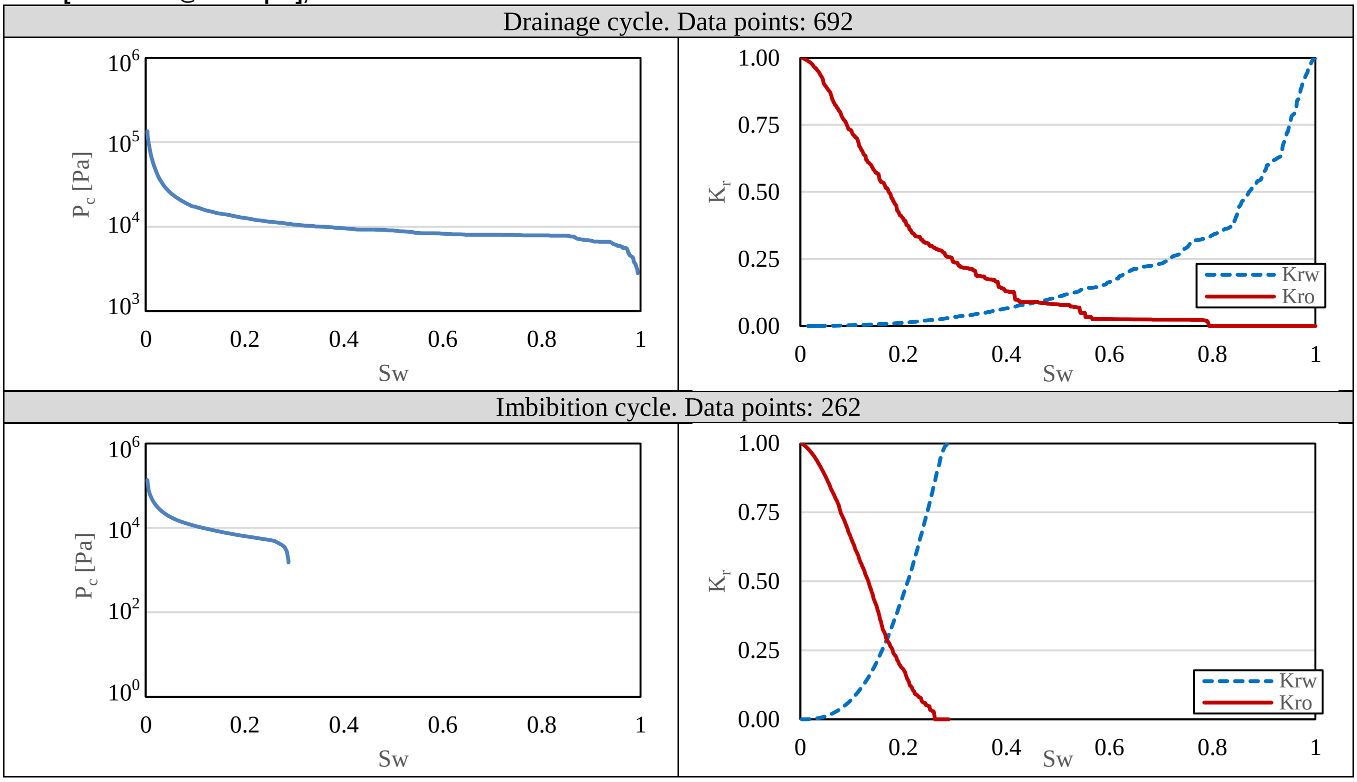

Berea [205 voxel^3 @ 13.859 µm]; Reduction factor=0.2002

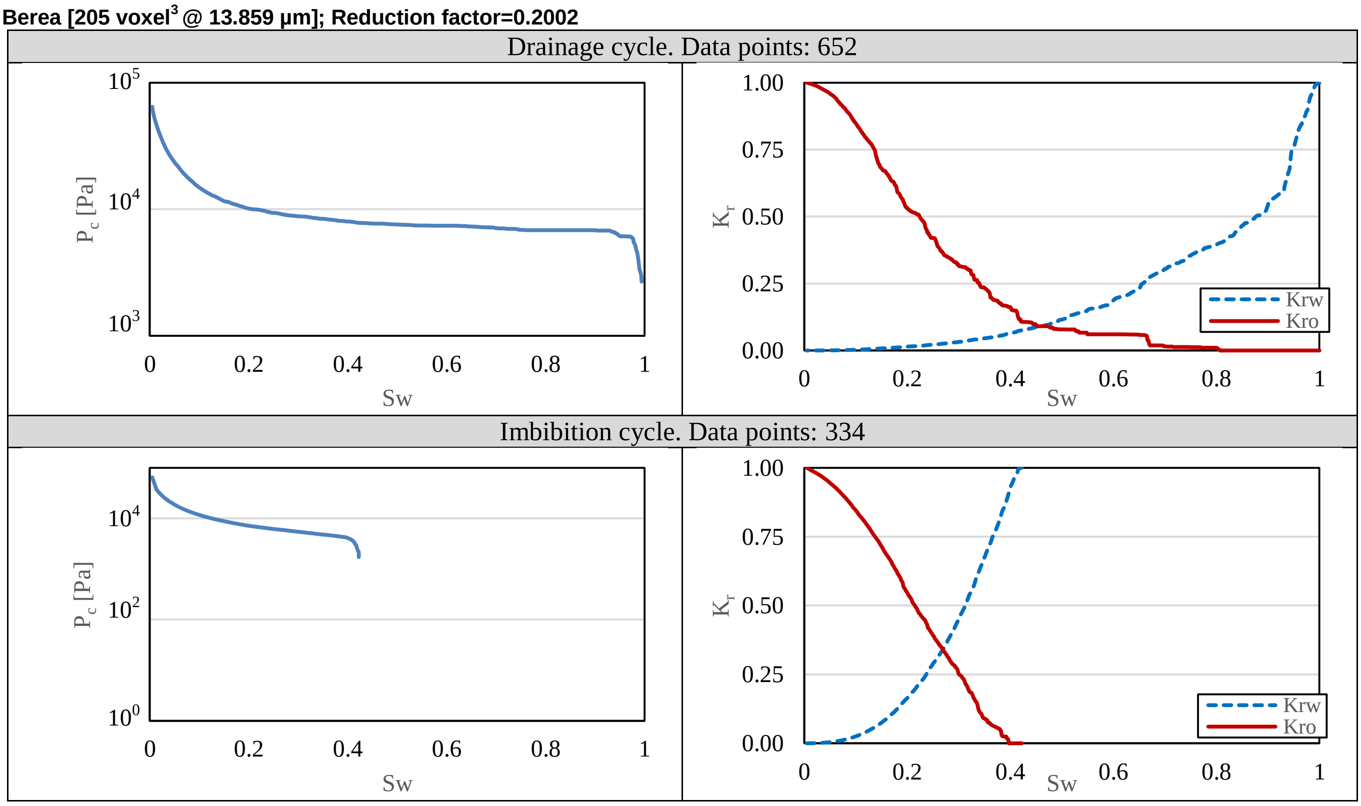

Berea [103 voxel^3 @ 27.583 μm]; Reduction factor=0.1006

Drainage cycle. Data points: 154

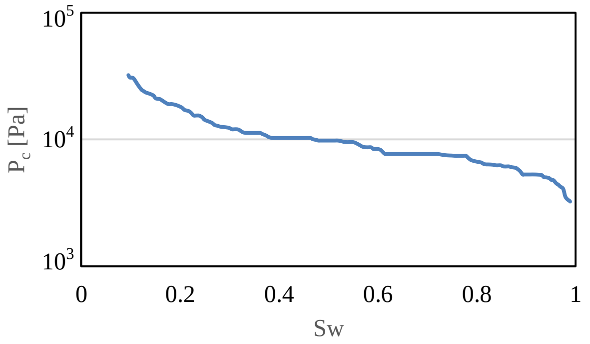

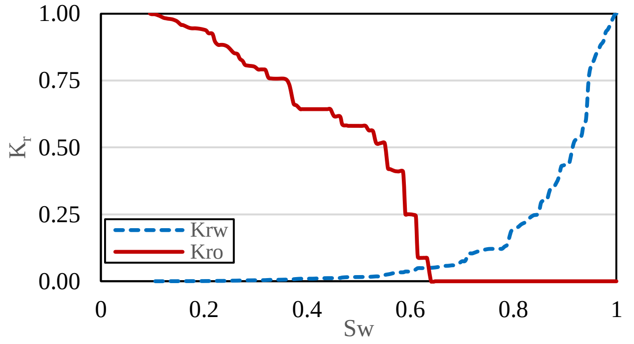

Imbibition cycle. Data points: 64

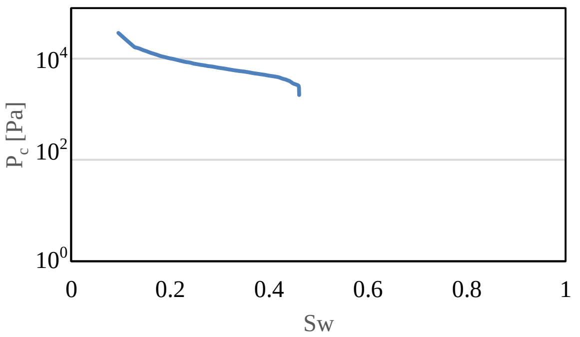

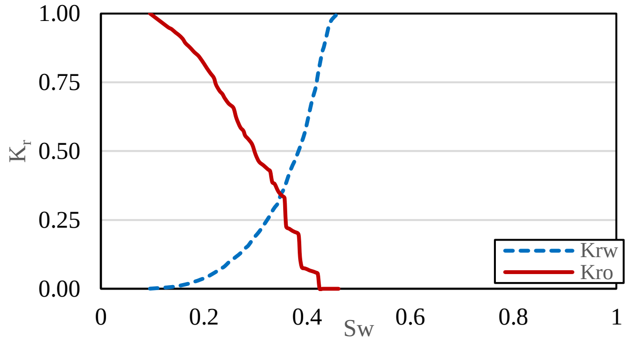

Doddington [615 voxel³ @ 4.620 μm]; Reduction factor=0.6006

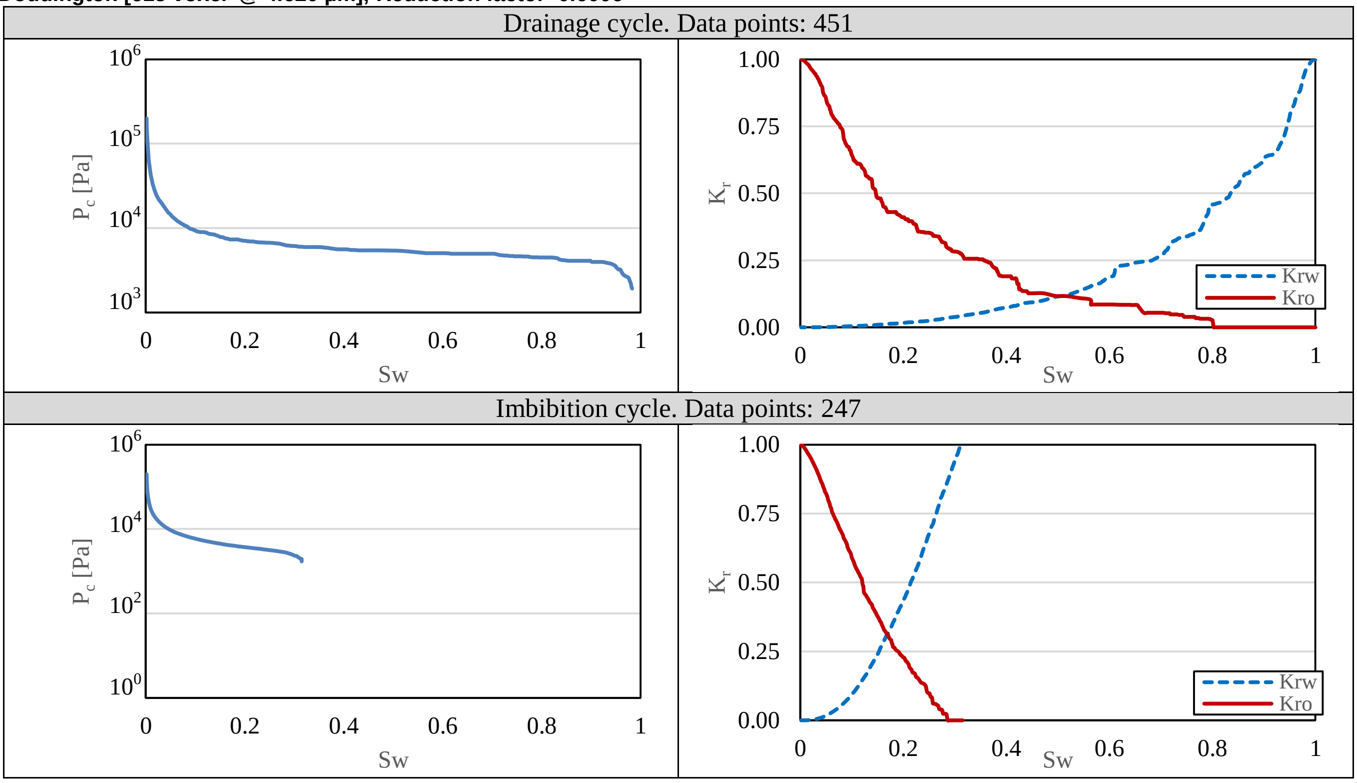

Doddington [410 voxel³ @ 6.929 μm]; Reduction factor=0.4004

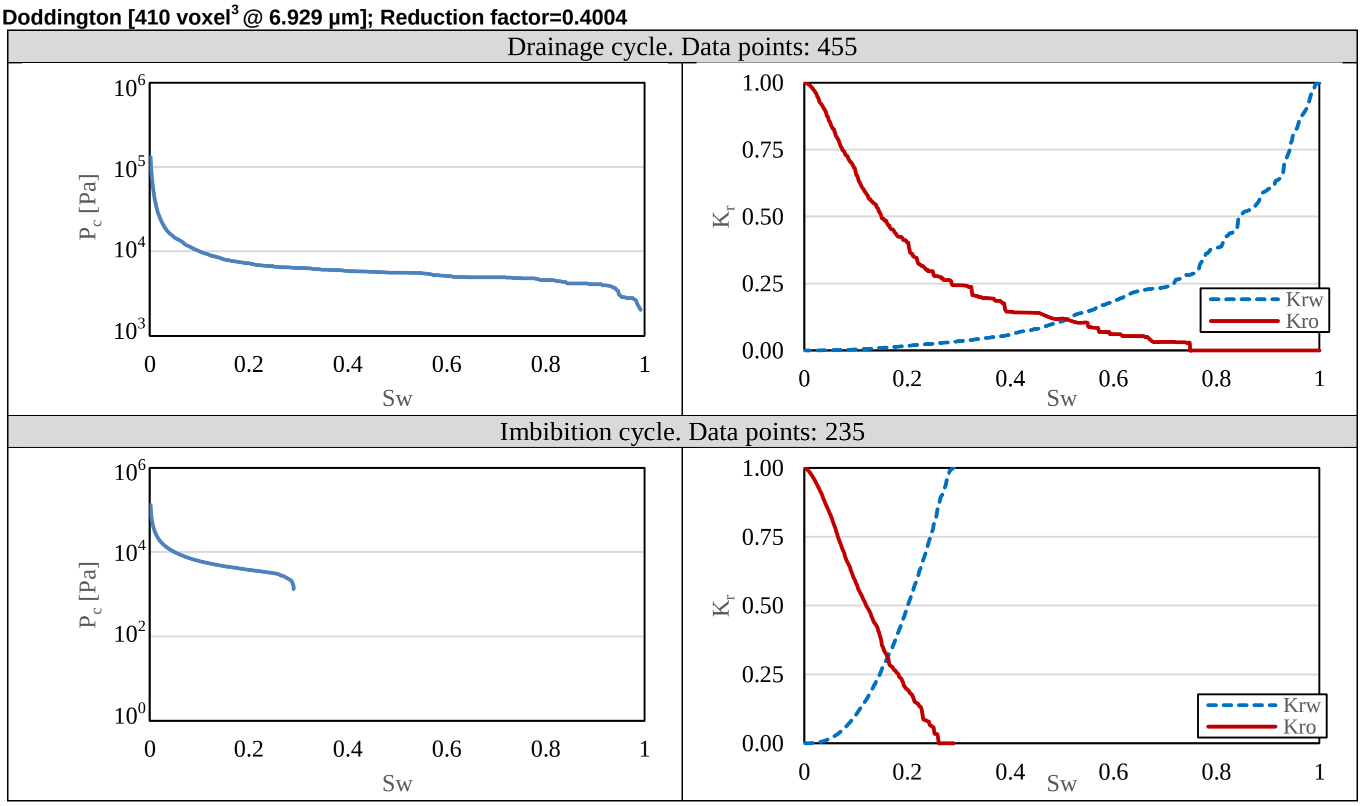

Doddington [205 voxel^3 @ 13.859 µm]; Reduction factor=0.2002

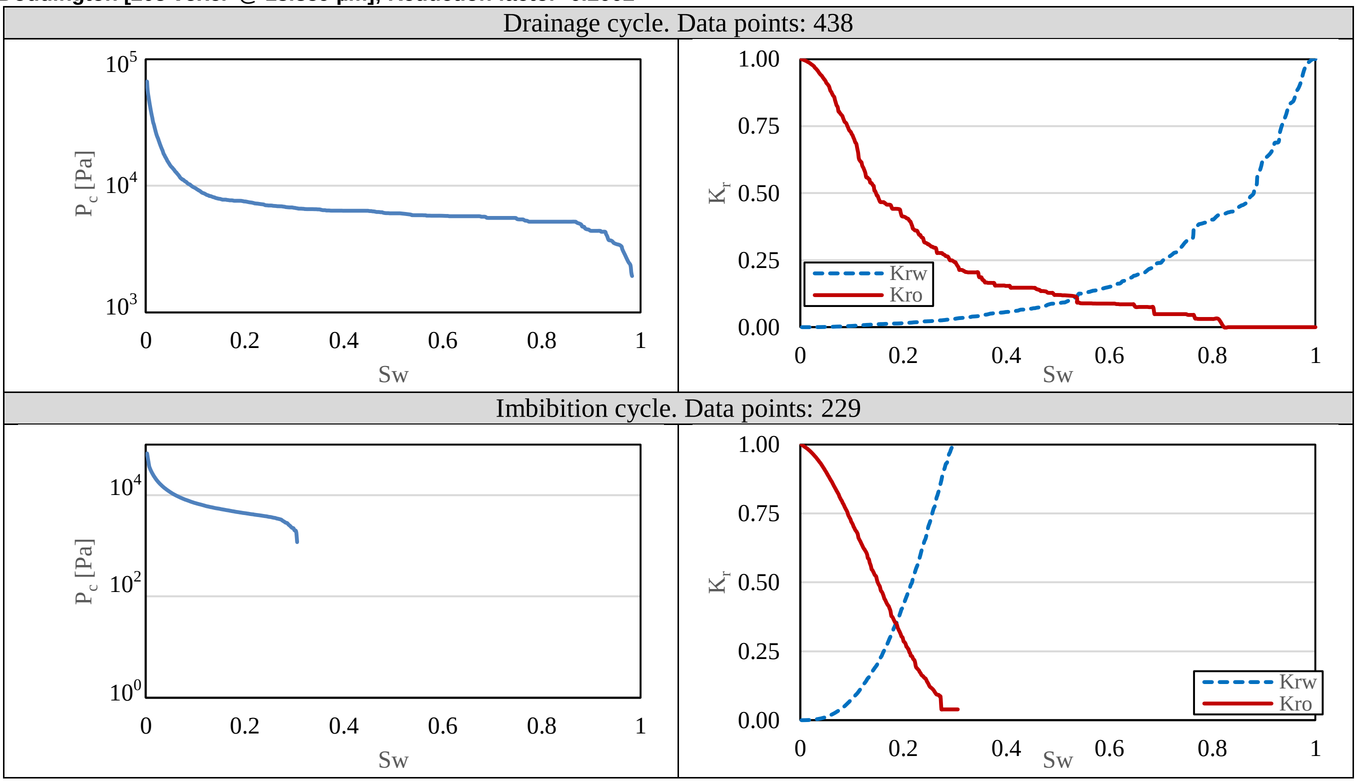

Doddington [103 voxel^3 @ 27.583 µm]; Reduction factor=0.1006

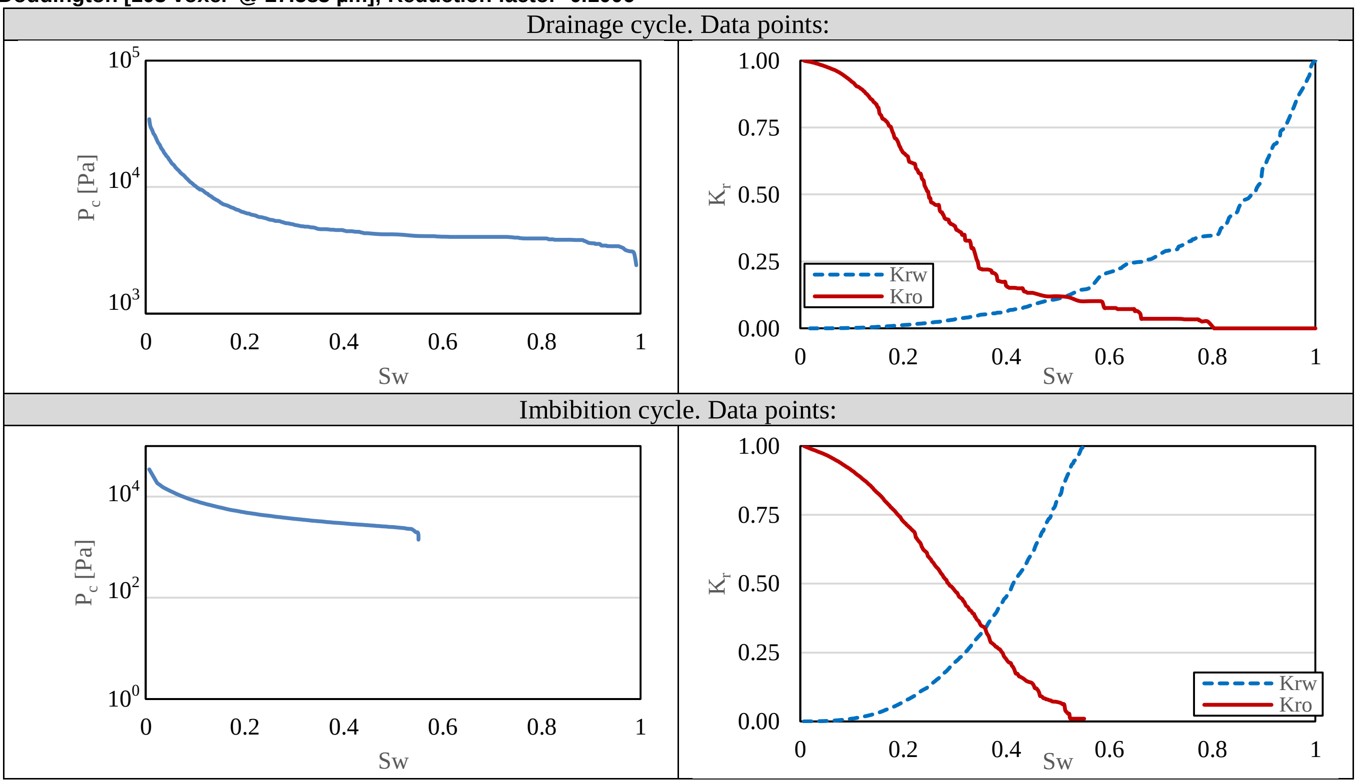

Estaillades [819 voxel^3 @ 3.354 µm]; Reduction factor=0.7998

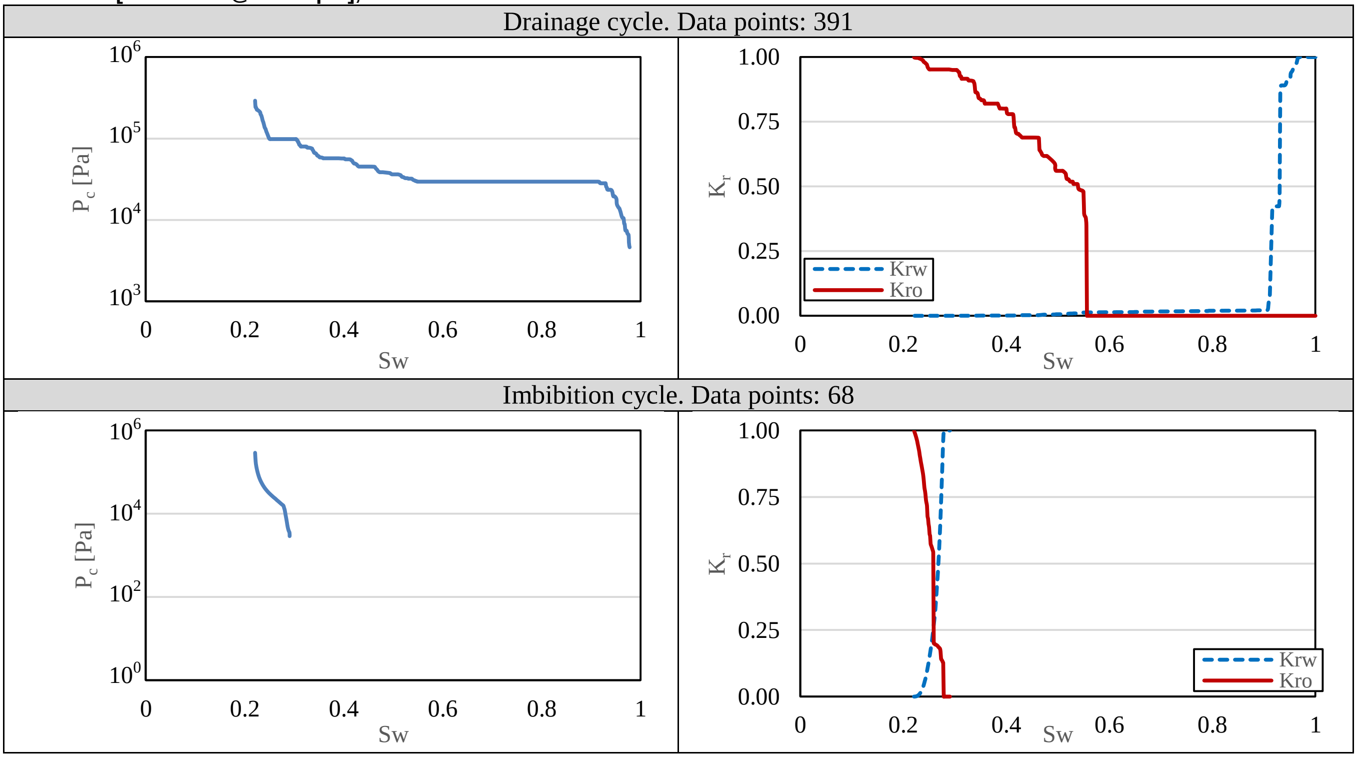

Estaillades [615 voxel^3 @ 4.466 µm]; Reduction factor=0.6006

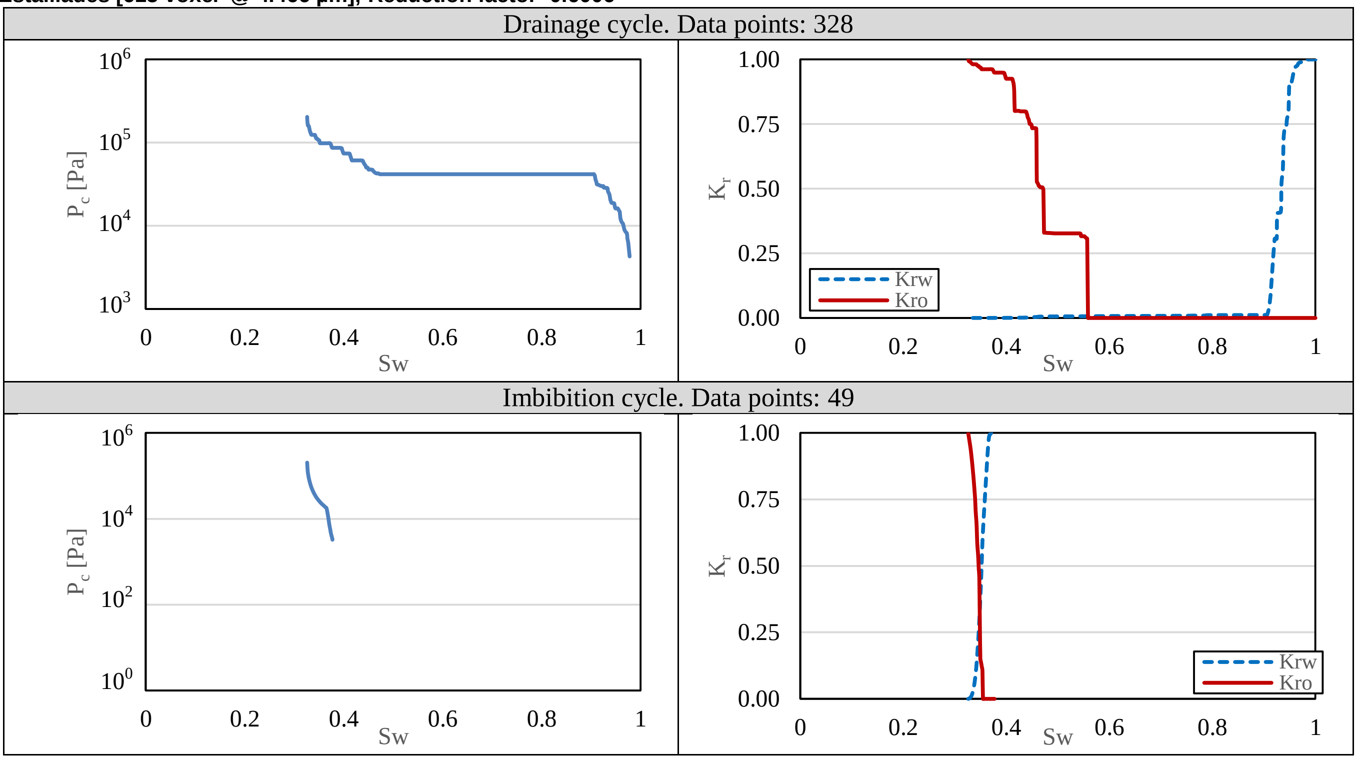

Estaillades [410 voxel³ @ 6.699 μm]; Reduction factor=0.4004

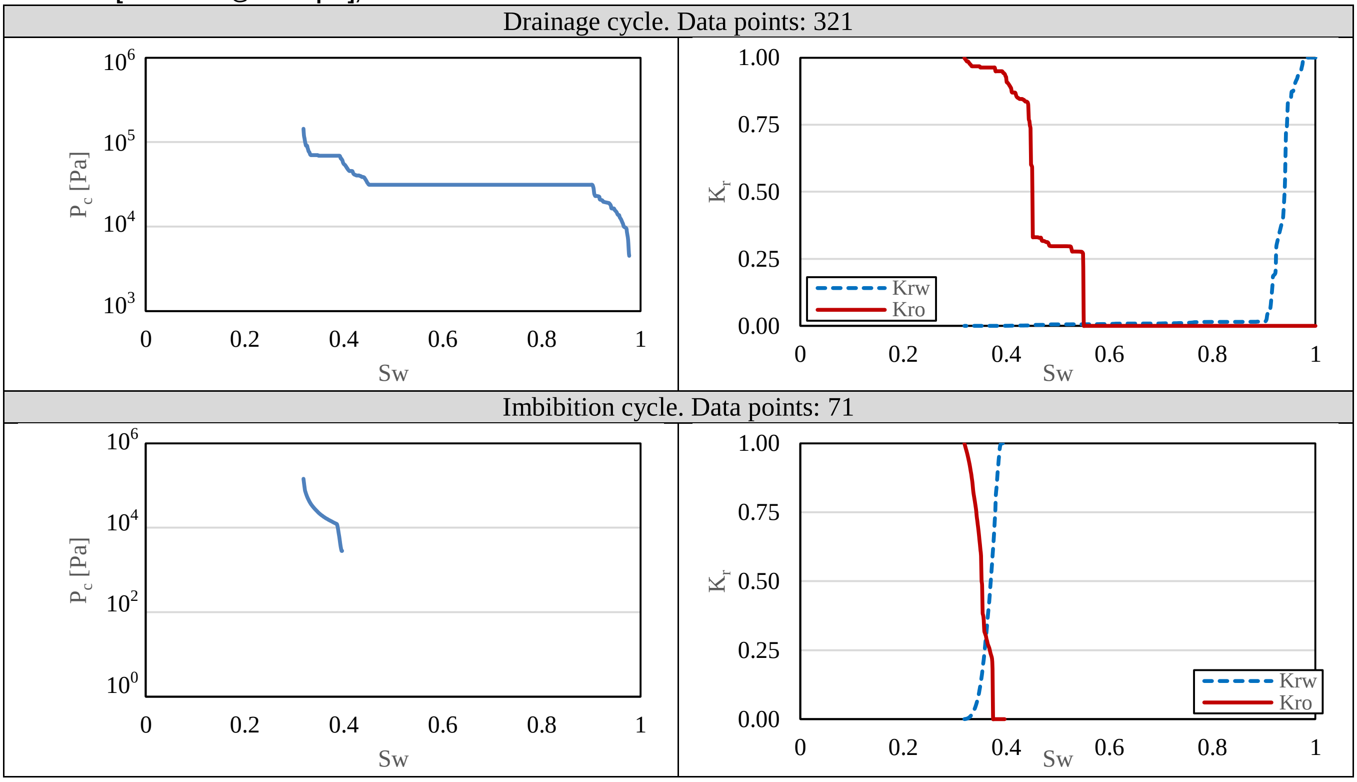

Estaillades [205 voxel³ @ 13.399 μm]; Reduction factor=0.2002

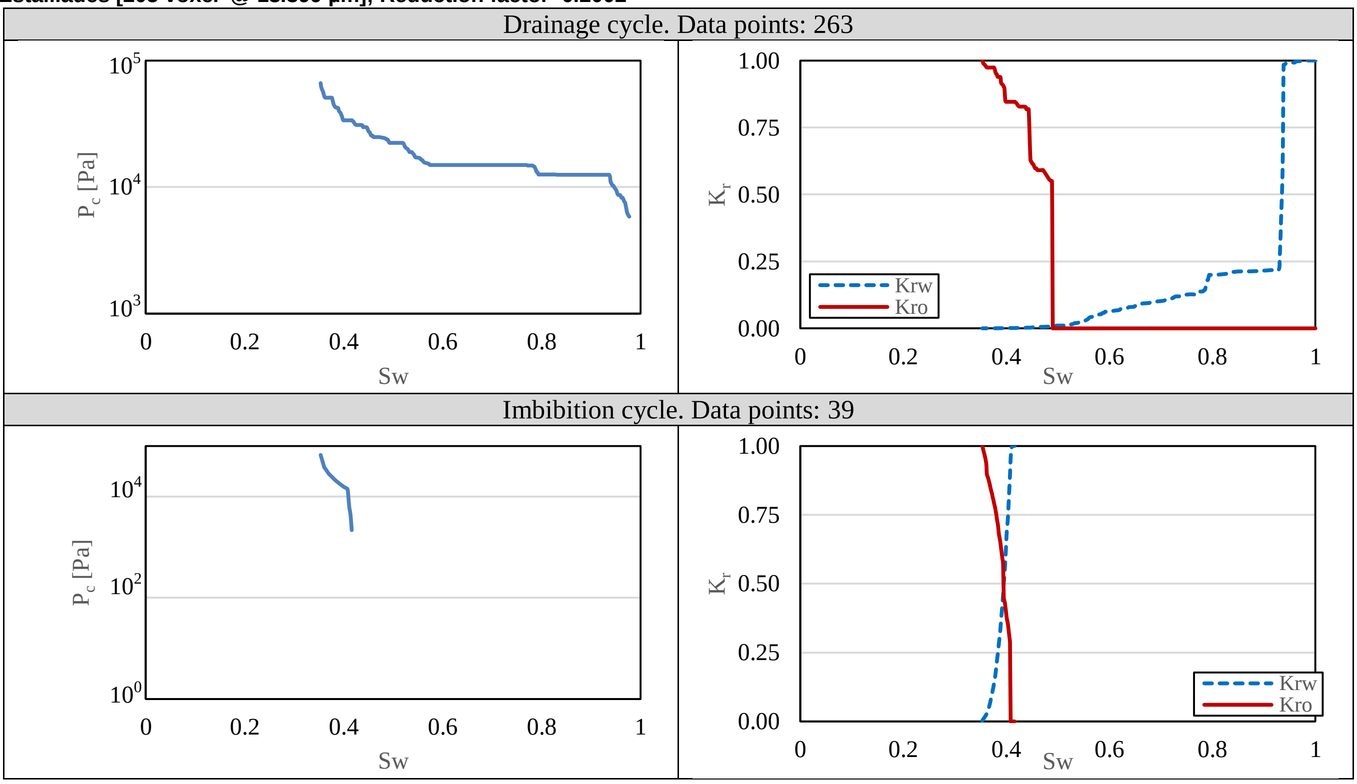

Estaillades [103 voxel^3 @ 26.668 μm]; Reduction factor=0.1006

Drainage cycle. Data points: 85

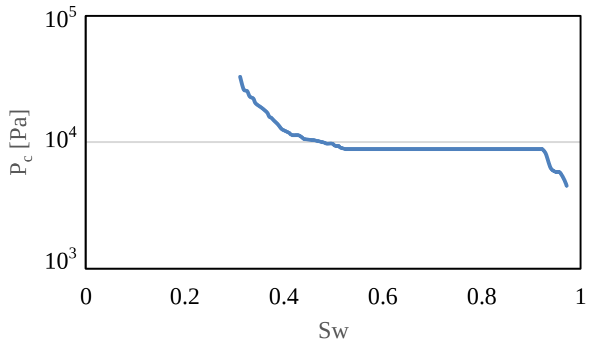

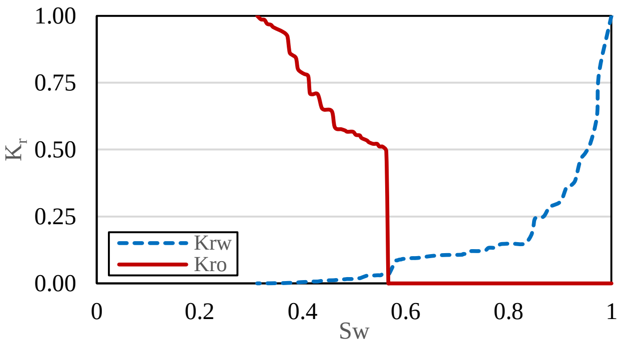

Imbibition cycle. Data points: 25

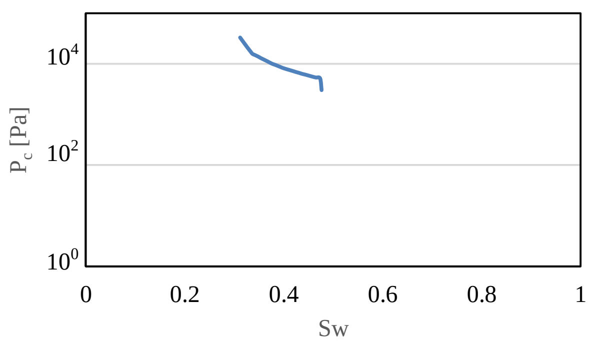

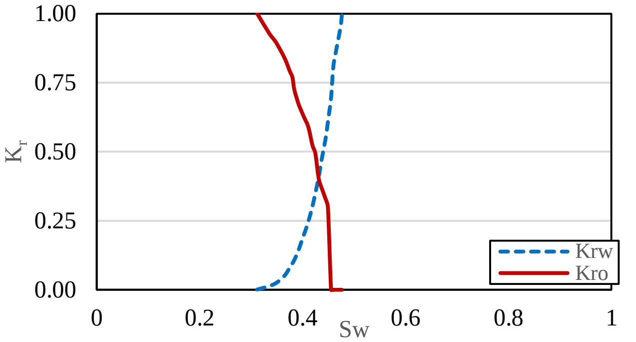

Ketton [512 voxel^3 @ 4.419 μm]; Reduction factor=0.6006

Drainage cycle. Data points: 184

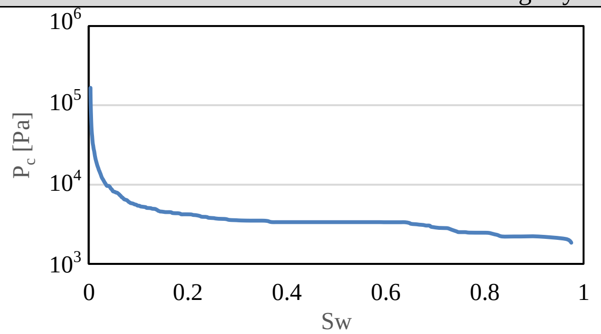

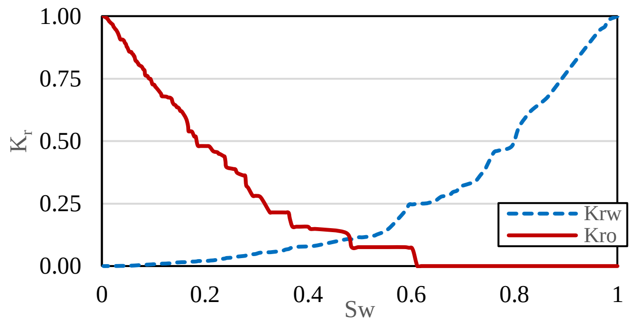

Imbibition cycle. Data points: 138

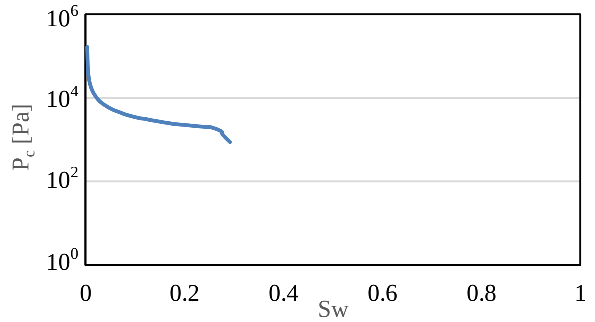

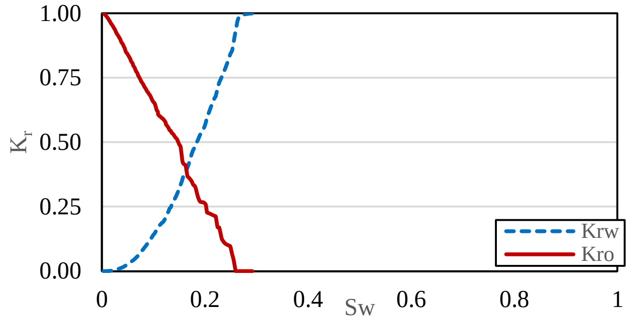

Ketton [410 voxel^3 @ 6.629 μm]; Reduction factor=0.4004

Drainage cycle. Data points:

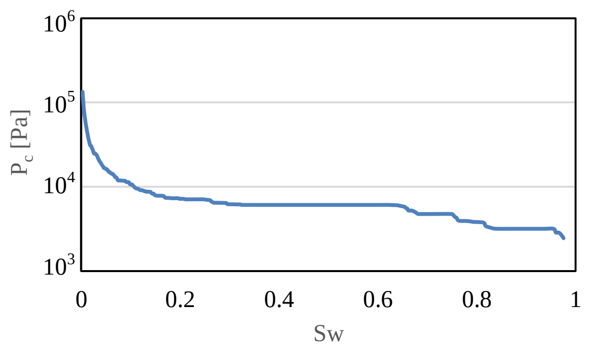

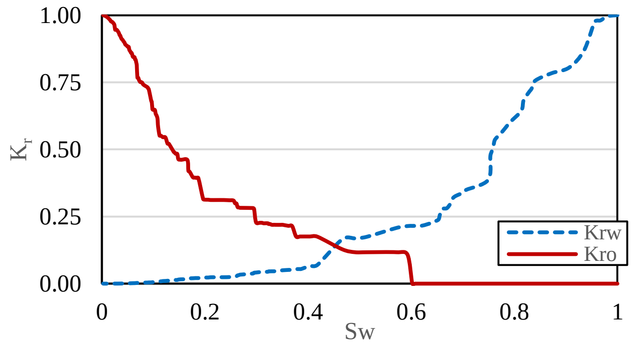

Imbibition cycle. Data points:

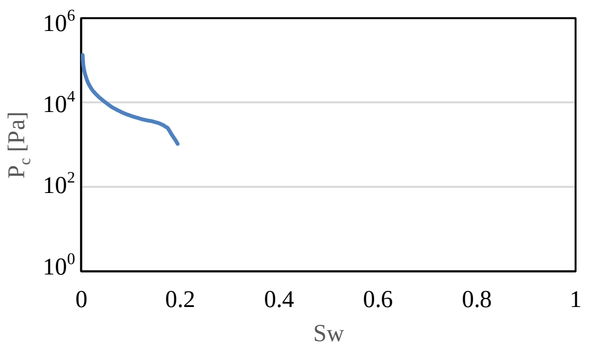

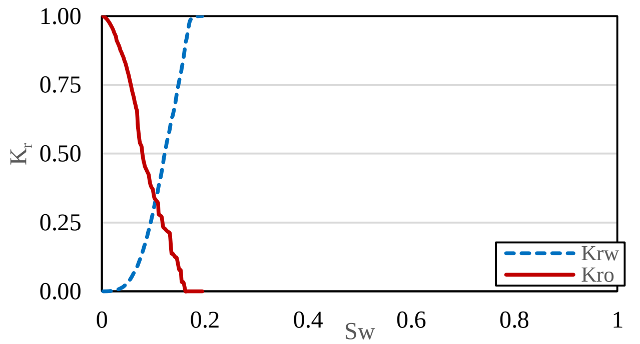

Ketton [205 voxel^3 @ 13.257 µm]; Reduction factor=0.2002

Drainage cycle. Data points:

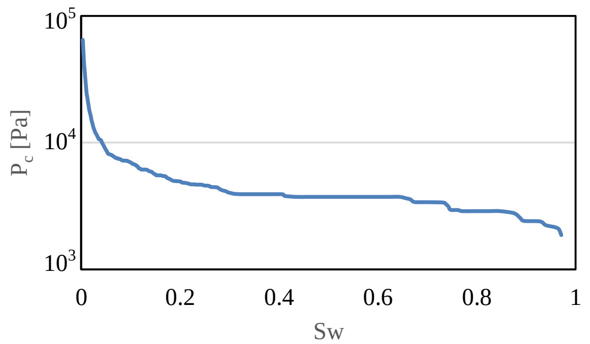

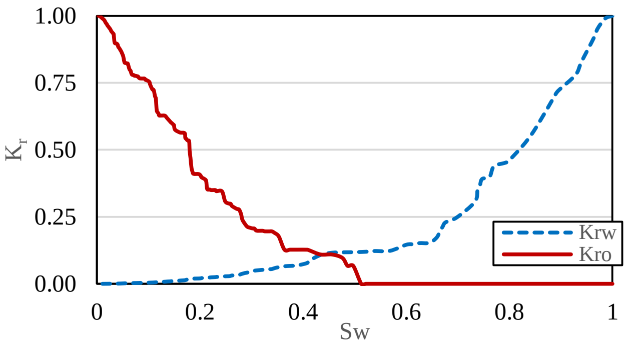

Imbibition cycle. Data points:

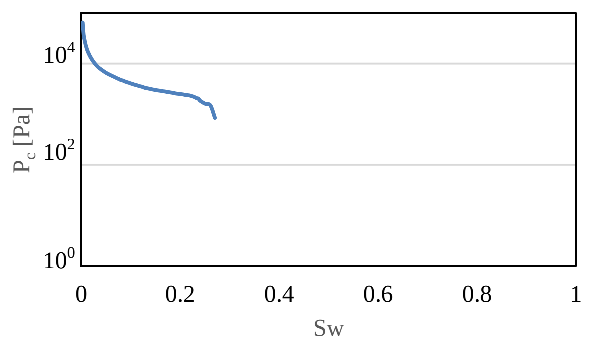

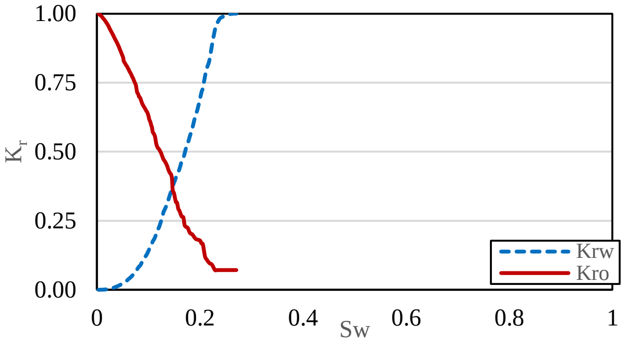

Ketton [103 voxel^3 @ 26.385 µm]; Reduction factor=0.1006

Drainage cycle. Data points: 128

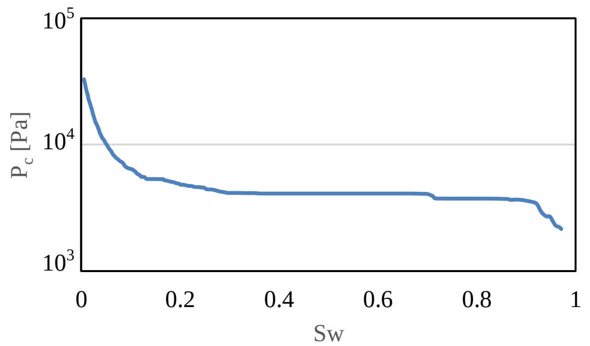

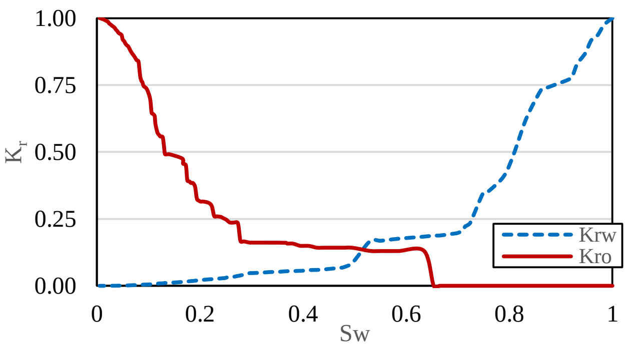

Imbibition cycle. Data points: 93

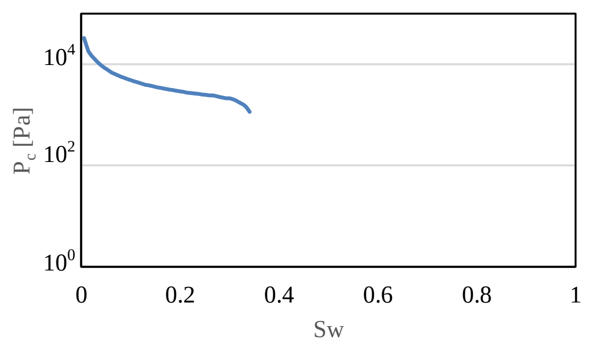

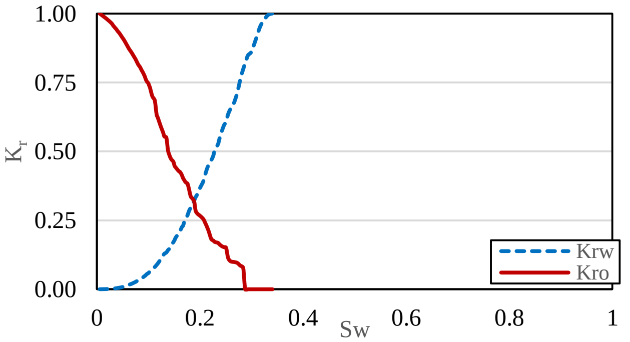

Appendix-VII: Extracted Network Properties

In this appendix, the network properties are tabulated for the subvolume and resolution study cases. It is included to show the effect of changing subvolume and resolution on properties that are not discussed in details in the main text.

Berea Subvolume

Cube size (Voxel^3)	100	199	400	800	1024
Resolution (µm)	2.7745	2.7745	2.7745	2.7745	2.7745
Number of pores	47	451	3224	27712	54979
Number of throats	87	747	5368	47833	96267
Average connection number	3.45	3.20	3.25	3.42	3.48
Number of connections to inlet	4	30	115	448	750
Number of connections to outlet	8	21	128	501	630
Number of physically isolated elements	3	71	532	4981	9522
Number of singlets removed	0	0	0	0	0
Number of triangular shaped elements	136	1193	8563	75268	150784
Number of square shaped elements	0	7	31	279	464
Number of circular shaped elements	0	0	0	0	0
Median throat length to radius ratio	18.05	19.36	19.68	20.12	20.20
Net porosity TwoPhase	0.24	0.18	0.21	0.21	0.20
Clay bound porosity	0	0	0	0	0
Absolute permeability (mD)	2844	439	1076	1195	1281.27
Absolute permeability (m^2)	2.81E-12	4.33E-13	1.06E-12	1.18E-12	1.26E-12
Formation factor	7.3	25.6	12.6	11.7	11.4389

Berea Resolution

Interpolation factor	1	0.800	0.601	0.500	0.400	0.350	0.300	0.200	0.150	0.120	0.101
Cube size(Voxel^3)	1024	819	615	512	410	358	307	205	154	123	103
Resolution (µm)	2.7745	3.47	4.62	5.5	7	8	9.3	14	18.4	23.1	27.6
Number of pores	54979	40400	26799	20270	15212	12601	10177	5813	3714	2529	667
Number of throats	96267	75913	55012	42689	34261	29301	24401	15060	10527	7693	972
Average connection number	3.48	3.73	4.07	4.17	4.45	4.60	4.73	5.10	5.58	5.98	2.78
Number of connections to inlet	750	650	546	457	398	359	321	239	165	124	43
Number of connections to outlet	630	550	471	410	357	337	307	221	177	133	45
Number of physically isolated elements	9522	4817	1800	1034	420	269	101	15	6	2	82
Number of singlets removed	0	0	0	0	0	0	0	0	0	0	0
Number of triangular shaped elements	150784	115990	81575	62762	49331	41775	34483	20815	14195	10187	1633
Number of square shaped elements	464	325	238	199	143	129	97	60	48	37	8
Number of circular shaped elements	0	0	0	0	1	0	0	0	0	0	0
Median throat length to radius ratio	20.20	20.39	20.72	20.90	21.30	21.51	21.37	20.40	18.93	17.63	18.22
Net porosity TwoPhase	0.20	0.201	0.201	0.200	0.201	0.199	0.200	0.198	0.198	0.199	0.083
Clay bound porosity	0	0	0	0	0	0	0	0	0	0	0
Absolute permeability (mD)	1281.27	1108	891	850	768	737	773	961	1320	1877	95
Absolute permeability (m^2)	1.26E-12	1.09E-12	8.79E-13	8.39E-13	7.58E-13	7.27E-13	7.63E-13	9.48E-13	1.30E-12	1.85E-12	9.37E-14
Formation factor	11.4389	12.76	14.58	15.55	16.90	17.80	18.24	19.57	19.28	18.56	243.76

Doddington Subvolume

Cube size (Voxel^3)	100	199	400	600	800	1024
Resolution (µm)	2.7745	2.7745	2.7745	2.7745	2.7745	2.7745
Number of pores	17	134	1515	4061	10865	38390
Number of throats	30	221	3097	7581	19650	69271
Average connection number	2.88	3.09	3.99	3.67	-	3.60
Number of connections to inlet	4	16	101	113	-	164
Number of connections to outlet	7	12	44	148	-	335
Number of physically isolated elements	0	17	200	568	-	1318
Number of singlets removed	0	0	0	0	-	0
Number of triangular shaped elements	49	357	4596	11605	-	85623
Number of square shaped elements	0	0	18	39	-	22040
Number of circular shaped elements	0	0	0	0	-	0
Median throat length to radius ratio	12.11	18.33	19.87	21.61	-	18.7891
Net porosity TwoPhase	0.186	0.276	0.241	0.229	-	0.216
Clay bound porosity	0	0	0	0	-	0
Absolute permeability (mD)	1789	3514	5903	6626	-	1811
Absolute permeability (m^2)	1.77E-12	3.47E-12	5.83E-12	6.54E-12	-	1.79E-12
Formation factor	16.90	7.91	6.26	6.40	-	13.3945

Doddington Resolution

Interpolation factor	1	0.800	0.601	0.5	0.400	0.345	0.3	0.200	0.150	0.120	0.101
Cube size (Voxel^3)	1024	818	615	512	410	358	307	205	154	123	103
Resolution (µm)	2.7745	3.74	4.62	5.5	7	8	9.3	14	18.4	23.1	27.6
Number of pores	38390	9991	11101	8281	6447	5371	4550	2854	2133	1651	1243
Number of throats	69271	23041	23289	17917	14756	12642	11068	7525	5824	4758	3764
Average connection number	3.60	-	4.14	4.27	4.50	4.63	4.78	5.17	5.34	5.64	5.91
Number of connections to inlet	164	-	297	251	237	202	202	149	123	99	91
Number of connections to outlet	335	-	289	253	243	215	203	157	128	105	87
Number of physically isolated elements	1318	-	773	406	194	106	53	7	4	2	0
Number of singlets removed	0	-	0	0	0	0	0	0	0	0	0
Number of triangular shaped elements	85623	-	34290	26119	21137	17953	15568	10353	7933	6387	4998
Number of square shaped elements	22040	-	102	81	68	62	52	28	26	24	11
Number of circular shaped elements	0	-	0	0	0	0	0	0	0	0	0
Median throat length to radius ratio	18.7891	-	21.23	21.21	21.35	22.30	22.05	22.55	21.25	19.81	18.47
Net porosity TwoPhase	0.216	-	0.215	0.212	0.215	0.215	0.215	0.216	0.214	0.213	0.212
Clay bound porosity	0	-	0	0	0	0	0	0	0	0	0
Absolute permeability (mD)	1811	-	4262	3715	3440	2873	2798	2643	2583	3291	3407
Absolute permeability (m^2)	1.79E-12	-	4.21E-12	3.67E-12	3.39E-12	2.84E-12	2.76E-12	2.61E-12	2.55E-12	3.25E-12	3.36E-12
Formation factor	13.3945	-	8.70	9.32	9.99	10.66	11.17	12.74	14.76	14.61	16.28

Estaillades Subvolume

Cube size (Voxel^3)	100	199	400	800	1024
Resolution (µm)	2.6824	2.6824	2.6824	2.6824	2.6824
Number of pores	4	431	5995	39439	75014
Number of throats	3	428	8504	52256	95916
Average connection number	1.00	1.87	2.80	2.63	2.54
Number of connections to inlet	0	10	36	292	505
Number of connections to outlet	2	42	181	515	691
Number of physically isolated elements	7	778	2685	28961	53391
Number of singlets removed	0	0	0	0	0
Number of triangular shaped elements	9	856	14457	91439	170512
Number of square shaped elements	0	5	44	258	420
Number of circular shaped elements	0	0	0	0	0
Median throat length to radius ratio	10.56	15.32	18.99	18.04	17.99
Net porosity TwoPhase	0.000	0.030	0.096	0.070	0.072
Clay bound porosity	0	0	0	0	0
Absolute permeability (mD)	0	0	0	8	3
Absolute permeability (m^2)	0.E+00	0.E+00	1.81E-16	8.17E-15	3.19E-15
Formation factor			1330	672	977.50

Estaillades Resolution

Interpolation factor	1	0.8	0.601	0.5	0.400	0.350	0.3	0.200	0.150	0.120	0.101
Cube size (Voxel^3)	1024	819	615	512	410	358	307	205	154	123	103
Resolution (µm)	2.6824	3.47	4.62	5.5	7	8	9.3	14	18.4	23.1	27.6
Number of pores	75014	45451	24112	16209	10882	8426	6111	2528	1234	691	423
Number of throats	95916	62991	36256	24473	17620	13988	10517	4599	2320	1249	737
Average connection number	2.54	2.75	2.98	2.99	3.20	3.28	3.39	3.56	3.66	3.50	3.35
Number of connections to inlet	505	382	302	232	182	166	135	77	50	28	22
Number of connections to outlet	691	540	383	311	264	204	185	116	73	52	33
Number of physically isolated elements	53391	29590	17008	8961	6693	3831	2686	1133	619	237	132
Number of singlets removed	0	0	0	0	0	0	0	0	0	0	0
Number of triangular shaped elements	170512	108161	60223	40585	28431	22365	16585	7104	3551	1934	1160
Number of square shaped elements	420	283	147	99	73	51	45	25	5	8	2
Number of circular shaped elements	0	0	0	0	0	0	0	0	0	0	0
Median throat length to radius ratio	17.99	18.68	19.14	19.02	18.47	18.34	18.03	17.21	16.53	16.20	15.97
Net porosity TwoPhase	0.072	0.071	0.070	0.069	0.069	0.070	0.069	0.067	0.065	0.063	0.061
Clay bound porosity	0	0	0	0	0	0	0	0	0	0	0
Absolute permeability (mD)	3	1	1	3	2	2	1	2	5	1	14
Absolute permeability (m^2)	3.19E-15	1.03E-15	5.65E-16	2.88E-15	1.73E-15	1.64E-15	8.97E-16	1.85E-15	5.05E-15	4.94E-16	1.34E-14
Formation factor	977.50	1474	1973	1434	1505	1992	2675	2172	1606	3681	1198

Ketton Subvolume

Cube size (Voxel^3)	199	400	600	800	1024
Resolution (µm)	2.654	2.654	2.654	2.654	2.654
Number of pores	51	564	1616	1937	19827
Number of throats	73	889	2298	3456	36352
Average connection number	2.63	3.08	2.78	-	3.66
Number of connections to inlet	6	16	37	-	72
Number of connections to outlet	6	25	62	-	100
Number of physically isolated elements	7	144	492	-	1417
Number of singlets removed	0	0	0	-	0
Number of triangular shaped elements	125	1451	3905	-	46436
Number of square shaped elements	1	4	11	-	9745
Number of circular shaped elements	0	0	0	-	0
Median throat length to radius ratio	22.32	25.45	31.62	-	22.8361
Net porosity TwoPhase	0.249	0.130	0.152	-	0.151
Clay bound porosity	0	0	0	-	0
Absolute permeability (mD)	187	95	11350	-	19419
Absolute permeability (m2)	1.84E-13	9.37E-14	1.12E-11	-	1.92E-11
Formation factor	38.8	82.9	11.2	-	8.54

Ketton Resolution

Interpolation factor	1	0.800	0.601	0.5	0.400	0.350	0.3	0.200	0.150	0.120	0.101
Cube size (Voxel^3)	1024	818	614	512	410	358	307	205	154	123	103
Resolution (µm)	2.654	3.32	4.42	5.5	7	8	9.3	14	18.4	23.1	27.6
Number of pores	19827	2853	1312	2416	1887	1431	1143	741	535	434	379
Number of throats	36352	5899	3204	4563	4190	3051	2524	1750	1290	1063	943
Average connection number	3.66	-	-	3.70	4.34	4.17	4.30	4.57	4.65	4.71	4.78
Number of connections to inlet	72	-	-	64	65	47	50	46	42	39	35
Number of connections to outlet	100	-	-	123	116	94	78	65	52	45	41
Number of physically isolated elements	1417	-	-	513	128	154	91	22	15	5	2
Number of singlets removed	0	-	-	0	0	0	0	0	0	0	0
Number of triangular shaped elements	46436	-	-	6966	6070	4471	3663	2487	1822	1497	1322
Number of square shaped elements	9745	-	-	15	9	13	6	6	5	2	2
Number of circular shaped elements	0	-	-	0	0	0	0	0	0	0	0
Median throat length to radius ratio	22.8361	-	-	22.65	26.67	21.23	20.93	20.26	22.41	21.76	21.47
Net porosity TwoPhase	0.151	-	-	0.148	0.115	0.149	0.149	0.149	0.149	0.149	0.149
Clay bound porosity	0	-	-	0	0	0	0	0	0	0	0
Absolute permeability (mD)	19419	-	-	6653	926	4797	4965	3445	3305	1807	2315
Absolute permeability (m2)	1.92E-11	-	-	6.57E-12	9.13E-13	4.73E-12	4.90E-12	3.40E-12	3.26E-12	1.78E-12	2.28E-12
Formation factor	8.54	-	-	13.04	28.9	16.0	16.0	18.8	20.6	28.2	28.2